Near Field Performance of Staged Diffusers in Shallow Water

by

E. Eric Adams and John H. Trowbridge

Energy Laboratory Report No. MIT-EL 79-015
April 1979

NEAR FIELD PERFORMANCE OF STAGED DIFFUSERS IN SHALLOW WATER

by

E. Eric Adams

and

John H. Trowbridge

Energy Laboratory

and

Ralph M. Parsons Laboratory
for
Water Resources and Hydrodynamics
Department of Civil Engineering

Massachusetts Institute of Technology
Cambridge, Massachusetts 02139

sponsored by

New England Power Service Company
Eastern Utilities Associates

under the

M.I.T. Energy Laboratory Electric Utility Program

Energy Laboratory Report No. MIT-EL 79-015

April 1979

ABSTRACT

Submerged diffusers are commonly used to dilute condenser cooling water from coastal power plants. A staged diffuser, in which the diffuser centerline is perpendicular to shore and the nozzles are directed essentially offshore, is often used at sites where there is a longshore, reversing current. Because of the symmetry of this design, dilution is improved by a longshore current in either direction, and the diffuser's position perpendicular to shore allows it to intercept a crossflow effectively.

The performance of a staged diffuser in shallow water of constant depth has been analysed previously by treating the diffuser as a continuously distributed line source of momentum (Almquist and Stolzenbach, 1976). This theory has been reviewed and extended to consider the case of a sloping bottom and to compute the external (entrainment) flow field set up by the diffuser. In these analyses the important parameters are the gross diffuser dimensions, including total flow rate, discharge velocity, water depth and diffuser length. Length scales are on the order of one diffuser length, and the characteristics of the individual jets are assumed to be insignificant in describing diffuser performance at this level.

A more detailed analysis of staged diffuser performance in the near field is useful if one wishes to describe the temperatures and shear stresses experienced by organisms that are entrained into the diffuser plume. Length scales in this problem are on the order of the port spacing, and characteristics of the individual jets are very important at this level. Relevant diffuser dimensions are discharge velocity, port diameter D_o, port spacing, port elevation h, water depth H, and discharge orientation.

A description of the near field at this level has been obtained by solving for the trajectories, velocities, temperatures and flow rates of individual jets. Boundary layer approximations are made similar to those used in the classical analysis of free turbulent jets, and the analysis includes the effects of shallow water, the flowfield set up by adjacent jets, and an ambient current. Theoretical predictions are compared with the results of an experimental program. The analysis is then used to evaluate different diffuser designs from the standpoint of temperature and shear stress exposure of entrained organisms.

ACKNOWLEDGEMENTS

This study was sponsored jointly by New England Power Service Company and Eastern Utilities Associates under the M.I.T. Energy Laboratory Electric Utility Program, OSP 85232. The cooperation and suggestions of Mr. Bradley Schrader of NEPSCO, Messrs. Stephen Doret and Dennis Ahearn of Yankee Atomic and Mr. Robert Dinnie of EUA are greatfully acknowledged.

This work was performed by Mr. John H. Trowbridge, graduate research assistant in the Department of Civil Engineering as part of his masters thesis. Supervision was provided by Dr. E. Eric Adams, Research Engineer at the Energy Laboratory. Computation was performed at the M.I.T. Information Processing Center. The report was skillfully typed by Mrs. Zigrida Garnis and Mrs. Carole Solomon.

TABLE OF CONTENTS

I. INTRODUCTION

A. PROBLEM DEFINITION

The production of a large amount of waste heat is a necessary consequence of the use of a steam cycle for the generation of electricity. One method for disposal of this waste heat is a "once-through" cooling system, in which cold water is withdrawn from a nearby water body, circulated through the power plant condensers where it absorbs the waste heat, and then discharged back into the water body. In order to minimize the impact of the heated discharge on aquatic life in the receiving water body, a diffuser, or series of turbulent jets, is often used to speed the mixing of the warm discharge water with the cold receiving water. General configurations now in use are tee, coflowing, oblique, alternating, and staged diffusers. (See Figure 1-1.)

This study is concerned with staged diffusers. The centerline of a staged diffuser is perpendicular to shore and the jets are directed essentially offshore. This diffuser design is often used at sites where there is a longshore, reversing current. Because of symmetry, mixing is generally improved by a current from either direction, and the diffuser's position perpendicular to shore enables it to intercept a current effectively. Since the diffuser momentum is directed offshore, the heated discharge tends to move away from the shallow water near the shore and into regions where mixing can be increased by currents and large scale turbulence. The variables describing a staged diffuser are defined in Figure 1-2.

This study is limited to sites where the water is relatively shallow and where the shoreline is fairly straight and "open", as opposed to enclosed locations in bays and inlets. These site characteristics are

typical of much of the northeastern United States and in particular they characterize the site of the proposed NEP-1 and 2 near Charlestown, R.I. Variables which describe the diffuser at this site are included in Table 1.1, and the reader is referred to Brocard (1977) and Brocard and Hsu (1978) for further site-specific analysis.

Table 1.1

Variables Describing the Diffuser at the Charlestown Site of NEP-1 and 2

Q_o = 856,000 gpm

ΔT_o = 37°F

L = 1200 feet

H = 30-33 feet

N = 34

D_o = 2 feet

γ = ± 20°

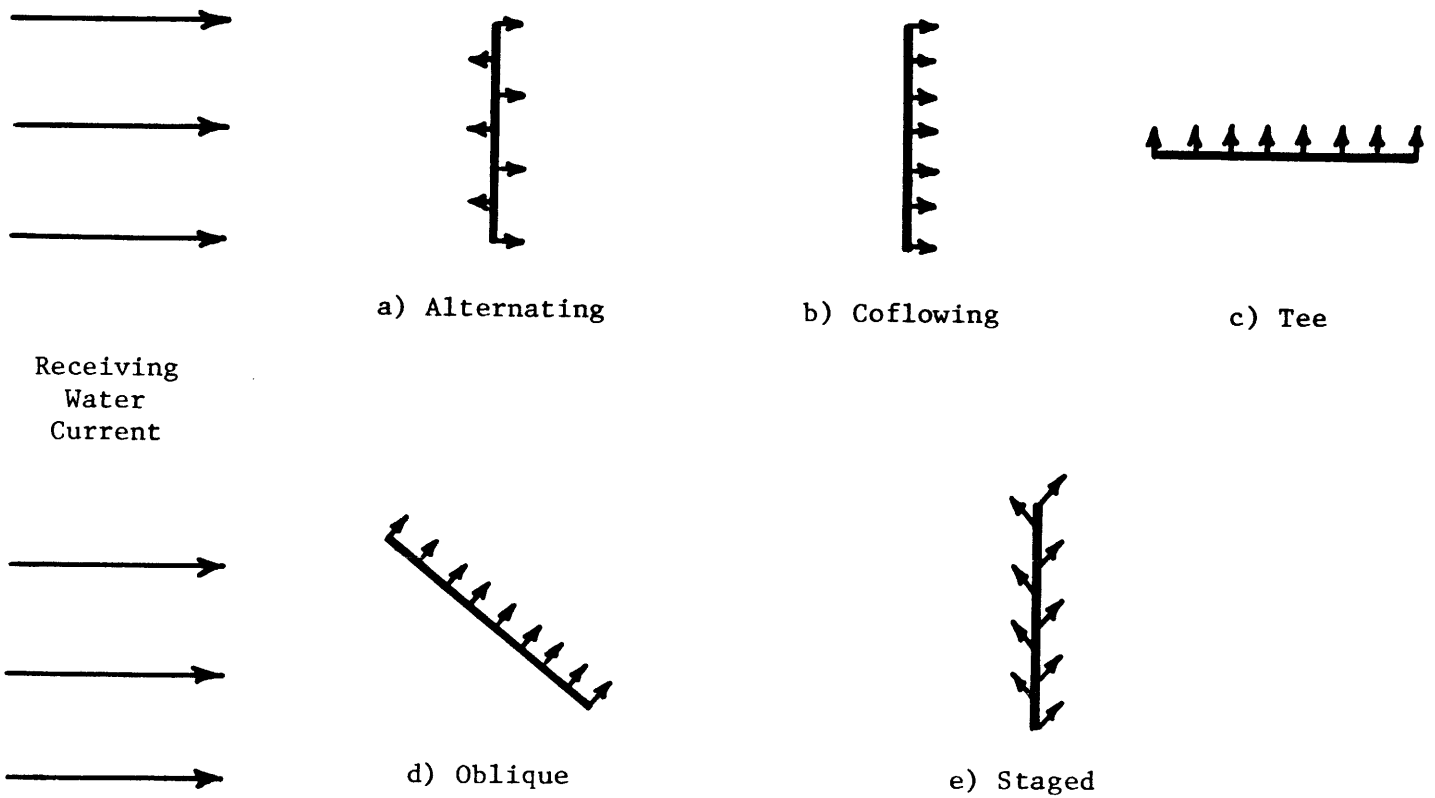

Figure 1-1 Diffuser Design Alternatives

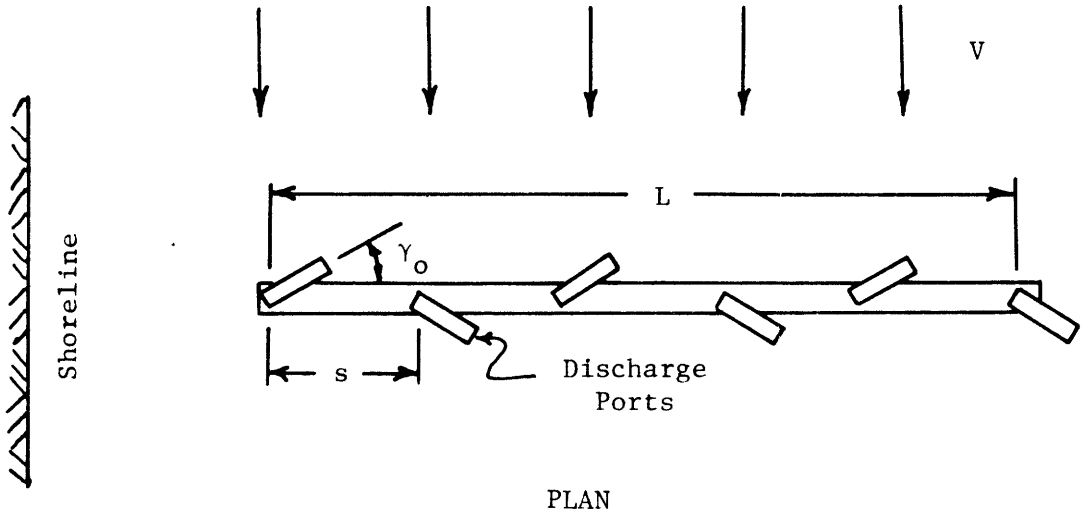

PLAN

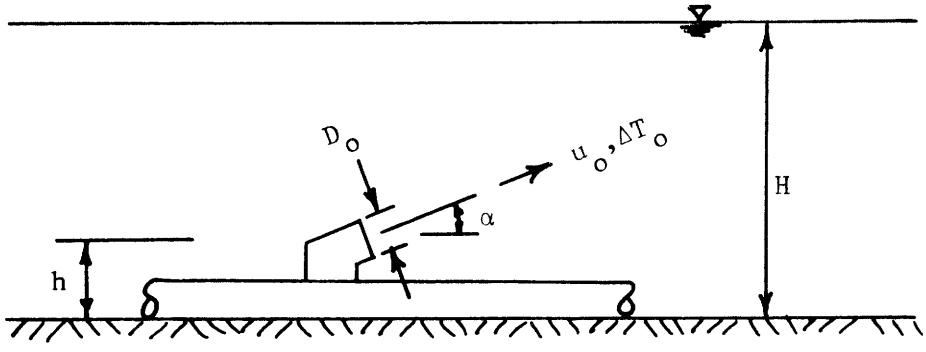

PROFILE

a_o = port area = $\frac{\pi}{4} D_o^2$

M_o = initial kinematic momentum flux = $Q_o u_o$

N = number of ports

Q_o = initial volume flux = $Na_o u_o$

ΔT_o = discharge temperature excess

u_o = discharge velocity

V = ambient current velocity

Figure 1-2 Staged Diffuser Definition Sketch

The flow field induced by a diffuser can be divided into a "near field" and a "far field." (See Figure 1-3.) In the near field, mixing is controlled by the characteristics of the diffuser and by the local features of the receiving water body such as depth and current velocity. Length scales range from the order of the port spacing, s, to the order of the diffuser length, L. The far field is dominated by large scale characteristics of the receiving water body, such as turbulence, surface heat loss, and time-varying current structure. Length scales are an order of magnitude or more greater than the diffuser length, L.

Several studies have examined the near field of different types of diffusers. These studies have been directed toward determining the overall mixing characteristics of the near field, such as total dilution and area of isotherms. The detailed behavior of the individual jets is less important at this level. The most important parameters are the gross diffuser dimensions, including total flow rate Q_o, discharge velocity u_o, water depth H, and diffuser length L. Length scales are on the order of one diffuser length. Examples of this type of study include the work of Adams (1972) and Lee et al. (1977) on tee diffusers, Jirka and Harleman (1973) on alternating diffusers, and Almquist and Stolzenbach (1976) on staged diffusers. These four studies are reviewed by Adams and Stolzenbach (1977); a copy of this review is included as Appendix H.

A more detailed analysis of diffuser performance in the near field is useful if one wishes to determine the temperatures and shear stresses experienced by organisms that are entrained into the diffuser plume. Length scales in this problem are on the order of the port spacing, and characteristics of the individual jets are very important

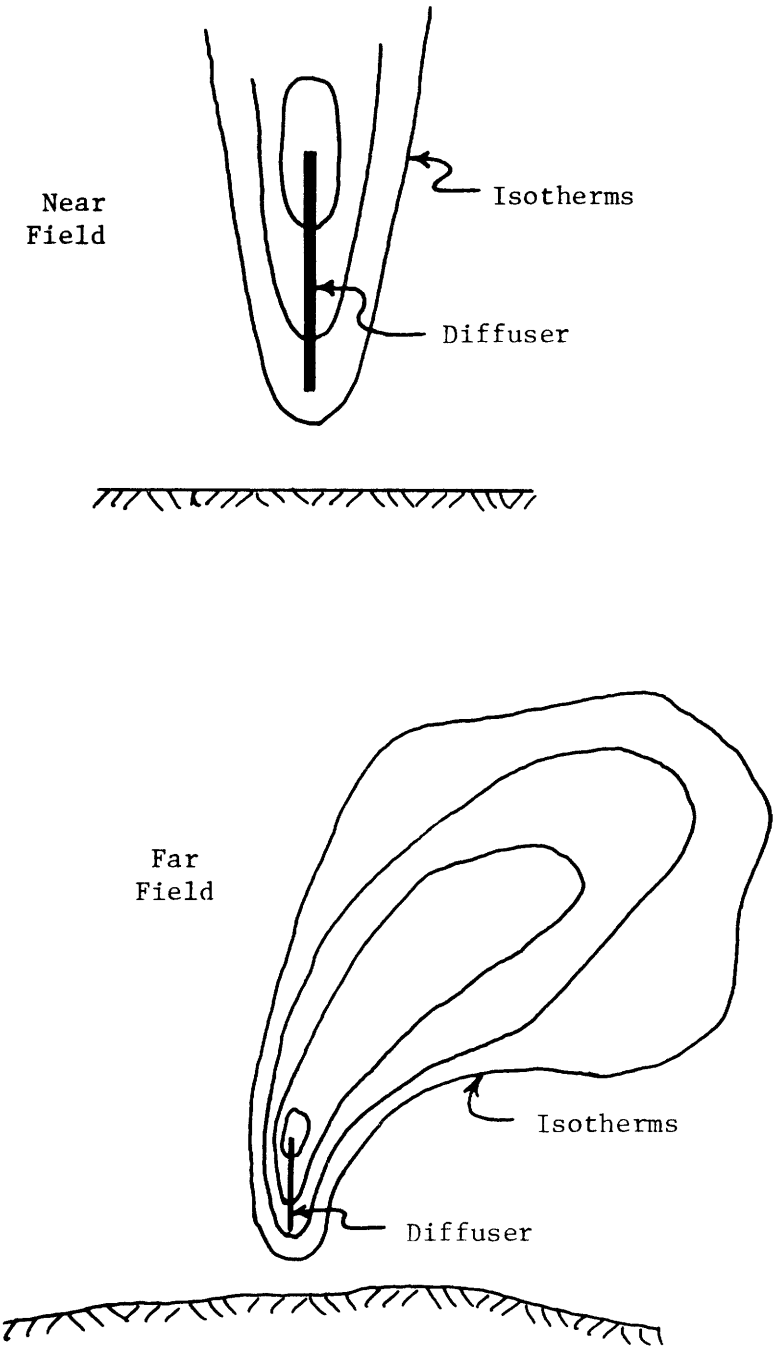

Figure 1-3 Near and Far Field of a Staged Diffuser

at this level. Relevant dimensions are discharge velocity u_o, port diameter D_o, port spacing s, port elevation h, water depth H, and discharge orientation γ_o and α.

The purpose of this report is to examine further the near field of staged diffusers, both on the level of the previous investigations, and on a more detailed level in which the characteristics of the individual jets are important. It is hoped that this study will be of use in understanding staged diffuser performance, in optimizing design, in comparing staged diffusers with other types of diffusers, and in providing tools to predict impacts on aquatic life in the receiving water.

B. APPROACH TO THE PROBLEM

There are two general approaches to problems in fluid mechanics. An Eulerian description of a flowfield gives flow variables at points that are fixed in space. Fluid velocities, accelerations, temperatures and shear stresses are presented as functions of position and time. Traditional measures of thermal plume impact, such as temperature at a point or the area within a given isotherm, are Eulerian descriptions.

In a Lagrangian description, individual particles are identified and flow variables are presented as functions of time following these individual particles through the flowfield. Impact analyses based on the time-history of organism exposure within a plume are based on Lagrangian descriptions.

Our approach has been first to obtain Eulerian descriptions of the near field of a staged diffuser. Jet widths, dilutions, temperatures, velocities and turbulence quantities are presented as functions of position. These variables depend on diffuser parameters such as port

spacing, port size, water depth, and discharge velocity. It has been assumed that the Eulerian flowfield does not change with time over the time scale of interest.

From the Eulerian descriptions, one can in principle obtain Lagrangian descriptions that indicate what a particle experiences as it moves through the diffuser plume. Because of the large turbulent fluctuations in the flow quantities, however, an accurate model of what a moving particle actually experiences is very difficult to obtain. By making simplifying assumptions we have generated Lagrangian descriptions that indicate trends and give an estimate of the "worst case".

In Schubel and Marcy (1978), methods are suggested for predicting the impact of various levels and durations of exposure to excess temperature and to shear stress. By using such models together with a Lagrangian description of the temperatures and shear stresses that an organism experiences as it moves through the diffuser plume, it should be possible to estimate the impact of a diffuser on aquatic life. The biological details of such work, however, are beyond the scope of this report.

Because of the orientation of the jets of a staged diffuser, it is difficult to avoid a certain amount of interaction between adjacent jets. It is desirable from both an Eulerian and a Lagrangian point of view to minimize this jet interaction, since interaction interferes with dilution and causes organisms to be re-entrained successively into a series of jets. An Eulerian model of jet trajectories can be used to improve design by indicating ways to avoid jet interaction.

C. SUMMARY OF THE REPORT

Chapter Two presents an analysis of a staged diffuser as a line source of momentum. The conclusions that can be drawn from such an approach as well as its limitations are summarized. In Chapter Three, Eulerian and Lagrangian descriptions of an individual, non-buoyant jet are obtained. Conclusions are presented as if each jet in a staged diffuser acted independently of the other jets. Chapter Four modifies the results of Chapter Three where possible to account for the effects of an ambient current and interaction with other jets. Applications to design, comparisons with other diffuser types and additional conclusions are given in Chapter Five.

II. STAGED DIFFUSER AS A LINE SOURCE OF MOMENTUM

A. INTRODUCTION

A simple Eulerian description of the flowfield near a staged diffuser can be developed by neglecting the effects of the individual jets and treating the diffuser as a source of momentum that is continuously distributed over the diffuser length. This type of analysis is best suited to describing the flow regions that are controlled by the characteristics of the diffuser as a whole, and in which individual jet behavior is not important. The relevant parameters are the gross diffuser dimensions, including total flow rate Q_o, discharge velocity u_o, water depth H, and diffuser length L.

In this chapter, we will first review the study of Almquist and Stolzenbach (1976), which gives an Eulerian description of a staged diffuser in stagnant water of constant depth, treating the diffuser as a line source of momentum. We will then use this theory to develop a Lagrangian description of a staged diffuser plume, and to solve for the entrainment flowfield surrounding the plume. The theory of Almquist and Stolzenbach will then be modified to account for a small bottom slope. Using this modified theory, a corresponding Lagrangian description will be developed and the entrainment flowfield for a sloping bottom will be analyzed.

B. REVIEW OF ALMQUIST AND STOLZENBACH THEORY

Almquist and Stolzenbach (1976) analyzed staged diffusers for the case of a stagnant, shallow receiving body of water with constant depth and infinite lateral dimensions. Their theory developed Eulerian expressions for mean velocity, plume width, temperature, and flow ra for the diffuser as a whole in the near field. Since the stagnant case is the

worst case for a staged diffuser, their theory provides a conservative estimate of staged diffuser performance.

The theory divided the near field into a 3-D region, a 2-D momentum region, and a 2-D jet region. (See Figure 2-1.) In the 3-D region, the diffuser plume does not intersect the water surface and it was assumed to behave like a classical, round, turbulent jet with continuous addition of momentum. The plume in the 2-D momentum region was assumed to be well mixed over the whole water depth so that it could be treated as a plane, turbulent jet with continuous momentum addition. In the 2-D jet region there is no momentum added and the plume was again treated as a plane jet. The analysis was based on a set of integrated continuity and momentum equations, and typical boundary layer approximations were made. Lateral velocity profiles were assumed to be kinematically similar and an entrainment hypothesis was used, relating plume centerline velocity and entrainment velocity. Buoyancy effects were neglected.

The results of the theory can be summarized briefly as follows.

3-D region

$$u_c \sim \frac{1}{\mathbb{K}} x^{-\frac{1}{2}}$$

$$\Delta T \sim \frac{1}{\mathbb{K}} x^{-\frac{1}{2}} \qquad (2.1)$$

$$S^* \sim \mathbb{K} \; x^{\frac{1}{2}}$$

3-D momentum region

$$u_c \sim \frac{1}{\mathbb{K}}$$

$$\Delta T \sim \frac{1}{\mathbb{K}} \qquad (2.2)$$

$$S^* \sim \mathbb{K}$$

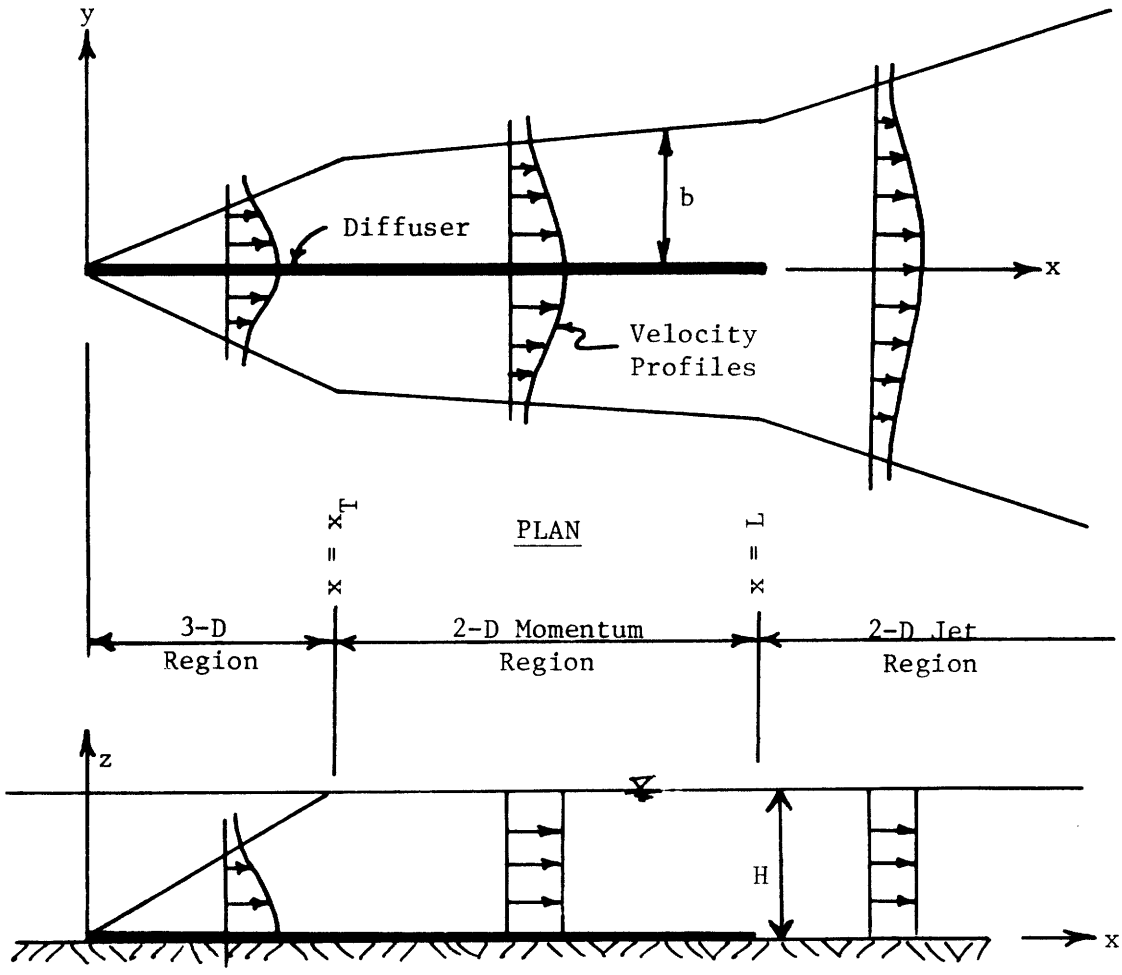

b = plume width

u = longitudinal velocity

u_c = centerline longitudinal velocity

ΔT = temperature excess

ΔT_c = centerline temperature excess

Q_E = entrained flowrate

$$S^* = \text{dilution} = \begin{cases} \dfrac{Q_E}{Q_o}\dfrac{x}{L} & \text{(3-D \& 2-D momentum regions)} \\ \dfrac{Q_E}{Q_o} & \text{(2-D jet region)} \end{cases}$$

Figure 2-1 Definition Sketch for Analysis of Almquist and Stolzenbach (1976)

2-D jet region

$$u_c \sim \frac{1}{K} x^{-\frac{1}{2}}$$

$$\Delta T \sim \frac{1}{K} x^{-\frac{1}{2}} \qquad (2.3)$$

$$S^* \sim K\ x^{\frac{1}{2}}$$

where

$$K = \sqrt{\frac{sH}{a_o}}$$

An important characteristic of this analysis is the heavy dependence of diffuser performance on the parameter K. Another important result is that the temperature, velocity and dilution are constant in the 2-D momentum region which includes most of the length of the diffuser. Also note that a discontinuity in ΔT will occur between the 3-D and the 2-D regions due to different lateral profiles and the required matching of integral quantities.

C. LAGRANGIAN DESCRIPTION

By assuming that an entrained organism moves through the diffuser plume as if it were a fluid particle, we can in principle develop Lagrangian expressions describing its motion and exposure history, based on the Eulerian expressions developed by Almquist and Stolzenbach. However, a staged diffuser plume is turbulent, and turbulence is characterized by large, random velocity fluctuations. If particle motion is to be described accurately, it must be treated as a stochastic process. Because of the non-linearity of the equations of motion, analytical expressions are difficult to obtain. In addition, the behavior of the individual jets in a staged diffuser can be important in determining

the motion of individual particles. A sophisticated analysis of random particle motion is not consistent with the simplification we have made in treating the diffuser as a line source of momentum.

For these reasons, we make simplifying assumptions in order to obtain Lagrangian equations. We assume that an entrained particle moves directly to the diffuser centerline and then travels along it at the mean centerline velocity. The temperatures that it experiences are assumed to be equal to the mean centerline temperatures. In order to model shear stress exposure, we assume that a characteristics shear stress is given by

$$\tau = C\rho u_c^2$$

where

τ = shear stress

ρ = water density

C = coefficient

The coefficient C should be of order .05, based on measurements made in turbulent jets (Rajaratnam (1976)). This assumption is reasonable for locations not too close to the receiving water bottom, and it is consistent with the accuracy of the assumptions concerning temperature exposure. It can be shown that the path along the centerline is the "worst case", as far as temperature exposure is concerned, of all the straight line paths that the particle could take. (See Appendix A.) In some sense, then, our analysis gives a conservative estimate of shear stress and temperature exposure within the limits of the line source of momentum assumption. This estimate should be fairly accurate for entrained particles that are not too near the bottom, and it should be useful in evaluating trends and

general behavior.

The Lagrangian equations we have developed under the above assumptions can be summarized briefly as follows.

3-D region

$$x \sim \mathbb{K}^{-2/3}\, t^{2/3}$$
$$\Delta T \sim \mathbb{K}^{-2/3}\, t^{-1/3} \qquad (2.4)$$
$$\tau \sim \mathbb{K}^{-4/3}\, t^{-2/3}$$

2-D momentum region

$$x \sim \mathbb{K}^{-1}\, t$$
$$\Delta T \sim \mathbb{K}^{-1} \qquad (2.5)$$
$$\tau \sim \mathbb{K}^{-2}$$

2-D jet region

$$x \sim \mathbb{K}^{-2/3}\, t^{2/3}$$
$$\Delta T \sim \mathbb{K}^{-2/3}\, t^{-1/3} \qquad (2.6)$$
$$\tau \sim \mathbb{K}^{-4/3}\, t^{-2/3}$$

where

x = particle location

t = time

These Lagrangian equations depend heavily on the diffuser parameter $\mathbb{K}$, as do the Eulerian equations on which they are based. The highest shear stresses and temperatures are experienced in the 3-D region, but the amount of time spent in this region by a moving particle is small compared

to the time spent in the 2-D momentum region and the 2-D jet region. A complete summary of the equations and the details of their development are given in Appendix B.

Sample curves showing shear stress and temperature exposure for a particle entrained at the extreme upstream end of a staged diffuser, with $x = t = 0$ at the point of entrainment, are presented in Figure 2-2. In order to find the exposure history of a particle entrained at a point further downstream, the curves can be "entered" at the value of x corresponding to the point of entrainment. Entrained flow rates have been plotted to allow estimates of the number of particles that experience a particular exposure history. All quantities have been normalized to provide generality.

As an example, suppose we have a staged diffuser with Q_o = 2000 cfs, H = 30', L = 1200', and K = 20. (These dimensions are approximately equal to those of the proposed diffuser for NEP-1 and NEP-2 at the Charlestown site, see Table 1.1). Suppose an organism enters the diffuser plume 240' from the upstream end of the diffuser. This corresponds to the point $\frac{x}{H} = 8$ in Figure 2-2, and the organism will experience the temperatures and shear stresses shown to the right of this point on the curve. From the dimensionless flowrate curve, we see that $\frac{Q_e}{Q_o} = 1.5$ where $\frac{x}{H} = 8$. Therefore, an amount of water per unit time $Q_e = 1.5\ Q_o = 3000$ cfs will enter the diffuser plume upstream of this point and will experience a temperature history equal to or worse than that experienced by the organism entering the diffuser plume at x = 240', If n is the density of organisms (e.g. number/ft^3) in the ambient water, the number of organisms that experience this temperature history per unit time is 3000 n. Using figures such as this, the total impact of a diffuser on entrained organisms

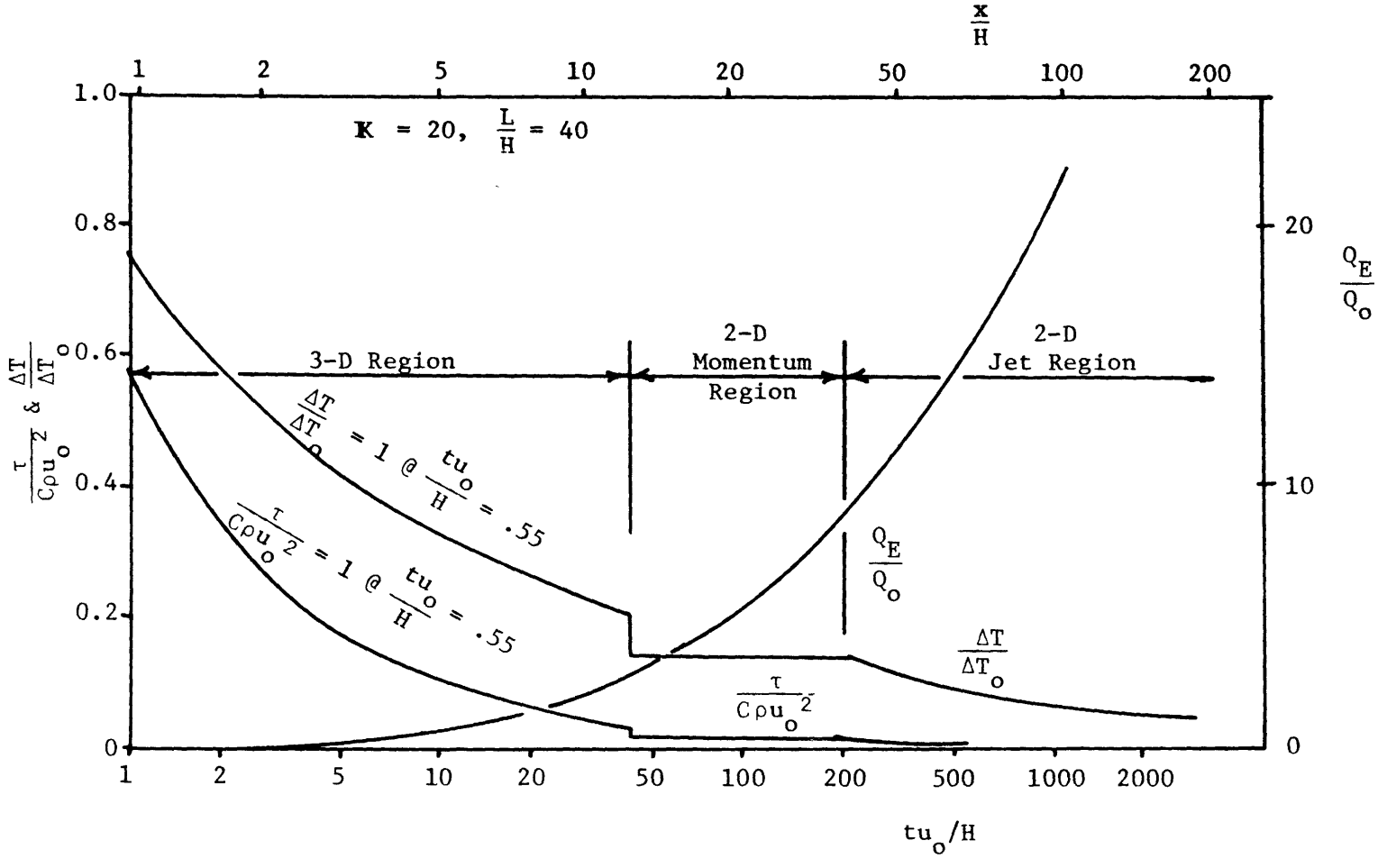

Figure 2-2 Particle Motion and Exposure History
(based on line source of momentum concept)

can be estimated if the response of the organisms to temperature increases is known.

In a real situation, a moving particle might periodically experience temperatures and shear stresses that are much different from those that our theory predicts, because of occasional contact with discrete jets and because of random, turbulent motions. As was disucssed above, this analysis can give only a general idea of the exposure histories of entrained particles and the effects of varying diffuser parameters.

D. SOLUTION FOR THE EXTERNAL FLOWFIELD

A description of the entrainment flowfield surrounding a staged diffuser could be useful in determining the origin of entrained water and the number and type of organisms likely to be drawn into a diffuser plume. We have obtained a potential flow solution for this flowfield by treating the diffuser as a line sink for entrained water, and by using the theory of Almquist and Stolzenbach to determine the flowrate at each point along the diffuser. Details of the solution and of the computer program used to perform the necessary numerical integration along the line sink are presented in Appendix C.

The receiving body of water is assumed to be stagnant and to have constant depth and semi-infinite horizontal dimensions. A definition sketch for our solution for the entrainment flowfield is shown in Figure 2-3. The solution is presented as a set of streamlines. A streamline is a curve that is tangent at every point to the local fluid velocity, so that there is no flow across a streamline. A value of the stream function, ψ, is associated with each streamline. ψ is equal to the volume of water flowing between the streamline and the shore per unit time. The flow rate between streamline "a" and streamline "b" is

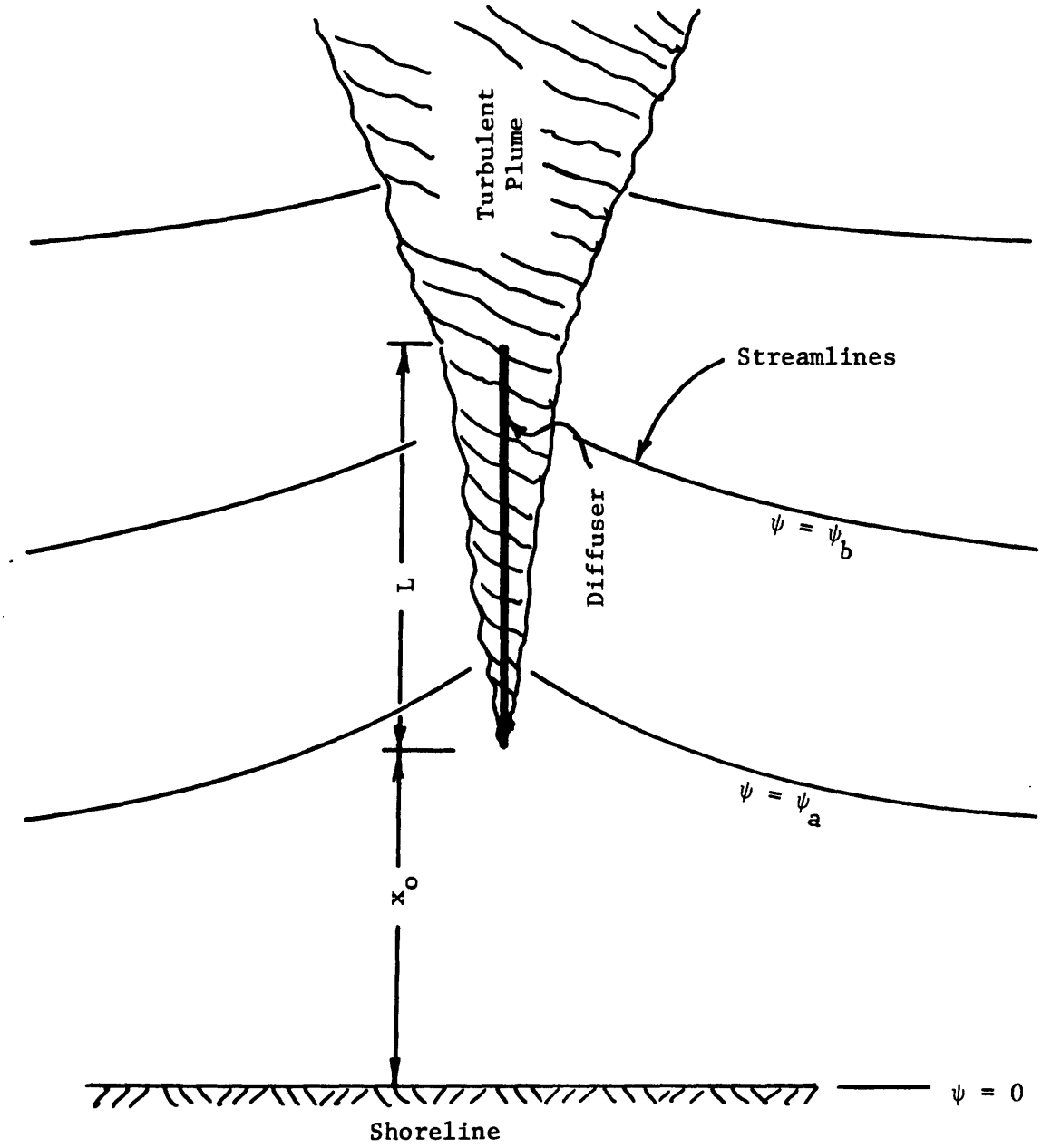

Figure 2-3 Definition Sketch of Entrainment Flowfield

is equal to $\psi_b - \psi_a$.

Our model for the entrainment flowfield gives streamlines and corresponding values of the stream function that are normalized with respect to the diffuser parameter $\mathbb{K}$ and the total discharge Q_o to provide generality. Lengths are normalized with respect to the water depth H. The distance between the diffuser and the shore, the diffuser length, and the extent of the region being considered can be varied. Examples of model results are shown in Figures 2-4 and 2-5.

E. APPLICATIONS TO SLOPING BOTTOM

We have modified the theory of Almquist and Stolzenbach in order to account for a small, constant bottom slope. In the modified theory, the staged diffuser is treated as a line source of momentum, and we assume a stagnant receiving body of water with semi-infinite lateral dimensions. The near field is divided into an initial region, a momentum region, and a jet region. (See Fig. 2-6.) In the initial region, the diffuser plume does not intersect the water surface and it is treated as a round jet with continuous momentum input. The plume in the momentum region is assumed to be well mixed over the whole water depth and it is treated as a confined jet with continuous momentum input. In the jet region, there is no momentum added and the plume is again assumed to be vertically well mixed so that it can be analyzed as a confined jet. It must be assumed that the bottom slope is small enough to allow the plume to intersect the water surface within a reasonably short distance. This condition is met at most coastal sites in the northeastern United States.

The analysis is based on a set of integrated continuity and

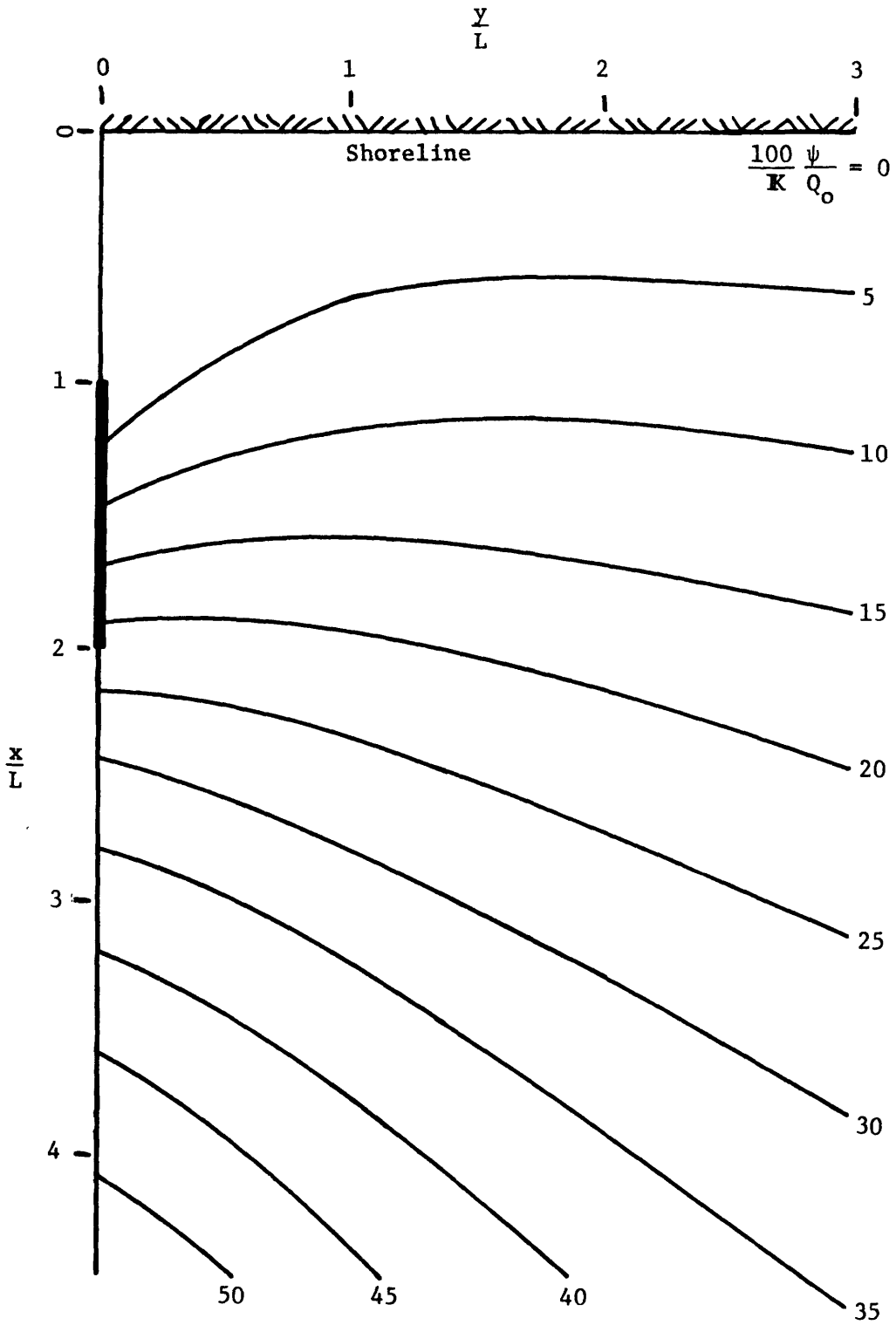

Figure 2-4 Entrainment Flowfield to a Staged Diffuser on a Horizontal Bottom for L/H = 40, $x_o/L = 1$.

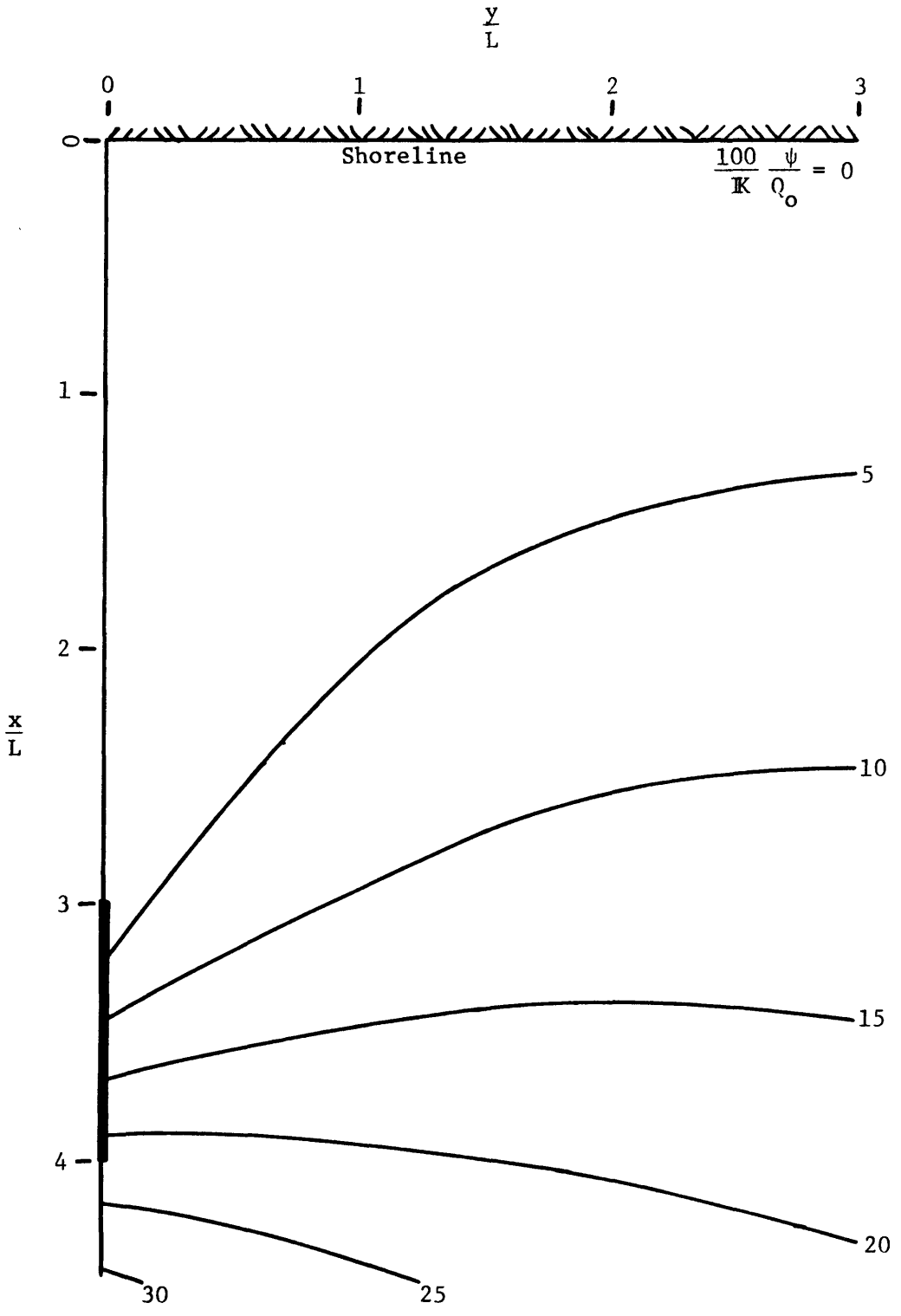

Figure 2-5 Entrainment Flowfield to a Staged Diffuser on a Horizontal Bottom for L/H = 40, $x_o/L = 3$.

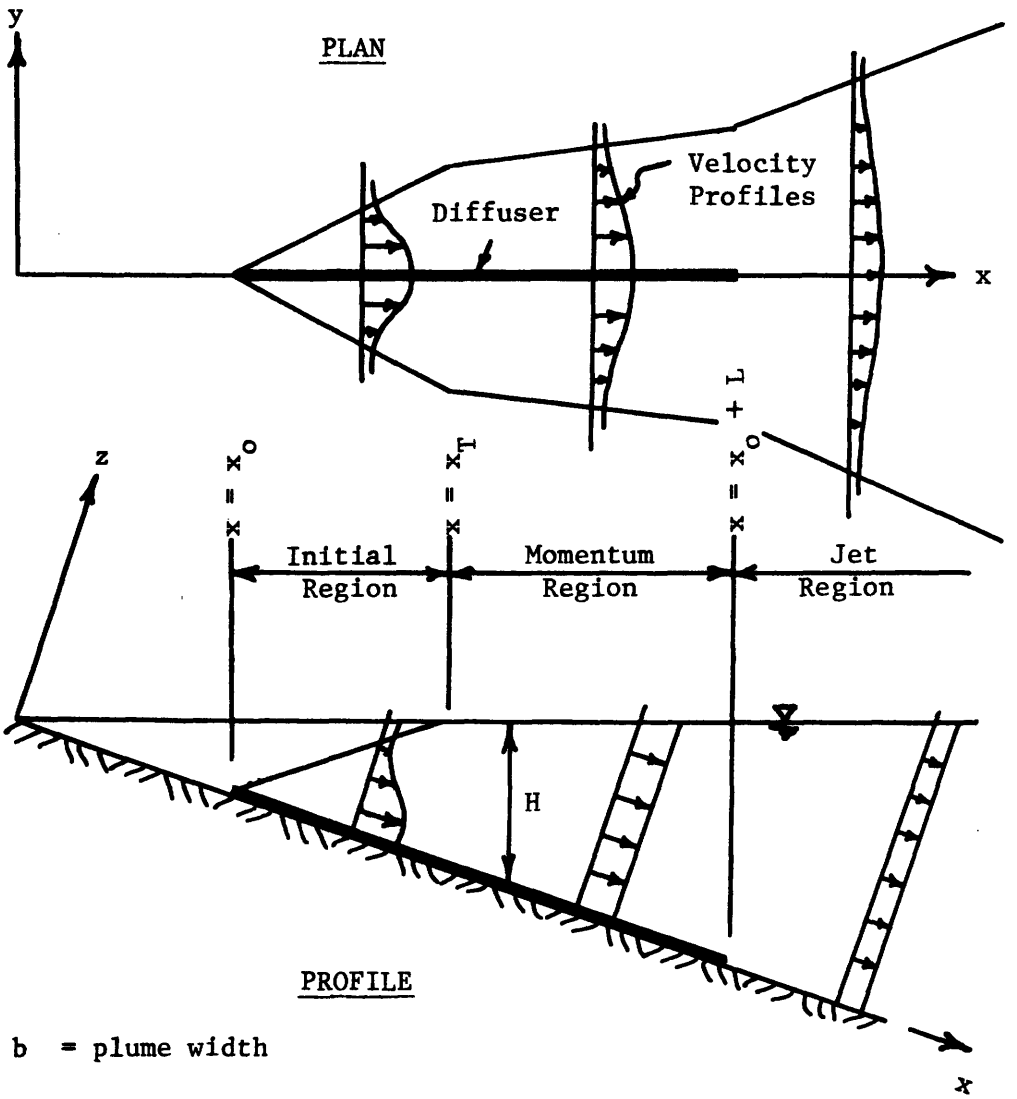

b = plume width

H_o = water depth at $x=x_o$

u = longitudinal velocity

u_c = centerline longitudinal velocity

ΔT = temperature excess

ΔT_c = centerline temperature excess

Q_E = entrained flowrate

$$S^* = \text{dilution} = \frac{Q_E}{Q_o \frac{x}{L}} \quad \text{(initial \& momentum regions)}$$

$$= \frac{Q_E}{Q_o} \quad \text{(jet region)}$$

Figure 2-6 Definition Sketch of Staged Diffuser on Sloping Bottom

momentum equations similar to those used by Almquist and Stolzenbach. Velocity profiles are assumed to be kinematically similar, and an entrainment hypothesis relating plume centerline velocity and entrainment velocity is used. Buoyancy effects are neglected. The Eulerian equations we obtain can be summarized briefly as follows.

Initial region

$$\begin{aligned} u_c &\sim \mathbb{K}_o^{-1} x^{-\frac{1}{2}} \\ \Delta T &\sim \mathbb{K}_o^{-1} x^{-\frac{1}{2}} \\ S^* &\sim \mathbb{K}_o x^{\frac{1}{2}} \end{aligned} \tag{2.7}$$

Momentum region

$$\begin{aligned} u_c &\sim \mathbb{K}_o^{-1} x^{-\frac{1}{2}} \\ \Delta T &\sim \mathbb{K}_o^{-1} x^{-\frac{1}{2}} \\ S^* &\sim \mathbb{K}_o x^{\frac{1}{2}} \end{aligned} \tag{2.8}$$

Jet region

$$\begin{aligned} u_c &\sim \mathbb{K}_o^{-1} x^{-1} \\ \Delta T &\sim \mathbb{K}_o^{-1} x^{-1} \\ S^* &\sim \mathbb{K}_o x \end{aligned} \tag{2.9}$$

where

$$\mathbb{K}_o = \sqrt{\frac{sH_o}{a_o}}$$

Diffuser performance depends heavily on the parameter $\mathbb{K}_o$, which is

similar to the parameter K used by Almquist and Stolzenbach. Dilutions are greater with a sloping bottom than with a horizontal bottom, since an increasing water depth provides a larger area over which entrainment can occur. In the constant depth case, temperature, centerline velocity and dilution are constant in the 2-D momentum region. There is no region for which this is true if the bottom is sloping. A complete summary of the Eulerian equations for the sloping bottom case, and the details of their development, are presented in Appendix D.

Using the Eulerian equations for a staged diffuser on a sloping bottom, we have developed corresponding Lagrangian equations that describe the motion and exposure history of an entrained particle. The Lagrangian equations are based on the same assumptions that were used in the constant depth case. We assume that an entrained particle moves directly to the diffuser centerline and then moves along it at the mean centerline velocity. We assume that it experiences the mean centerline temperature and that it is subject to a shear stress characterized by

$$\tau = C\rho u_c^2$$

where

C = constant of order .05.

The Lagrangian equations can be summarized briefly as follows.

Initial region

$$\begin{aligned} x &\sim K_o^{-2/3}\, t^{2/3} \\ \Delta T &\sim K_o^{-2/3}\, t^{-1/3} \\ \tau &\sim K_o^{-4/3}\, t^{-2/3} \end{aligned} \qquad (2.10)$$

Momentum region

$$x \sim K_o^{-2/3} t^{2/3}$$
$$\Delta T \sim K_o^{-2/3} t^{1/3} \qquad (2.11)$$
$$\tau \sim K_o^{-4/3} t^{-2/3}$$

where

x = location of particle

t = time

No explicit solution was possible in the jet region. Sample curves showing these relationships are presented in Figure 2-7. A complete summary of the Lagrangian equations and the details of their development are given in Appendix E.

To describe the entrainment flowfield surrounding a staged diffuser on a sloping bottom, we have obtained a potential flow solution by treating the diffuser as a line sink for entrained water. The entrainment demand along the diffuser can be specified by using either the theory for a horizontal bottom or the theory for a sloping bottom. Because of the relatively uniform depth at the site for NEP-1 and NEP-2 the former assumption would be most appropriate for that site. Details of the solution and the computer program necessary to perform the necessary numerical integration are also presented in Appendix F. The solution for the entrainment flowfield is again shown as a set of streamlines, with corresponding values of the stream function normalized with respect to

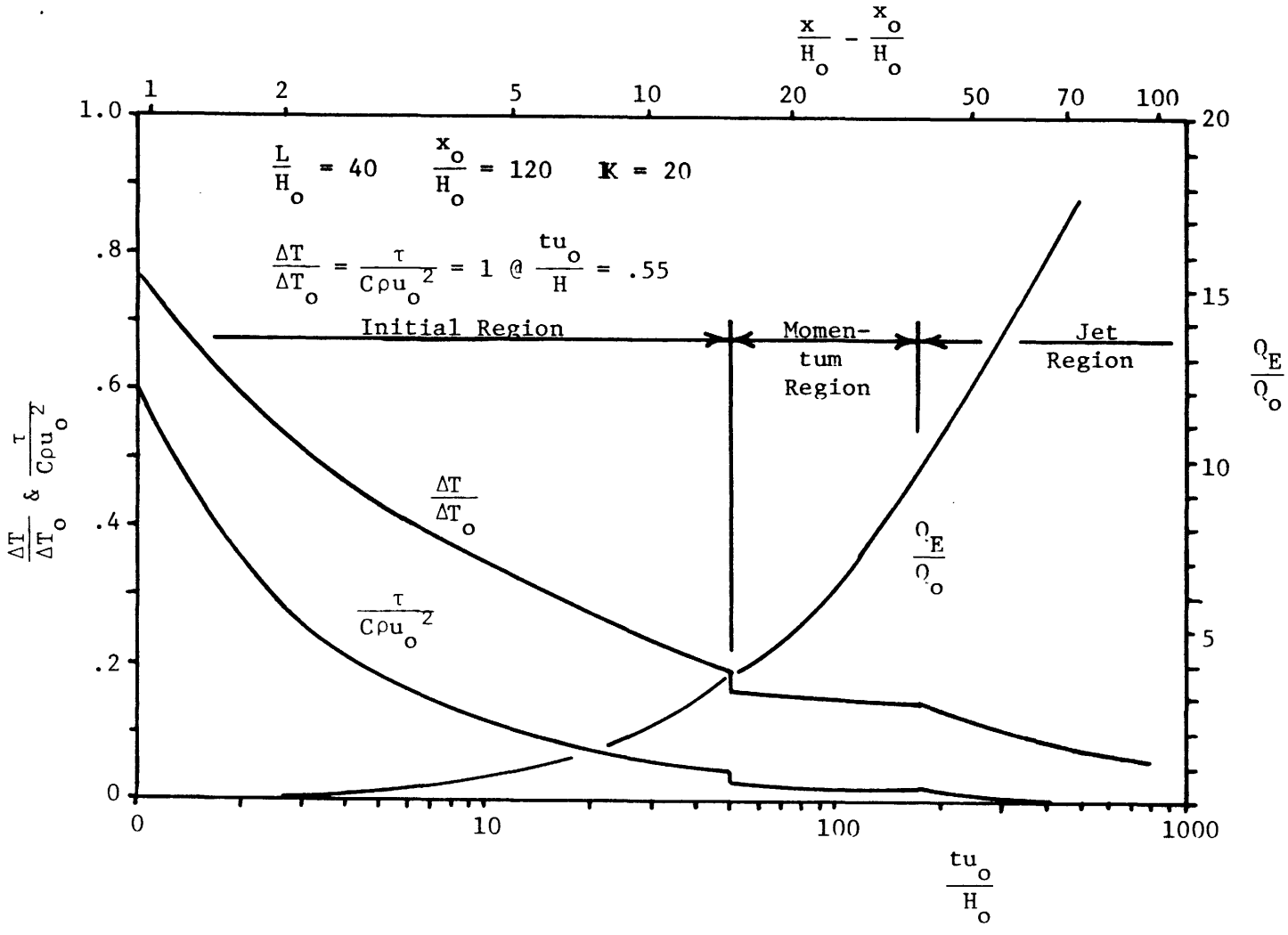

Figure 2-7 Particle Motion and Exposure History for a Staged Diffuser on a Sloping Bottom (Based on the line source of momentum comcept)

the diffuser parameter K_o and the total discharge Q_o to provide generality. Lengths are normalized with respect to the diffuser length L. The distance between the diffuser and the shore and the extent of the region being considered can be varied. Examples of model results are shown in Figures 2-8 and 2-9.

F. SUMMARY OF CHAPTER II

In Chapter II we have shown the Eulerian and Lagrangian descriptions of the near field of a staged diffuser that can be obtained by treating the diffuser as a line source of momentum. In addition, we have presented simple models of the entrainment flowfield surrounding a staged diffuser.

In using the equations developed in this chapter, the simplifications on which they are based should be kept in mind. Basically, these include the line source of momentum assumption, which neglects the effects of individual jets, and the assumption of a stagnant semi-infinite receiving body of water. In addition, the Lagrangian equations for shear stress and temperature exposure are based on simple, straight line paths for particle motion.

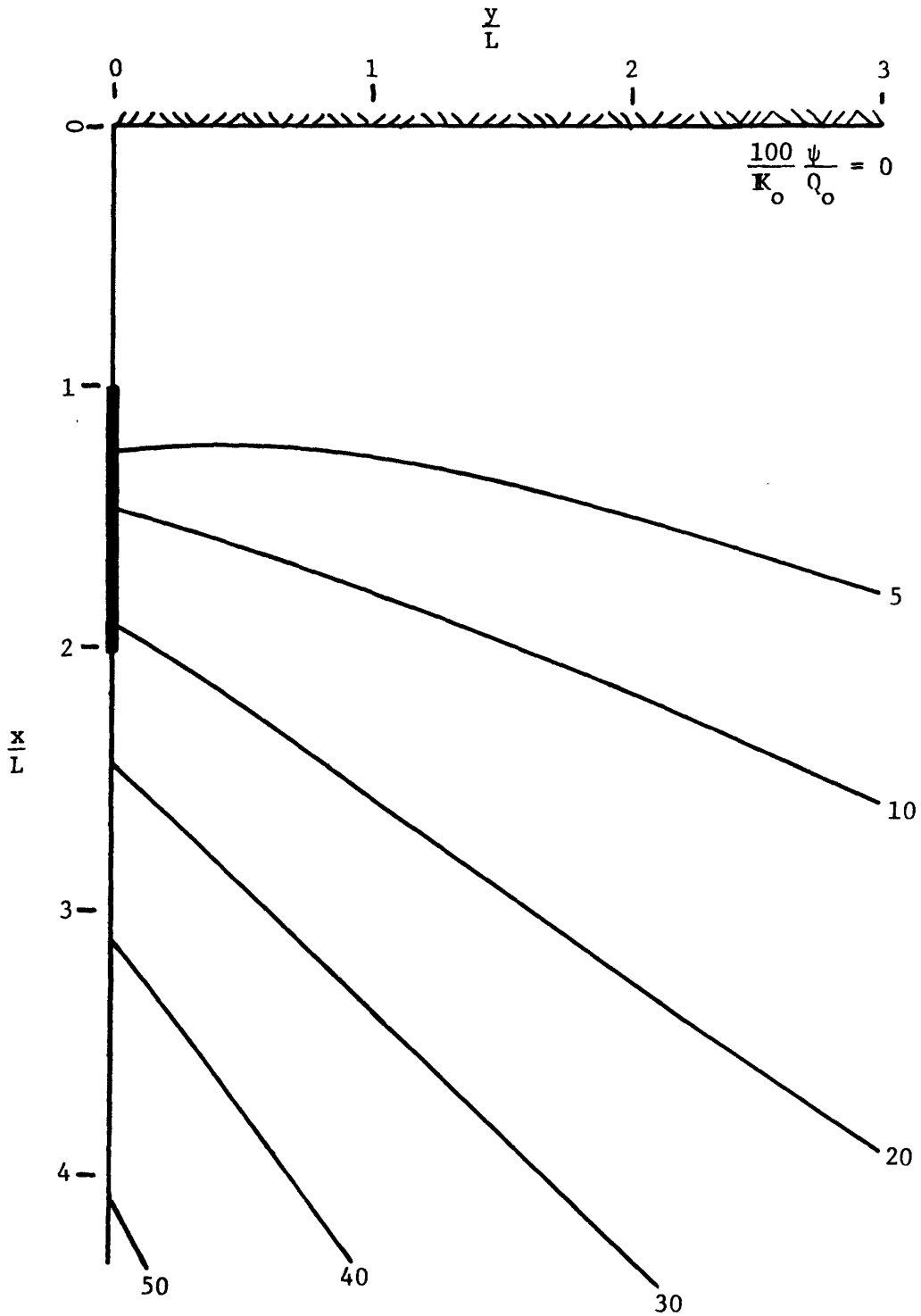

Figure 2-8 Entrainment Flowfield to a Staged Diffuser on a Sloping Bottom for $x_o/L = 1$

(Inner Solution is Almquist and Stolzenbach Theory (1976).)

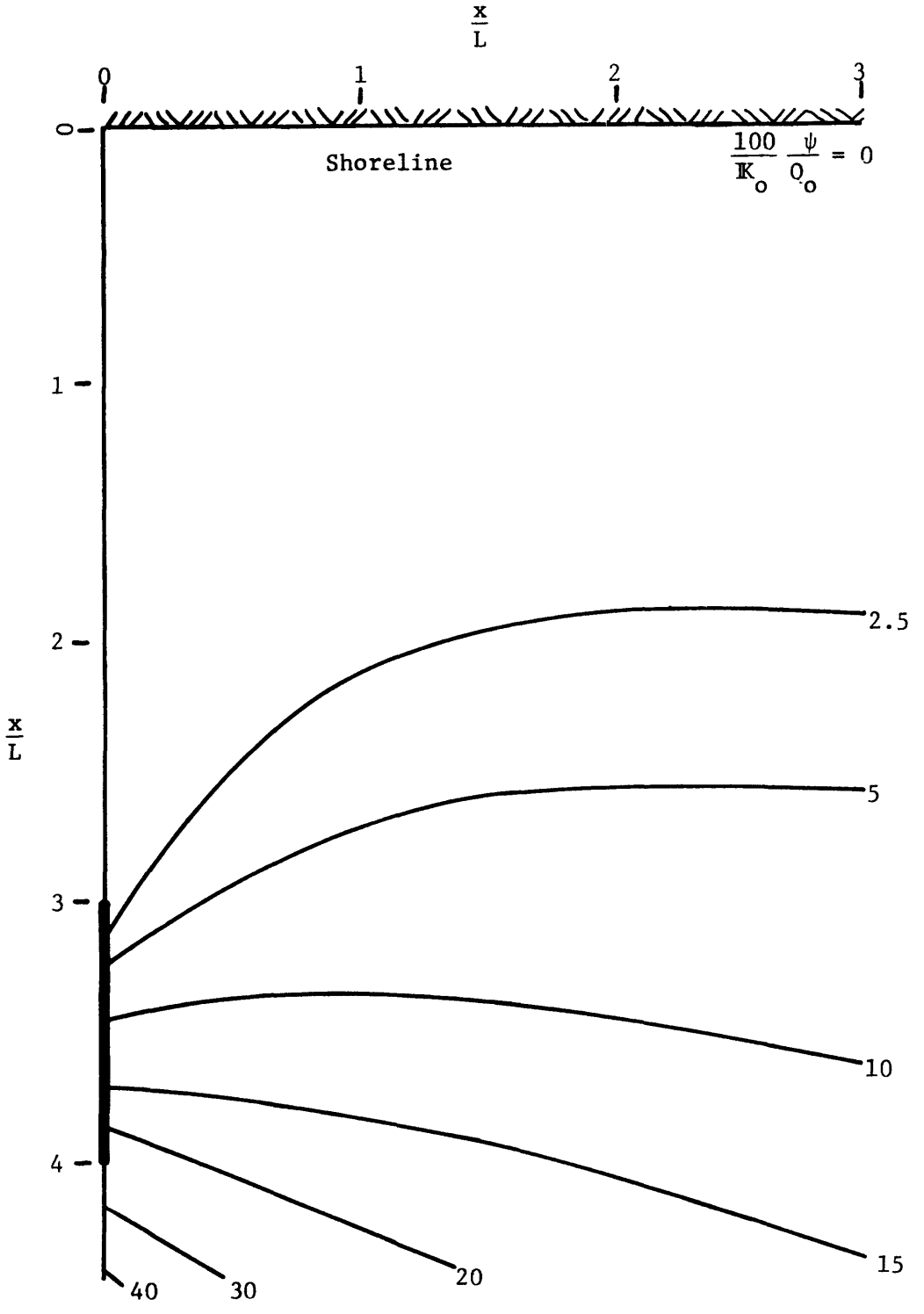

Figure 2-9 Entrainment Flowfield to a Staged Diffuser on a Sloping Bottom for $x_o/L = 3$

(Inner Solution is Almquist and Stolzenbach Theory (1976))

III. A SINGLE, NONBUOYANT JET IN WATER OF FINITE DEPTH

A. INTRODUCTION

In Chapter II, we discussed one approach to describing the behavior of staged diffusers. The fundamental assumption made was that the behavior of individual jets is unimportant in describing staged diffuser performance and that the series of jets may be represented adequately by a line source of momentum. This simplification is useful for describing gross features of the near field (e.g. dilution and the entrainment field), but the behavior of the individual jets may be very important in determining the motion, shear stress exposure and temperature exposure of a moving particle.

Another approach to describing staged diffuser performance is to model the diffuser as a series of round jets that are subject to interference from adjacent jets and to the effects of ambient currents and intersection with the water surface and bottom. This is a more realistic approach than that of Chapter II, but it is difficult to obtain a set of Eulerian and Lagrangian equations that include all of these effects.

In this chapter, we will introduce the description of a staged diffuser as a series of round jets by discussing a single jet in water of finite depth. In Chapter IV, we will show where possible how the results of Chapter III are changed due to ambient currents and interaction with other jets.

B. EULERIAN DESCRIPTION

Figure 3-1 shows a single jet in water of finite depth. The jet is divided into three regions: a zone of flow establishment, a 3-D zone and a 2-D zone. A circular cylindrical coordinate system (x,r,θ) is used to describe the zone of flow establishment and the 3-D zone. In these

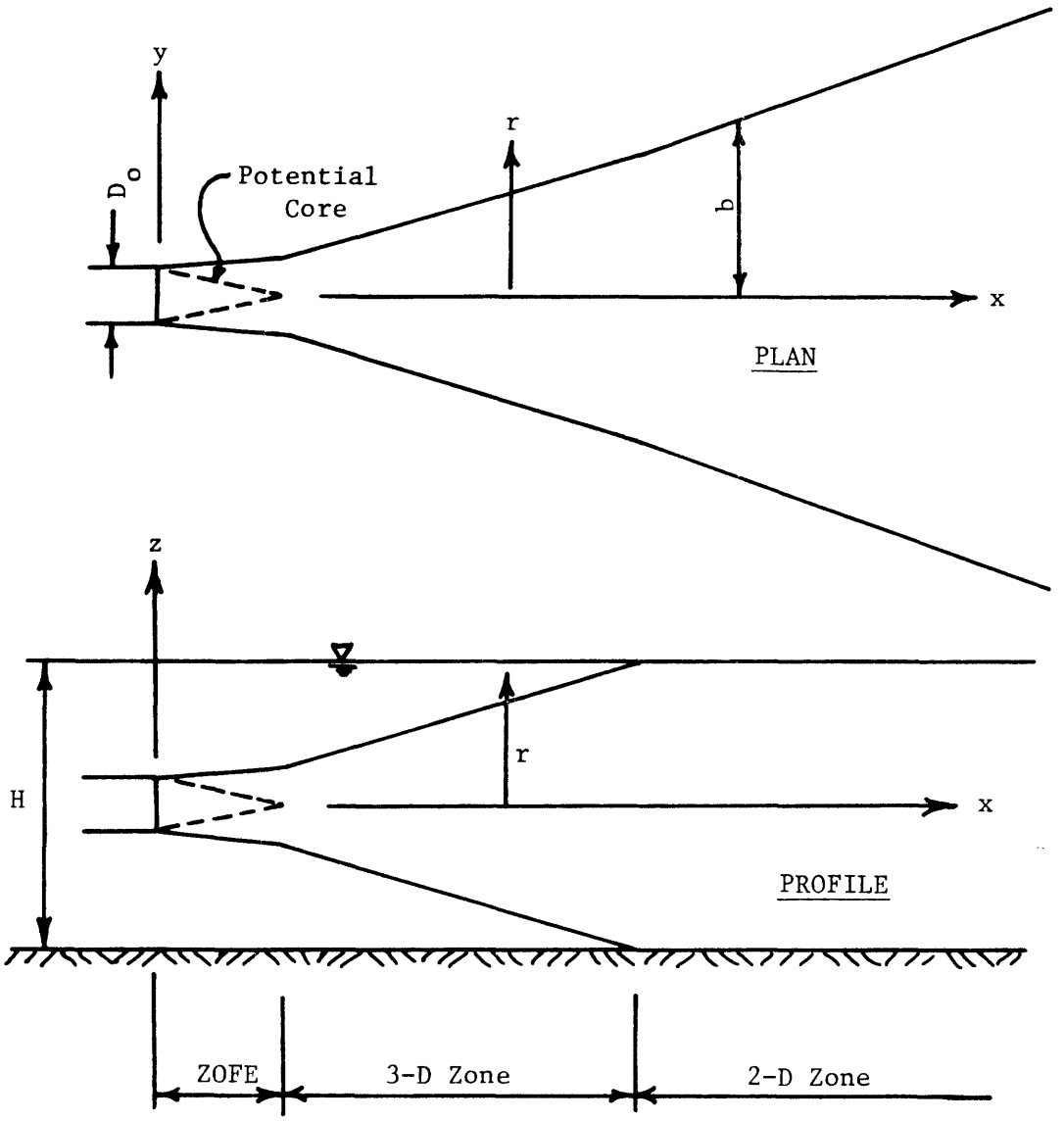

A_c = jet cross section area

b = plume width

u = longitudinal velocity

u_c = centerline longitudinal velocity

u_o = discharge velocity

ΔT = temperature excess

ΔT_c = centerline temperature excess

ΔT_o = discharge temperature excess

Q_i = jet flow rate = $\int_{A_c} udA$

Q_{io} = discharge flow rate

ZOFE = zone of flow establishment

Figure 3-1 Definition Sketch of a Single Jet in Finite Depth Water

zones, the jet is assumed to behave like a classical, round, turbulent jet. A rectangular coordinate system (x,y,z) is used to describe the 2-D zone. In this zone, the jet is assumed to behave like a classical, plane, turbulent jet with boundary conditions determined from the 3-D zone. We assume that the temperature of the discharged water is not too much greater than that of the ambient water, so that the jet can be treated as nonbuoyant and the temperature excess can be treated as a tracer that is dispersed by the mixing process. This is generally justified in dealing with staged diffusers in shallow water. (See Almquist and Stolzenbach (1976)).

In the zone of flow establishment, an unsheared, potential core is surrounded by a turbulent mixing layer. The length of this region is taken to be 6.2 D_o, where D_o is the diameter of the discharge port. (See Rajaratnam (1976)). Because the core is unsheared, the centerline temperature and velocity are the same as the discharge temperature and velocity:

$$u_c = u_o \tag{3.1}$$

$$\Delta T_c = \Delta T_o \tag{3.2}$$

The quantity $\overline{\rho u'v'} = \rho \mathrm{cov}(u,v)$, where

ρ = water density

u = longitudinal velocity component

v = radial velocity component

appears as the only important turbulent shear stress in the equations that describe the turbulent mixing layer. From dimensional analyses

$$\overline{u'v'} = Cu_o^2 \tag{3.3}$$

where, from experiments, we estimate C to be of order .05. (See Rajaratnam (1976)).

In the 3-D zone, the jet is turbulent across its whole width. The centerline velocity and temperature excess decrease with distance away from the discharge, while the total volume flux and the jet width increase. The lateral velocity, temperature and shear stress profiles have been shown to be kinematically similar for a large range of values of x. Assuming that heat and mass diffuse at the same rate (Reynolds analogy; turbulent Prandtl number equal one) then the temperature and velocity profiles can be written

$$\frac{\Delta T(x,r)}{\Delta T_c(x)} = \frac{u(x,r)}{u_c(x)} = f(r/b) \tag{3.4}$$

where b is a length scale in the radial (r) direction. If it is further assumed that the turbulent viscosity defined by

$$\overline{u'v'} = \nu_T \frac{\partial u}{\partial y} \tag{3.5}$$

is constant over a given crossection (i.e. $\nu_T = Cu_c b$), then the profile for shear stress may be given by

$$\frac{\overline{u'v'}(x,r)}{u_c^2(x)} = g(r/b) = C \frac{\partial f}{\partial (r/b)} \tag{3.6}$$

Experiments suggest that the value of C is of the order of .05 (Rajaratnam, 1976).

Because the jet diameter is relatively small compared to the scale of the 3-D region, the jet can be replaced by an equivalent point source. By using turbulent boundary layer assumptions and defining appropriate integral balances based on the above profiles, it can be easily shown that, at reasonable distance from the source,

$$\begin{aligned} b &\sim x \\ A_c &\sim x^2 \\ u_c &\sim x^{-1} \\ Q_i &\sim x \\ \Delta T_c &\sim x^{-1} \\ \overline{u'v'} &\sim x^{-2} \end{aligned} \tag{3.7}$$

Coefficients in these proportionalities must be determined experimentally. Assuming Gaussian velocity profiles, i.e.

$$f(r/b) = e^{-r^2/b^2} \tag{3.8}$$

and the experimental results of Albertson et al. (1950) it follows that

$$b = 0.11\, x \tag{3.9}$$

$$\frac{u_c}{u_o} = 6.2\, \frac{D_o}{x} \tag{3.10}$$

$$\frac{Q_i}{Q_{io}} = 0.32\, \frac{x}{D_o} \tag{3.11}$$

and accepting the Reynolds analogy

$$\frac{\Delta T_c}{\Delta T_o} \sim 6.2 \frac{x}{D_o} \tag{3.12}$$

The remaining variable of interest, $\overline{u'v'}$ can be determined from equations 3.6 and 3.10.

In the 2-D zone, the jet has boundary layer characteristics similar to those in the 3-D zone. These characteristics include kinematically similar temperature and velocity profiles and an entrainment rate that depends only on local velocity and length scales. In this analysis the jet is assumed to be well-mixed over the water depth so that there is no variation in the vertical direction. Using similar profile assumptions as for the 2-D regions

$$\frac{\Delta T(x,r)}{\Delta T_c(x)} = \frac{u(x,r)}{u_c(x)} = f(y/b) \tag{3.13}$$

$$\frac{\overline{u'v'}(x,y)}{u_c^2(x)} = g(\frac{y}{b}) = C \frac{\partial f}{\partial (y/b)} \tag{3.14}$$

where b is a length scale in the lateral (y) direction.

Because the plume has grown to a substantial size by the time it reaches the 3-D region, it is not reasonable to derive simple expressions for the longitudinal dependence of jet width, velocity, temperature etc. as in equations 3.7 for the 3-D region. Instead, results must be obtained by integrating in x based on initial conditions defined at the transition between 3-D and 2-D regions. (See discussion below).
We make an entrainment hypothesis

$$v_e = \alpha u_c \tag{3.15}$$

where v_e is the entrainment velocity normal to the jet at the jet boundary, and α is an entrainment coefficient, assumed constant. Writing the volume flux in the jet as

$$Q_i = 2 \int_o^\infty Hudy = 2\ Hbu_c C_Q \tag{3.16}$$

where

$$C_Q = \int_o^\infty f(\frac{y}{b})d(\frac{y}{b})$$

the kinematic momentum flux in the jet as

$$M_i = 2 \int_o^\infty Hu^2 dy = 2\ Hbu_c{}^2 C_m \tag{3.17}$$

where

$$C_m = \int_o^\infty f^2(\frac{y}{b})d(\frac{y}{b})$$

and the kinematic thermal energy flux in the jet as

$$J_i = 2 \int_o^\infty Hu\Delta T dy = 2\ H\ bu_c \Delta T_c\ C_Q \tag{3.18}$$

the continuity equation for the jet becomes

$$\frac{dQ_i}{dx} = 2\ Hv_e \tag{3.19}$$

the momentum equation becomes

$$M_i = M_{io} = \frac{\pi}{4} D_o{}^2 u_o{}^2 \tag{3.20}$$

and the thermal energy equation becomes

$$J_i = J_{io} = \frac{\pi}{4} D_o^2 u_o \Delta T_o \tag{3.21}$$

By combining equations 3.15 - 3.21 and carrying out the integrations, we can solve for the jet width,velocity, temperature rise and flow rate. Thus

$$\frac{b}{D_o} = \frac{2\,\alpha x}{C_Q D_o} + \frac{\pi}{8C_m}\frac{D_o}{x} C_1 \tag{3.22}$$

$$\frac{u_c}{u_o} = \frac{\Delta T_c}{\Delta T_o} = \left\{\frac{16 C_m \alpha}{\pi C_Q}\frac{H}{D_o}\frac{x}{D_o} + C_1\right\}^{-\frac{1}{2}} \tag{3.23}$$

$$\frac{Q_i}{Q_{io}} = \left\{\frac{16\ C_Q \alpha}{C_m}\frac{H}{D_o}\frac{x}{D_o} + C_1\left(\frac{C_Q}{C_m}\right)^2\right\}^{\frac{1}{2}} \tag{3.24}$$

where C_1 is a constant of integration. If we again use Gaussian profiles,

$$f\left(\frac{y}{b}\right) = e^{-y^2/b^2} \tag{3.25}$$

$$g\left(\frac{y}{b}\right) = -2C\,\frac{y}{b}\,e^{-y^2/b^2} \tag{3.26}$$

we find that

$$C_Q = \frac{\sqrt{\pi}}{2}$$
$$C_M = \frac{\sqrt{\pi}}{2\sqrt{2}} \tag{3.27}$$
$$\alpha = .069$$

where α has been determined experimentally for plane jets. (See Rajaratnam (1976)). We choose to evaluate the integration constant C_1 by equating the volume flux in the 2-D zone with the volume flux in the 3-D zone at

at the point of transition between the two zones, x_t. By doing this, we find that

$$C_1 = .051 \tag{3.28}$$

Using equation 3.28, equations 3.22 - 3.24 can be rewritten

$$\frac{b}{D_o} = .16\,\frac{x}{D_o} + .032\left(\frac{x_T}{D_o}\right)^2\left(\frac{D_o}{H}\right) - .16\left(\frac{x_T}{D_o}\right) \tag{3.29}$$

$$\frac{u_c}{u_o} = \frac{\Delta T_c}{\Delta T_o} = \left\{.25\,\frac{H}{D_o}\,\frac{x}{D_o} + .051\left(\frac{x_T}{D_o}\right)^2 - .25\,\frac{H}{D_o}\,\frac{x_T}{D_o}\right\}^{-\frac{1}{2}} \tag{3.30}$$

$$\frac{Q_i}{Q_{io}} = \left\{.50\,\frac{H}{D_o}\,\frac{x}{D_o} + .102\left(\frac{x_T}{D_o}\right)^2 - .50\,\frac{H}{D_o}\,\frac{x_T}{D_o}\right\}^{\frac{1}{2}} \tag{3.31}$$

One way of finding x_T is to define it as the point where the lateral length scale b in the 3-D zone becomes equal to the water depth H. This gives

$$x_T = 9H \tag{3.32}$$

Using equation 3.32 for x_T, and C = .05, the Eulerian equations that have been developed in this section are summarized below.

Zone of flow establishment ($0 \leq x \leq 6.2\ D_o$)

$$\frac{u_c}{u_o} = \frac{\Delta T_c}{\Delta T_o} = 1 \tag{3.33}$$

$$\frac{\overline{u'v'}}{u_o^2} = .05 \tag{3.34}$$

3-D zone ($6.2\ D_o \leq x \leq 9H$)

$$\frac{b}{D_o} = 0.11\,\frac{x}{D_o} \tag{3.35}$$

$$\frac{u}{u_o} = \frac{\Delta T}{\Delta T_o} = 6.2 \frac{D_o}{x} e^{-(r/b)^2} \tag{3.36}$$

$$\frac{Q_i}{Q_{io}} = 0.32 \frac{x}{D_o} \tag{3.37}$$

$$\frac{\overline{u'v'}}{u_o^2} = -3.8 \left(\frac{r}{b}\right)\left(\frac{D_o}{x}\right)^2 e^{-(r/b)^2} \tag{3.38}$$

2-D zone ($9H < x$)

$$\frac{b}{D_o} = .16 \frac{x}{D_o} + 1.15 \frac{H}{D_o} \tag{3.39}$$

$$\frac{u}{u_o} = \frac{\Delta T}{\Delta T_o} = \left\{\frac{.25\ x\ H}{D_o^2} + \frac{1.88H^2}{D_o^2}\right\}^{-\frac{1}{2}} e^{-(y/b)^2} \tag{3.40}$$

$$\frac{Q_i}{Q_{io}} = \left\{\frac{.50\ Hx}{D_o^2} + \frac{3.76H^2}{D_o^2}\right\}^{\frac{1}{2}} \tag{3.41}$$

$$\frac{\overline{u'v'}}{u_o^2} = -.10 \frac{y}{b} \frac{D_o^2}{.25Hx + 1.88H^2} e^{-(y/b)^2} \tag{3.42}$$

Note that, beyond the zone of flow establishment, it is possible to express the solutions independently of the discharge diameter. In fact using the previously defined kinematic momentum and thermal energy fluxes the expressions for the 3-D and 2-D regions can be written as follows:

3-D zone ($6.20\ D_o \leq x \leq 9H$)

$$\frac{b}{x} = 0.11 \tag{3.43}$$

$$\frac{ux}{\sqrt{M_{io}}} = \frac{\Delta T x \sqrt{M_{io}}}{J_{io}} = 7.0\ e^{-(r/b)^2} \tag{3.44}$$

$$\frac{Q_i}{x\sqrt{M_{io}}} = .36 \tag{3.45}$$

$$\frac{\overline{u'v'}\ x^2}{M_{io}} = -4.8\ \frac{r}{b}\ e^{-(r/b)^2} \tag{3.46}$$

2-D zone (9H < x)

$$\frac{b}{H} = .16\ \frac{x}{H} + 1.15 \tag{3.47}$$

$$\frac{uH}{\sqrt{M_{io}}} = \frac{\Delta T\ H\sqrt{M_{io}}}{J_{io}} = (.20\ \frac{x}{H} + 1.48)^{-\frac{1}{2}}\ e^{-(y/b)^2} \tag{3.48}$$

$$\frac{Q_i}{\sqrt{M_{io}}H} = (.56\ \frac{x}{H} + 4.2)^{\frac{1}{2}} \tag{3.49}$$

$$\frac{\overline{u'v'}\ H^2}{M_{io}} = -12.7\ \frac{y}{b}\ \{\frac{1}{.25\ x/H + 1.88}\}\ e^{-(y/b)^2} \tag{3.50}$$

Curves showing these relationships are presented in Figure 3-2.

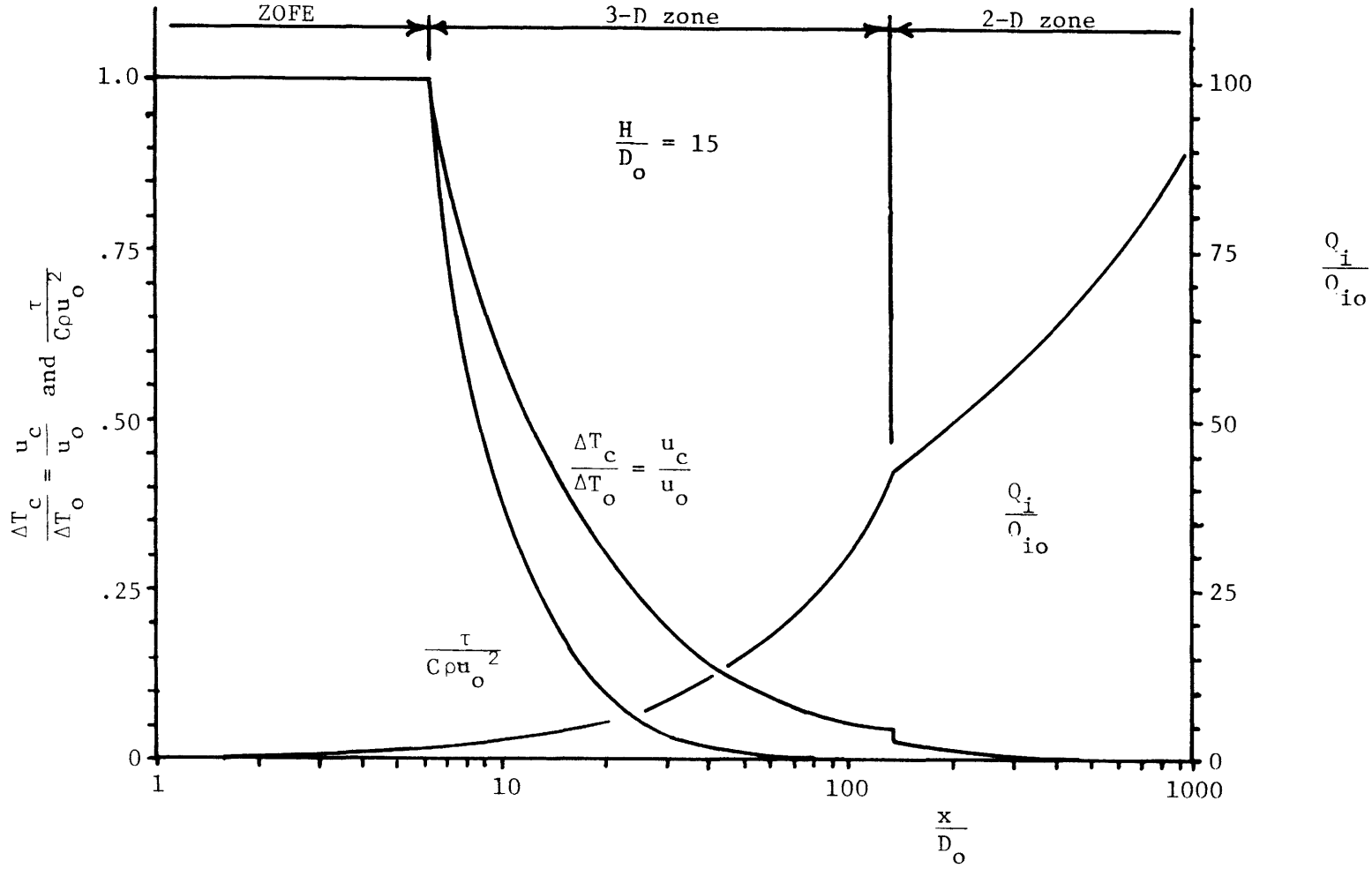

Figure 3-2 Eulerian Description of a Single Round Jet in Finite Depth Water

C. LAGRANGIAN DESCRIPTION

Using the Eulerian equations developed above, it is possible in principle to obtain Lagrangian equations that describe the trajectory, shear stress history and temperature history of a small particle moving through a jet. As was discussed in Chapter II, however, an accurate mathematical description of the path that a moving particle takes cannot easily be obtained because of the large velocity fluctuations and the nonhomogeneous velocity field that are characteristic of turbulent jets.

For this reason, we make simplifying assumptions about particle motion similar to those made in Chapter II. We assume that an entrained particle moves directly to the jet centerline and then moves along it at the mean centerline velocity. We assume that the particle experiences the mean centerline temperature, and a shear stress equal to $C\rho u_c^2$, where C is a constant of order .05. It is shown in Appendix A that the centerline path is the worst in terms of temperature exposure of any straight line path that the particle could take. The estimate of shear stress that the particle experiences, $C\rho u_c$, is approximately equal to the highest shear stress in the jet cross section. The Lagrangian shear stress and temperature histories obtained under our assumptions about particle motion will therefore approximate the "worst case" for an entrained organism.

To obtain our Lagrangian description of the jet, we solve the equation

$$\frac{dx}{dt} = u_c \tag{3.51}$$

to find the particle position x as a function of time t. We then combine this expression with the Eulerian equations for temperature excess and shear stress as functions of x to get the corresponding Lagrangian equations.

This procedure is presented below for each of the three zones.

In the zone of flow establishment, we have

$$\frac{dx}{dt} = u_c = u_o \tag{3.52}$$

This expression can be integrated to give

$$\frac{x}{D_o} = \frac{x_{e,f}}{D_o} + \frac{tu_o}{D_o} - \frac{t_{e,f}u_o}{D_o} \tag{3.53}$$

where

x = particle position

t = time

$x_{e,f}$ = position at which the particle enters the ZOFE

$t_{e,f}$ = time at which the particle enters the ZOFE

The Eulerian expressions for temperature excess and shear stress are

$$\frac{\Delta T}{\Delta T_o} = 1 \tag{3.54}$$

$$\frac{\overline{u'v'}}{u_o^2} = C \tag{3.55}$$

Since these quantities do not vary with x in the zone of flow establishment, equations 3.54 - 3.55 are also Lagrangian equations for temperature excess and shear stress.

In the 3-D zone, we have

$$\frac{dx}{dt} = u_c = 6.2\, u_o \frac{D_o}{x} \tag{3.56}$$

This expression can be integrated to give

$$\frac{x}{D_o} = \left[12.4 \left(\frac{tu_o}{D_o} - \frac{t_{e,3}u_o}{D_o}\right) + \left(\frac{x_{e,3}}{D_o}\right)\right]^{1/2} \tag{3.57}$$

where

$x_{e,3}$ = position at which the particle enters the 3-D zone

$t_{e,3}$ = time at which the particle enters the 3-D zone

The Eulerian expressions for temperature excess and shear stress are

$$\frac{\Delta T_c}{\Delta T} = 6.2 \frac{D_o}{x} \tag{3.58}$$

$$\frac{\overline{u'v'}}{u_o^2} = 38.4\ C\left(\frac{D_o}{x}\right)^2 \tag{3.59}$$

These can be combined with equation 3.57 to give the corresponding Lagrangian expressions

$$\frac{\Delta T}{\Delta T_o} = 6.2\ \left[12.4\left(\frac{tu_o}{D_o} - \frac{t_{e,3}u_o}{D_o}\right) + \left(\frac{x_{e,3}}{D_o}\right)^2\right]^{-1/2} \tag{3.60}$$

$$\frac{\overline{u'v'}}{u_o^2} = 38.4\ C\left[12.4\left(\frac{tu_o}{D_o} - \frac{t_{e,3}u_o}{D_o}\right) + \left(\frac{x_{e,3}}{D_o}\right)^2\right]^{-1} \tag{3.61}$$

In the <u>2-D region</u> we have

$$\frac{dx}{d\tau} = u_c = u_o \left\{.25 \frac{H}{D_o}\frac{x}{D_o} + .051\left(\frac{x_T}{D_o}\right)^2 - .25 \frac{H}{D_o}\frac{x_T}{D_o}\right\}^{-1/2} \tag{3.62}$$

This expression can be integrated to give

$$\frac{x}{D_o} = \frac{x_T}{D_o} - 0.20 \frac{D_o}{H}\left(\frac{x_T}{D_o}\right)^2 + 4.0 \frac{D_o}{H}\left\{\left[.25 \frac{H}{D_o}\frac{x_{e,2}}{D_o} + .051\left(\frac{x_T}{D_o}\right)^2 - .25 \frac{H}{D_o}\frac{x_T}{D_o}\right]^{3/2} + .38 \frac{H}{D_o}\left(\frac{tu_o}{D_o} - \frac{t_{e,2}u_o}{D_o}\right)\right\}^{2/3} \tag{3.63}$$

where

$x_{e,2}$ = position at which the particle enters the 2-D zone

$t_{e,2}$ = time at which the particle enters the 2-D zone

The Eulerian expressions for temperature excess and shear stress are

$$\frac{\Delta T_c}{\Delta T_o} = \{0.25 \frac{H}{D_o} \frac{x}{D_o} + .051(\frac{x_T}{D_o})^2 - .25 \frac{H}{D_o} \frac{x_T}{D_o}\}^{-\frac{1}{2}} \tag{3.64}$$

$$\frac{\overline{u'v'}}{u_o^2} = C\{.25 \frac{H}{D_o} \frac{x}{D_o} + .051(\frac{x_T}{D_o})^2 - .25 \frac{H}{D_o} \frac{x_T}{D_o}\}^{-1} \tag{3.65}$$

These can be combined with equation 3.63 to give the corresponding Lagrangian expressions

$$\frac{\Delta T}{\Delta T_o} = \{[.25 \frac{H}{D_o} \frac{x_{e,2}}{D_o} + .051(\frac{x_T}{D_o})^2 - .25 \frac{H}{D_o} \frac{x_T}{D_o}]^{3/2} + .38 \frac{H}{D_o}(\frac{tu_o}{D_o} - \frac{t_{e,2}u_o}{D_o})\}^{-1/3} \tag{3.66}$$

$$\frac{\overline{u'v'}}{u_o^2} = C\{[.25 \frac{H}{D_o} \frac{x_{e,2}}{D_o} + .051(\frac{x_T}{D_o})^2 - .25 \frac{H}{D_o} \frac{x_T}{D_o}]^{3/2} + .38 \frac{H}{D_o}(\frac{tu_o}{D_o} - \frac{t_{e,2}u_o}{D_o})\}^{-2/3} \tag{3.67}$$

A summary of the Lagrangian equations, evaluated with $x_T = 9H$ and $C = .05$ follows.

Zone of flow establishment ($0 \leq x \leq 6.2\ D_o$)

$$\frac{x}{D_o} = \frac{x_{e,f}}{D_o} + \frac{tu_o}{D_o} - \frac{t_{e,f}u_o}{D_o} \tag{3.68}$$

$$\frac{\Delta T}{\Delta T_o} = 1 \tag{3.69}$$

$$\frac{\overline{u'v'}}{u_o^2} = C \tag{3.70}$$

3-D zone ($6.2\ D_o \leq x \leq 9H$)

$$\frac{x}{D_o} = \left[12.4\left(\frac{tu_o}{D_o} - \frac{t_{e,3}u_o}{D_o}\right) + \left(\frac{x_{e,3}}{D_o}\right)^2\right]^{1/2} \tag{3.71}$$

$$\frac{\Delta T}{\Delta T_o} = 6.2\left[12.4\left(\frac{tu_o}{D_o} - \frac{t_{e,3}u_o}{D_o}\right) + \left(\frac{x_{e,3}}{D_o}\right)^2\right]^{-1/2} \tag{3.72}$$

$$\frac{\overline{u'v'}}{u_o^2} = 1.92\left[12.4\left(\frac{tu_o}{D_o} - \frac{t_{e,3}u_o}{D_o}\right) + \left(\frac{x_{e,3}}{D_o}\right)^2\right]^{-1} \tag{3.73}$$

2-D zone ($9H < x$)

$$\frac{x}{D_o} = -\frac{7.2\ H}{D_o} + 4.0\ \frac{D_o}{H}\left\{\left[.25\ \frac{H}{D_o}\frac{x_{e,2}}{D_o} + 1.88\ \frac{H^2}{D_o^2}\right]^{3/2} + .38\ \frac{H}{D_o}\left(\frac{tu_o}{D_o} - \frac{t_{e,2}\ u_o}{D_o}\right)\right\}^{2/3} \tag{3.74}$$

$$\frac{\Delta T}{\Delta T_o} = \left\{\left[.25\ \frac{H}{D_o}\frac{x_{e,2}}{D_o} + 1.88\ \frac{H^2}{D_o^2}\right]^{3/2} + .38\ \frac{H}{D_o}\left(\frac{tu_o}{D_o} - \frac{t_{e,2}\ u_o}{D_o}\right)\right\}^{-1/3} \tag{3.75}$$

$$\frac{\overline{u'v'}}{u_o^2} = .05\left\{\left[.25\ \frac{H}{D_o}\frac{x_{e,2}}{D_o} + 1.88\ \frac{H^2}{D_o^2}\right]^{3/2} + .38\ \frac{H}{D_o}\left(\frac{tu_o}{D_o} - \frac{t_{e,2}\ u_o}{D_o}\right)\right\}^{-2/3} \tag{3.76}$$

It should be noted that each of the expressions summarized above is valid only in the region for which it was derived. For example, if a particle is entrained into the zone of flow establishment, the equations derived for the zone of flow establishment (equations 3.68 - 3.70) should be used to describe the particle's history until it reaches the point $x = 6.2\ D_o$, which is the beginning of the 3-D zone. From here the equations for the

3-D zone (equations 3.71 - 3.73) should be used until the particle reaches $x = x_T$, which is the beginning of the 2-D zone. After this point, the equations derived for the 2-D zone (equations 3.74 - 3.76) should be used.

Sample curves showing position, temperature and shear stress as functions of time for a particle entrained at x=t=0 are shown in Figure 3-3. Flowrates have been plotted to allow estimates of the number of particles that experience a particular exposure history. All quantities have been normalized to provide generality.

Figure 3-3 can be used in the same way as Figure 2-2 in Chapter II . For example, in Figure 3-3, a particle entrained at $\frac{x}{D_o} = 10$ will experience the temperatures and shear stresses shown to the right of that point on the graph. Since $\frac{Q_i}{Q_{io}} = 3.2$ at that point, we conclude that a volume of water per unit time equal to 3.2 Q_{io} will enter the jet and undergo a temperature history that is equal to or worse than that of the particle entrained at $\frac{x}{D_o} = 10$.

Although an actual diffuser is made up of a number of interacting nozzles, it is possible to gain some understanding of organism exposure for a diffuser in the limiting case of no interaction - i.e. treating each jet independently. Consider the trade-offs in the thermal and shear stress exposure characteristics which exist under the following variations:

1) The number of jets N is varied with the condenser flow rate Q_o, temperature rise ΔT_o and exit velocity u_o maintained constant.

2) the discharge velocity u_o is varied with the number of jets N, the condenser flow rate Q_o and the temperature rise ΔT_o maintained constant, and

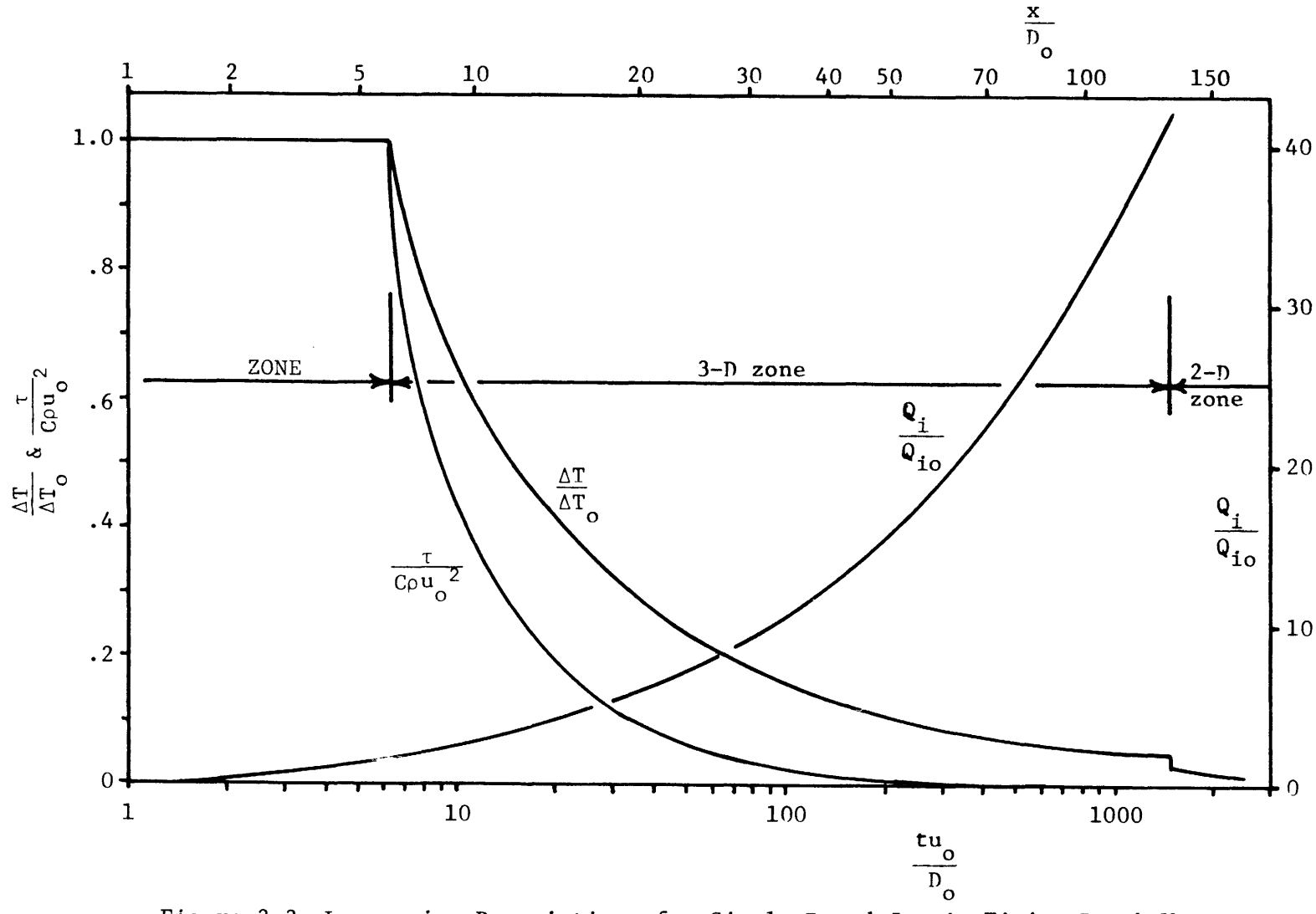

Figure 3-3 Lagrangian Description of a Single Round Jet in Finite Depth Water

3) the condenser temperature rise ΔT_o is varied with the number of jets N and the discharge velocity u_o maintained constant.

These cases are depicted in Figure 3-4 where the symbol I denotes the maximum level (intensity) of exposure, D corresponds to the relative duration of exposure to a level of temperature or shear stress above a certain threshold, and n represents the rate (number per time) of organisms exposed to levels greater than or equal to a given threshold. Subscripts T and τ refer to thermal impact and shear stress impact respectively.

The intensity of thermal exposure I_T is proportional to the discharge temperature rise and the intensity of shear stress exposure I_τ is proportional to the square of the discharge velocity. Therefore I_τ increases only with ΔT_o and I_τ increases only with u_o in the graphs of Figure 3-4.

The rate of exposure of organisms to temperature rises above a certain threshold n_T, is proportional to the cumulative flow NQ_i needed to dilute the individual plumes to the required threshold. For a threshhold temperature rise of ΔT, this flow is

$$n_T \sim NQ_i \sim \frac{NJ_{io}}{\Delta T} \tag{3.77}$$

For a constant station heat rejection NJ_{io}, n_T does not depend on any of the three variables considered. The number n_τ exposed to a given level of shear stress, however, depends on both the discharge velocity and the condenser flow rate. For example, in the 3-D zone,

$$\overline{u'v'} \sim \frac{u_o^2 D_o^2}{x^2} \tag{3.78}$$

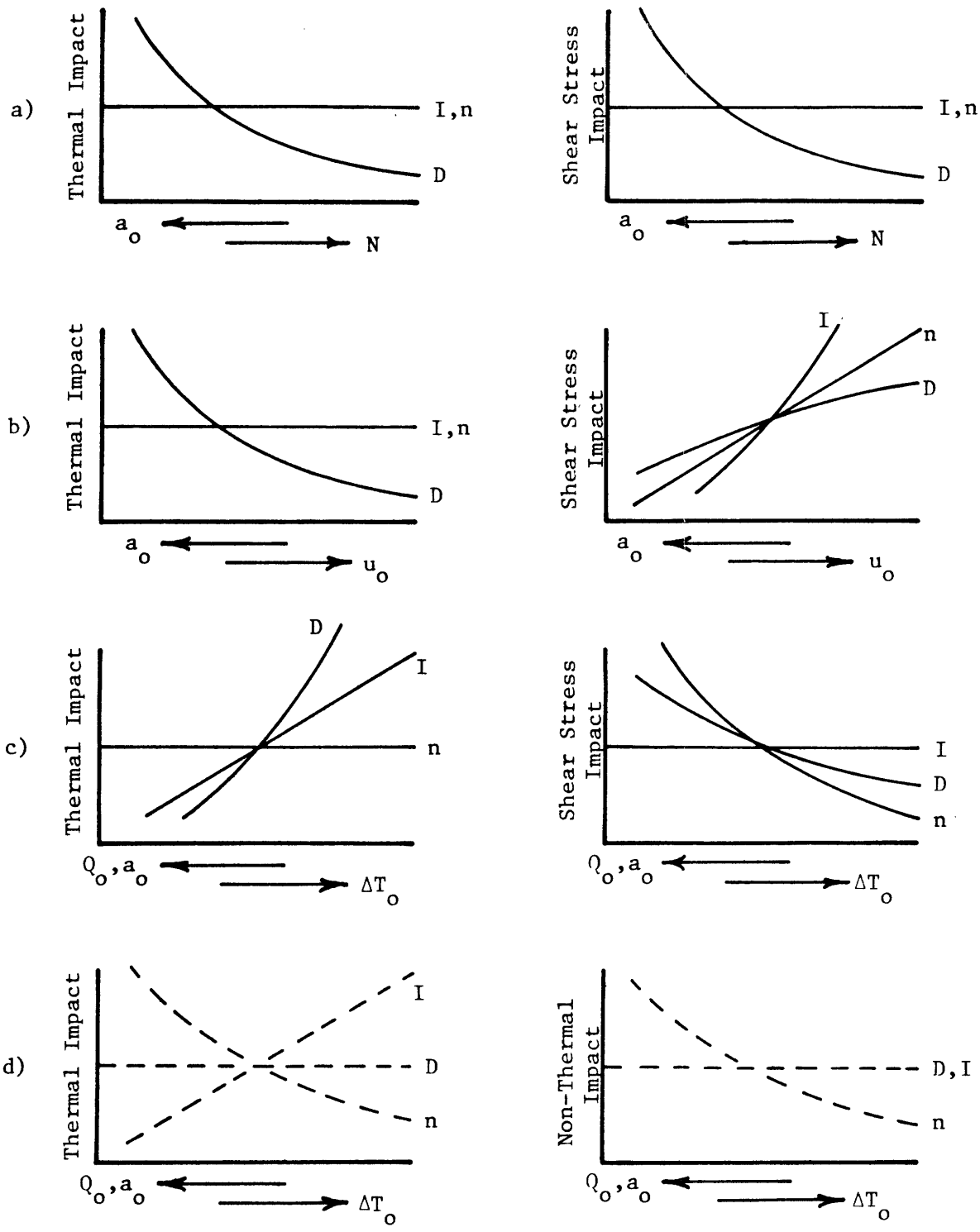

I = intensity of impact, D = duration of impact, n = no. of organisms exposed

Figure 3-4 Qualitative Impact Tradeoffs for Varying Diffuser Parameters

a) N, a_o vary; $Q_o, \Delta T_o, u_o$ constant (discharge impact)
b) u_o, a_o vary; $Q_o, \Delta T_o, N$ constant (discharge impact)
c) $\Delta T_o, Q_o, a_o$ vary; N, u_o constant (discharge impact)
d) $\Delta T_o, Q_o, a_o$ vary; N, u_o constant (intake impact)

while

$$\frac{NJ_{io}}{NQ_i} \sim \frac{\Delta T_o \, D_o}{x} \tag{3.79}$$

Combining,

$$n_\tau \sim NQ_i \sim \frac{NJ_{io} \, u_o}{\Delta T_o \sqrt{\overline{u'v'}}} \tag{3.80}$$

Since

$$NJ_{io} \sim N \, u_o \Delta T_o \, D_o^{\,2} \sim NQ_{io} \, \Delta T_o \tag{3.81}$$

it can easily be shown that for fixed NJ_{io} and $\overline{u'v'}$, n is independent of N (for fixed Q_o, ΔT_o, and u_o), is directly proportional to u_o (for fixed N, Q_o and ΔT_o) and inversely proportional to ΔT_o (for fixed N and u_o). Qualitatively similar results would hold for the 2-D zone.

The duration of exposure responds to variation in all three variables considered. Again consider the 3-D zone where travel time t is related to distance traveled x by

$$t \sim \frac{x^2}{u_o D_o} \tag{3.82}$$

x, in turn, varies as

$$x \sim \frac{\Delta T_o \, D_o}{\Delta T} \tag{3.83}$$

Combining equations 3.82 and 3.83, the maximum duration to temperature rises above ΔT is thus

$$D_T \sim t \sim \frac{\Delta T_o^{\,2} \, D_o}{\Delta T^2 \, u_o} \tag{3.84}$$

Employing equation 3.84 it can thus be shown that for fixed values of ΔT, D_T varies as $N^{-\frac{1}{2}}$ (for fixed Q_o, ΔT_o and u_o), as $u_o^{-3/2}$ (for fixed N, Q_o and

ΔT_o) and as $\Delta T_o^{3/2}$ (for fixed u_o and N). To compute exposure times to shear stress, equations 3.78 and 3.83 may be combined to yield

$$D_\tau \sim t \sim \frac{u_o D_o}{\overline{u'v'}} \tag{3.85}$$

Again employing equation 3.82, it follows that for a fixed $\overline{u'v'}$, that D_τ varies as $N^{-\frac{1}{2}}$ (for fixed u_o, Q_o and ΔT_o), as u_o (for fixed N, Q_o and ΔT_o) and as $\Delta T_o^{-\frac{1}{2}}$ (for fixed u_o and N). Again, qualitatively similar results can be expected for the 2-D zone.

Although the focus of the discussion has been in impacts associated with the discharge plumes, it is also possible to address, qualitatively, the dependence of the variables N, a_o, u_o, Q_o and ΔT_o on various impacts associated with the cooling water intake. Of these variables, the only ones which would influence intake impact are the last two, Q_o and ΔT_o. It may be reasonable to assume that the number of organisms (n) subjected to impingement on intake screens or subjected to various thermal, chemical or mechanical stresses associated with passage through the cooling system is proportional to the condenser flow rate Q_o, while the duration of exposure (d) would be independent of these parameters. The intensity of exposure (I) would also be nearly independent of Q_o and ΔT_o for the case of non-thermal impacts while for thermal impacts the intensity would increase with ΔT_o. These trends are summarized in Figure 3-4 d. A more detailed discussion is available in Schubel and Marcy (1978).

Based on the above observations, several conclusions can be drawn about the anticipated impacts associated with various diffuser parameters. These conclusions assume, of course, no jet interaction. To the extent

possible the effect of jet interaction will be treated in the following chapter.

1. Both temperature and shear stress-related impacts in the discharge zone decrease with increasing jet number N (fixed u_o, Q_o and ΔT_o) since duration of exposure decreases and intensity and exposure rate stay constant. Thus a diffuser with many nozzles tends to minimize these impacts.
2. Temperature-related impacts in the discharge zone decrease with increasing jet velocity u_o (fixed N, Q_o, ΔT_o) since duration of exposure decreases and level and exposure rate stay constant. This conclusion supports the selection of relatively high values of discharge velocity (order of 20 fps) found in recent submerged diffuser designs. However, shear stress-related impacts in the discharge zone increase with increasing u_o since intensity, duration and exposure rate all increase. Thus the choice of discharge velocity involves a trade-off between temperature-related and shear stress-related discharge impacts.
3. Temperature-related impacts in the discharge zone increase with increasing condenser temperature rise ΔT_o because duration and intensity increase while exposure rate remains constant. Conversely, shear stress-related impacts in the discharge zone decrease with increasing ΔT_o since duration and exposure rate decrease while intensity remains constant. Thus the choice of condenser temperature rise also involves a trade-off between temperature-related and shear stress-related impacts <u>within the discharge zone</u>.

With respect to impacts associated with organism passage through the cooling system (via the intake), it is not clear from the qualitative analysis presented herein whether temperature-related impacts increase or decrease with increasing ΔT_o since the exposure rate would decrease while the intensity would increase. However, mechanical, chemical and other non-temperature-related impacts would clearly decrease with increasing ΔT_o since the exposure rate would drop and the intensity and duration would remain essentially unchanged. Minimization of these impacts can be seen as one motivation for the selection of a high ΔT_o at stations such as NEP-1 and NEP-2.

D. SUMMARY

In Chapter III we have presented Eulerian and Lagrangian equations describing a turbulent jet in water of finite depth. The Eulerian equations are based on the classical analysis of turbulent jets, and the Lagrangian equations were developed by assuming simple, straight-line particle trajectories. This discussion of individual jets has been included as a basis for the description of a staged diffuser as a series of individual jets.

IV. INDIVIDUAL JETS IN A STAGED DIFFUSER

A. INTRODUCTION

The behavior of individual jets in a staged diffuser is of interest in obtaining an accurate Lagrangian description of what an entrained organism experiences as it moves through a diffuser plume. The important jet parameters are trajectory, temperature, velocity, shear stress, and dilution. These parameters are expected to be somewhat different from those predicted by the simple analysis of Chapter III, because of local currents and pressure gradients which were not considered in that analysis. These currents and pressure gradients arise primarily because of an ambient crossflow, influence of nearby jets, or both. Buoyancy is expected to be a secondary factor. In this chapter, we will first discuss these effects qualitatively. Then certain quantitative results will be presented.

B. QUALITATIVE DESCRIPTION

Figure 4-1 shows individual jet trajectories in a staged diffuser under stagnant conditions (part a) and with a crossflow (part b). In this section we will describe qualitatively first the stagnant case and then the crossflow case. Finally, general characteristics common to both cases will be discussed.

Stagnant Case

In the stagnant case, the behavior of an individual jet is affected to a large degree by the presence of nearby jets. The interaction among jets is very complicated because of the multiple length and velocity scales involved and because several physical processes are important.

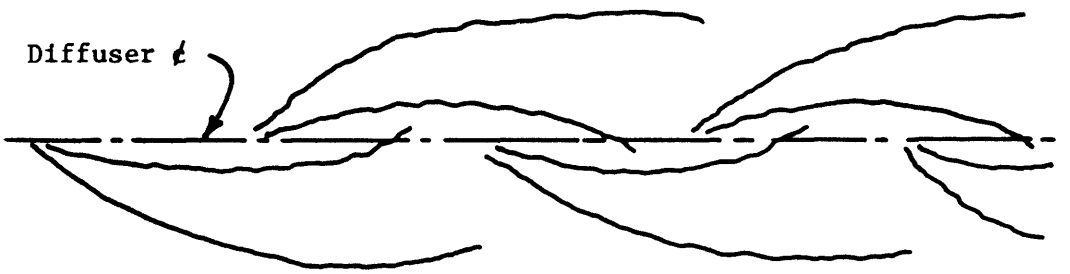

a) Stagnant Case

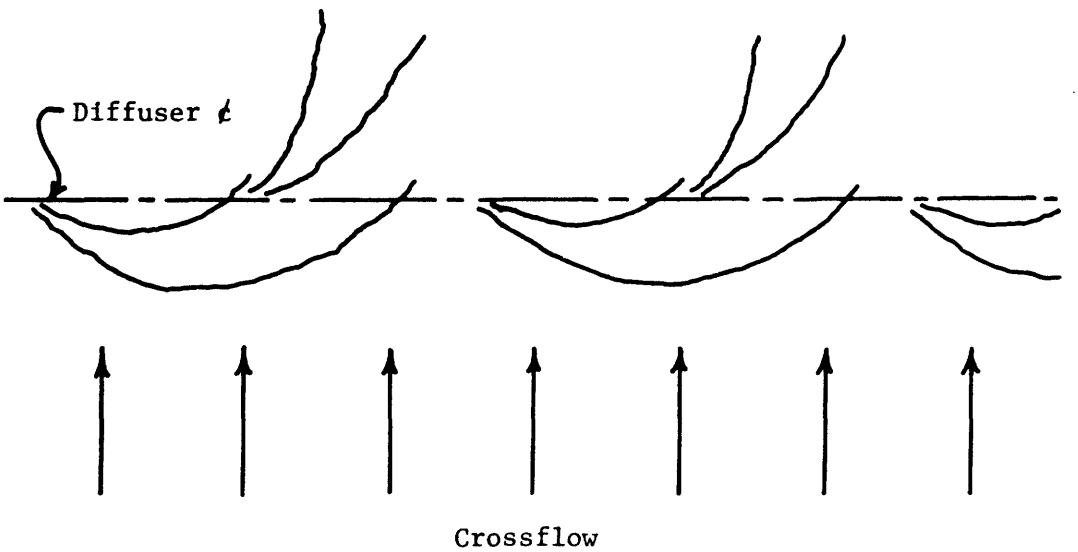

b) Crossflow Case

Figure 4-1 Jet Trajectories in a Staged Diffuser

However, much of the behavior of the individual jets can be described qualitatively in terms of the characteristics of the turbulent boundary layer that constitutes the near field of the diffuser.

A few port spacings past the upstream end of a staged diffuser in shallow water, a boundary layer forms whose width becomes much greater than the port diameter D_o, and whose characteristic velocity is an order of magnitude less than the discharge velocity, u_o. Its gross characteristics, including flowrate, velocity, temperature and width, are described by the near field analysis of Almquist and Stolzenbach (1976) that was discussed in Chapter II. Individual jets tend to curve toward the centerline of the diffuser, and they are distinguishable from the overall boundary layer for only a relatively short distance (order of the port spacing s) from their respective origins. Beyond this distance, individual jet velocities and temperatures blend in with those of the boundary layer. (See Figure 4-2)

The tendency of jets to bend toward the diffuser centerline can be explained by the relatively high centerline velocities of the boundary layer, the corresponding low dynamic pressures near the diffuser centerline, and the lateral flowfield set up near the diffuser. (See Figure 4-2)

Because of the longitudinal velocity in the overall boundary layer, and the initial orientation γ_o of the jet, a jet within the boundary layer is subject to an ambient crossflow of variable magnitude and variable turbulent intensity. A jet in crossflow is characterized by a kidney-shaped cross section, a pair of counter rotating vortices that substantially increase entrainment, and a relatively low pressure in the lee of the jet which results in drag. (See Figure 4-3). Because both the mean

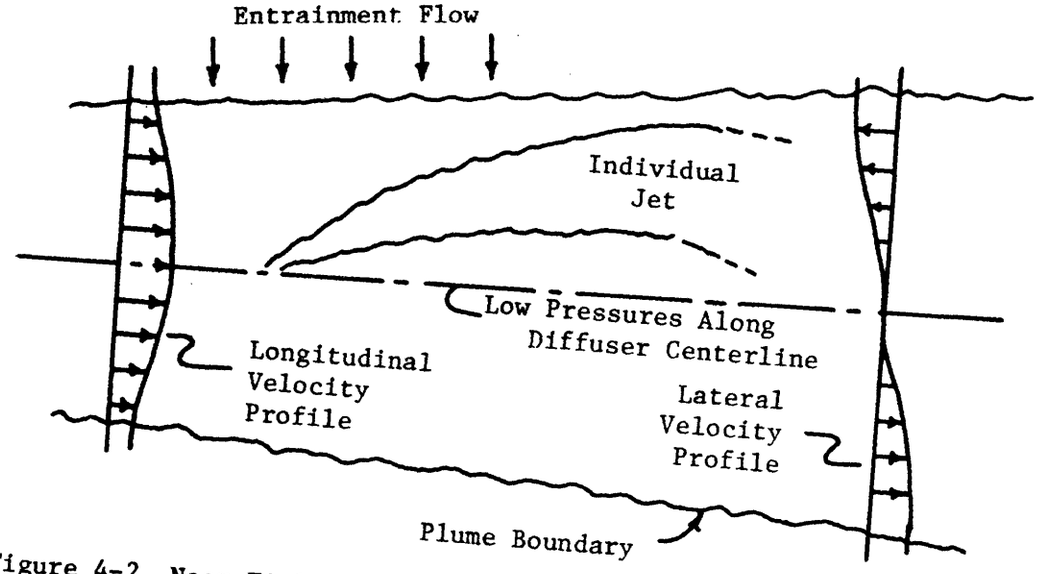

Figure 4-2 Near Field Plume & Individual Jet in a Staged Diffuser

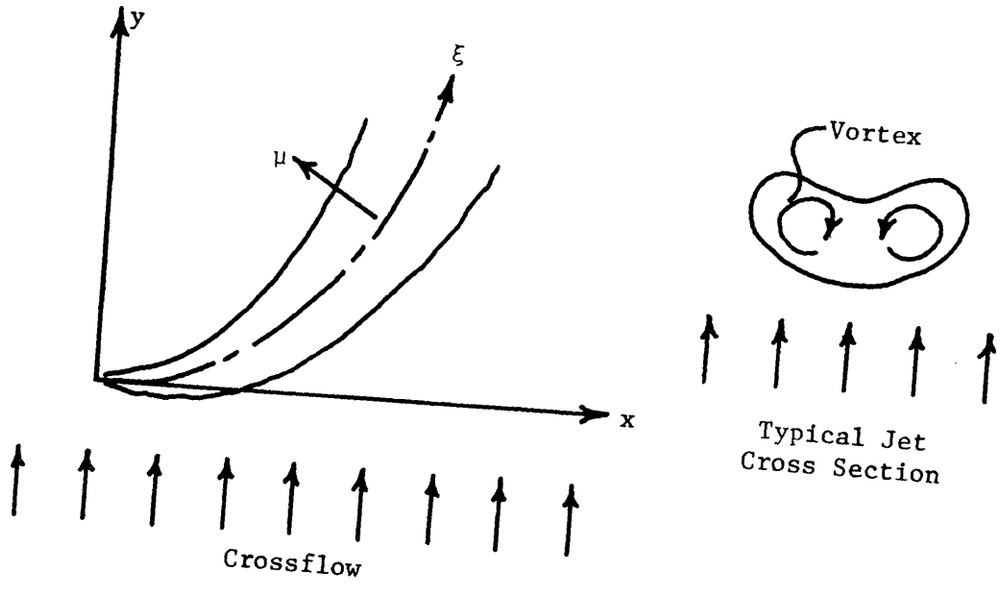

Figure 4-3 Jet in Crossflow

longitudinal and lateral velocities within the boundary layer have components directed perpendicular to the jet axis (see Figure 4-3) the entrainment and the drag tend to bend the jet towards the diffuser centerline. Also, the longitudinal velocity in the overall diffuser boundary layer is higher near the centerline than near the edges. Low fluid pressures are associated with the high velocities and turbulent fluctuations near the centerline, and this dynamic pressure gradient also causes individual jets to bend inward.

For jets outside of the diffuser boundary layer, the entrainment flowfield set up by the diffuser subjects individual jets to a lateral crossflow, causing them to bend toward the diffuser centerline by the crossflow mechanisms discussed above. Although the entrainment velocity is an order of magnitude smaller than the longitudinal velocity in the boundary layer, it is nearly perpendicular to the diffuser and can therefore cause significant jet deflection.

In the boundary layer associated with the near field of a staged diffuser, the longitudinal velocity is substantial and the temperature is higher than the ambient temperature of the receiving body of water. For this reason, the temperatures, velocities and turbulent shear stresses of an individual jet in a staged diffuser are expected to decay more slowly than they do in a free jet in infinite, stagnant surroundings.

Crossflow Case

Experiments show that even a relatively small ambient crossflow interferes substantially with the formation of the boundary layer that constitutes the near field of a staged diffuser in stagnant water. (See

Appendix G). When a crossflow is present, the individual jets are swept downstream and they do not form the kind of structure that can affect jets that are several jet spacings away. (See Figure 4-1b). Because of this, crossflow effects tend to have a substantial effect on individual jet behavior when even a relatively small crossflow is present, and the effects of interaction among jets are believed to be secondary.

As was discussed above, a jet in crossflow is characterized by a kidney shaped cross section and a pair of counter rotating vortices that substantially increase entrainment of ambient fluid. (See Figure 4-3). Dilutions are higher and velocities, temperatures, and shear stresses decay more rapidly than in jets in stagnant water. Deflection of the jets is caused by low pressures on the downstream side due to flow separation and eddy formation, and by entrainment of fluid that has a momentum component perpendicular to the jet. Intuitively, one expects the deflection force on a jet due to crossflow to increase as the water becomes shallower, because the ambient flow must be "squeezed" through a smaller area or be deflected laterally.

General

In both the stagnant and crossflow cases, proximity of the water surface and bottom will change the entrainment and spreading characteristics of a jet. Finite depth effects will vary along the length of a jet, since the jet width increases relative to the water depth with distance. These effects have been dealt with in a simple way in Chapter III.

Potential energy is associated with the buoyancy of jets in a staged diffuser, and this could affect entrainment characteristics and

pressure distributions. However, buoyancy effects will be small relative to inertial effects if the discharge densimetric Froude number, $\mathbb{F}_o$, is large enough. $\mathbb{F}_o$ is defined by

$$\mathbb{F}_o = \frac{u_o}{\sqrt{g\beta\Delta T_o D_o}} \tag{4.1}$$

where

u_o = discharge velocity
g = acceleration due to gravity
β = coefficient of thermal expansion of water
ΔT_o = discharge temperature excess
D_o = discharge port diameter

The densimetric Froude number measures the ratio of inertial forces to buoyancy forces. In most practical situations involving staged diffusers, $\mathbb{F}_o$ is large enough so that buoyancy can be neglected. (See Almquist and Stolzenbach (1976)).

C. ANALYTICAL DESCRIPTION

The influence of crossflow on the jets of a staged diffuser has been discussed qualitatively above. Because of the multiple length and time scales involved an analytical description of this influence is very difficult for a diffuser in stagnant water. Individual jet behavior in a staged diffuser subject to an ambient crossflow, on the other hand, seems more easily describable analytically. It appears from experiments (see Appendix G) that even for relatively small crossflows, crossflow is the most important factor affecting jet behavior, and that other effects such as jet interaction and buoyancy are secondary. Under these circum-

stances, the problem therefore reduces to that of a round jet in crossflow in finite water depth. There are difficulties, however, with the solution even to this simplified problem. These difficulties are discussed below.

An analytical description of a round jet in crossflow in finite water depth can be obtained by writing a continuity equation, which must include some assumption about entrainment, a ξ- momentum equation along the jet axis, and an η- momentum equation perpendicular to the jet, which includes the forces on the jet due to crossflow.

Several analytical solutions to this problem have been attempted for the case of nonbuoyant jets in infinite surroundings. (See Rajaratnam (1976) and Chan and Kennedy (1972)). In most of these, jet velocity profiles are assumed to be kinematically similar. Entrainment hypotheses are generally phenomenological, because the vortex structure that is important to the entrainment process is not easily analyzed. A typical hypothesis is

$$v_e = \alpha u_c + \beta V \tag{4.2}$$

where

v_e = average entrainment velocity

u_c = characteristic velocity in the jet

V = crossflow velocity

α, β = empirical coefficients

The "drag" force on the jet associated with low pressures on the downstream side is usually assumed to be of the form:

$$F_D = C_D \rho \frac{V^2}{2} \text{ (2b)} \tag{4.3}$$

and the "entrainment" force due to the entrainment of moving fluid is usually expressed as:

$$F_E = \rho V q_e \tag{4.4}$$

where:

F_D = drag force per unit jet length

F_E = entrainment force per unit jet length

C_D = empirical drag coefficient

ρ = fluid density

V = crossflow velocity

b = characteristic jet width

q_e = entrained flowrate into the jet per unit jet length

and where corrections for the jet inclination have been dropped for clarity. The drag force equation is based on an analogy to flow around a solid cylinder, and does not explicitly take into account the vortex structure that is important to flow separation around a jet in crossflow. Because of the simplifications inherent in the equations described above, solutions obtained from them are not entirely satisfactory and the constants must be varied substantially to match experimental data.

The problem of a jet in crossflow is complicated further when the jet is part of a staged diffuser, primarily because of finite water depth, and to a lesser extent because of jet interaction.

Since the available solutions to this problem are semi-empirical at best, we decided to use our own empirical results to describe individual jet behavior in a staged diffuser. The empirical results are discussed in the next section.

D. EMPIRICAL RESULTS

The complicated behavior of the individual jets in a staged diffuser suggests an empirical, rather than analytical, approach to describing them. The results reported herein apply only to trajectory which is the jet property most affected by crossflow. At present, it must be assumed that other jet properties remain the same as for non-interacting jets in stagnant water. This is a conservative assumption. Ongoing experiments are investigating other jet properties and these will be factored into future analysis.

In this section, we will begin by using dimensional analysis to determine the parameters that govern jet behavior in a staged diffuser. We will then present quantitative results.

Dimensional Analysis

Although jet behavior in a staged diffuser is not easily described analytically, we can use dimensional analysis to reduce the number of variables and to determine the dimensionless parameters that govern jet behavior in a staged diffuser. This is useful in increasing understanding and in interpreting experimental data.

The relevant variables are

Q_i = diluted flowrate of the jet

u = characteristic jet velocity

ΔT = characteristic jet temperature excess

y = characteristic jet displacement

x = position along diffuser axis

D_o = discharge diameter

Q_{io} = discharge volume flux = $\frac{\pi}{4} D_o^2 u_o$

M_{io} = discharge kinematic momentum flux = $\frac{\pi}{4} D_o^2 u_o^2$

ΔT_o = discharge temperature excess

s = port spacing

H = water depth

h = port elevation

V = crossflow velocity

α = vertical discharge angle

γ_o = horizontal discharge angle

ν = kinematic viscosity

g = acceleration due to gravity

There are seventeen variables in three dimensions (length, time and temperature). This implies that fourteen dimensionless quantities will describe the problem. We choose these to be

$$\frac{Q_i}{Q_{io}}, \frac{u}{u_o}, \frac{\Delta T}{\Delta T_o}, \frac{y}{D_o},$$

$$\frac{x}{D_o}, \frac{Q_{io}^2}{M_{io} Hs}, \gamma_o, \frac{H}{D_o}, \frac{h}{D_o}, \alpha, \frac{V}{U_o}, \tag{4.5}$$

$$\frac{u_o D_o}{\nu}, \frac{u_o}{\sqrt{g\beta\Delta T_o D_o}}, \frac{u_o}{\sqrt{gH}}$$

where β = coefficient of thermal expansion. We can reduce this list of parameters by observing that:

$\frac{u_o D_o}{\nu}$ = Reynolds number. This parameter can be dropped if it is large enough to insure turbulence in the jet.

$\frac{u_o}{\sqrt{g\beta\Delta T_o D_o}}$ = discharge densimetric Froude number. This parameter indicates the importance of buoyancy, and can be dropped if it is large enough, as was discussed in part B of this chapter.

$\frac{u_o}{\sqrt{gH}}$ = free surface Froude number. This parameter can be dropped since the effects of free surface waves are expected to be small.

We can write:

$$\frac{Q_{io}^2}{M_{io} Hs} = \frac{a_o^2 u_o^2}{a_o u_o^2 Hs} = \frac{a_o}{sH} \qquad a_o = \frac{\pi}{4} D_o^2$$

$$\frac{Q_{io}^2}{M_{io} Hs} = \mathbb{K}^{-2} \tag{4.6}$$

where $\mathbb{K} = \sqrt{\frac{sH}{a_o}}$, the parameter used by Almquist and Stolzenbach (1976).

The list of dimensionless variables can now be written as:

$$\frac{Q}{Q_{io}}, \frac{u}{u_o}, \frac{\Delta T}{\Delta T_o}, \frac{y}{D_o} = f\left(\frac{x}{D_o}, \sqrt{\frac{sH}{a_o}}, \gamma_o, \frac{H}{D_o}, \frac{h}{D_o}, \alpha, \frac{V}{u_o}\right) \tag{4.7}$$

In the case of a significant crossflow, individual jet characteristics seem to be largely independent of the other jets, as was discussed in part C of this chapter. For this case we can therefore drop the parameter $\mathbb{K} = \sqrt{\frac{sH}{a_o}}$. It is expected that $\frac{h}{D_o}$ and α will have only secondary effects on individual jet behavior, so that we can drop them for the purposes of this analysis. We now have:

$$\frac{Q_i}{Q_{io}}, \frac{u}{u_o}, \frac{\Delta T}{\Delta T_o}, \frac{y}{D_o} = f\left(\frac{x}{D_o}, \sqrt{\frac{sH}{a_o}}, \gamma_o, \frac{H}{D_o}\right)$$

(no crossflow case)

$$\frac{Q_i}{Q_{io}}, \frac{u}{u_o}, \frac{\Delta T}{\Delta T_o}, \frac{y}{D_o} = f\left(\frac{x}{D_o}, \frac{V}{u_o}, \gamma_o, \frac{H}{D_o}\right) \qquad (4.8)$$

(crossflow case)

Quantitative Results for Jet Deflection

For a staged diffuser in a current, jet behavior seems to depend primarily on the crossflow rather than interaction with other jets, as was discussed in part B of this chapter. This suggests that jet trajectories might be described by the empirical trajectory equations that have been obtained by various investigators (see Rajaratnam (1976) and Chan and Kennedy (1972)) for round jets in infinite surroundings. An example of an empirical trajectory equation is the one suggested by Rajaratnam (1976) for the centerline of a jet issuing perpendicular to an ambient crossflow (see Figure 4-3):

$$\frac{y}{D_o} = 0.077\left(\frac{V}{u_o}\right)^{2.6}\left(\frac{x}{D_o}\right)^{3.6} \qquad (4.9)$$

However, experiments show that actual deflections are much larger than those predicted by these equations. (See Appendix H). Other factors, probably including the water depth H, must affect jet deflections in a staged diffuser in crossflow. Our present best estimate of jet trajectory was obtained from experiments discussed in Appendix H and is given by the equation:

$$\frac{y}{D_o} = .6\left(\frac{V}{u_o}\right)\left(\frac{x}{D_o}\right)^2 + \left(\frac{x}{D_o}\right)\tan\gamma_o \qquad (4.10)$$

where γ_o is positive if the jet is inclined in the same direction as the crossflow.

Experiments were also conducted to determine jet trajectories in stagnant water. (See Table G-1 of Appendix G.) While these results have not been reduced to the form of an equation, it is apparent that an increase in either water depth or discharge angle γ_o results in "wider" trajectories while a decrease in either variable produces trajectories closer to the diffuser centerline. In contrast to the situation with a diffuser in a current, or a diffuser in stagnant water with $\gamma_o = 0$, there were no observations of individual jets interacting with downstream jets near the latters' origin. That is, interaction between an upstream and a downstream jet always occured at a substantial distance away from the diffuser centerline and after the downstream jet had incurred significant dilution. Thus, it appears that an appropriate way to consider interaction in a diffuser in stagnant water and $\gamma_o \neq 0$, is to model the behavior of an individual jet discharged into a background flowfield which has been set up by the diffuser as a whole.

Other Jet Parameters

Our present best estimates of jet dilution, temperature rise, excess velocity and shear stress for a jet in either an ambient current or in stagnant water, is that they are nearly the same as for the case of a non-interacting jet in stagnant water which was discussed in Chapter III. This assumption is based on the observation that the jet velocity is much greater than either the ambient crossflow or the current set-up by the flow of the diffuser as a whole. Ongoing experiments are being

performed to test this hypothesis and future analysis will be able to take these findings into account.

Based on this assumption, several observations can be made about the relationship between the behavior of individual jets and the diffuser as a whole. First, consider a staged diffuser with $\gamma_o = 0$ as suggested in Figure 4-4. Experiments suggest that it only requires a modest ambient current speed to deflect each jet such that it does not directly impinge on the downstream nozzle. If the performance of each jet is similar and is independent of adjacent jets until the point of interaction, then the formulae of Chapter III can be used to compute dilution for the diffuser as a whole. Clearly, this dilution increases as the current speed increases because the undisturbed trajectory lengths increase. This explains the increase in staged diffuser performance with increased current speed which is often observed. (See e.g., Stolzenbach et al., 1976.) For diffusers with a non-zero discharge angle γ_o, similar results should pertain for the diffuser as a whole although the behavior of the individual jets would depend on whether one were describing a jet pointing upstream or a jet pointing downstream.

As the current speed is reduced the jet trajectories become more and more co-linear. For some low current speed it could be expected that the trajectories would be barely overlapping as suggested in Figure 4.4b. At this point it is expected that the overall diffuser dilution would approach that obtained from the analysis of the diffuser as an equivalent slot which was presented in Chapter II.

For the 2-D momentum region in the analysis of a slot diffuser,

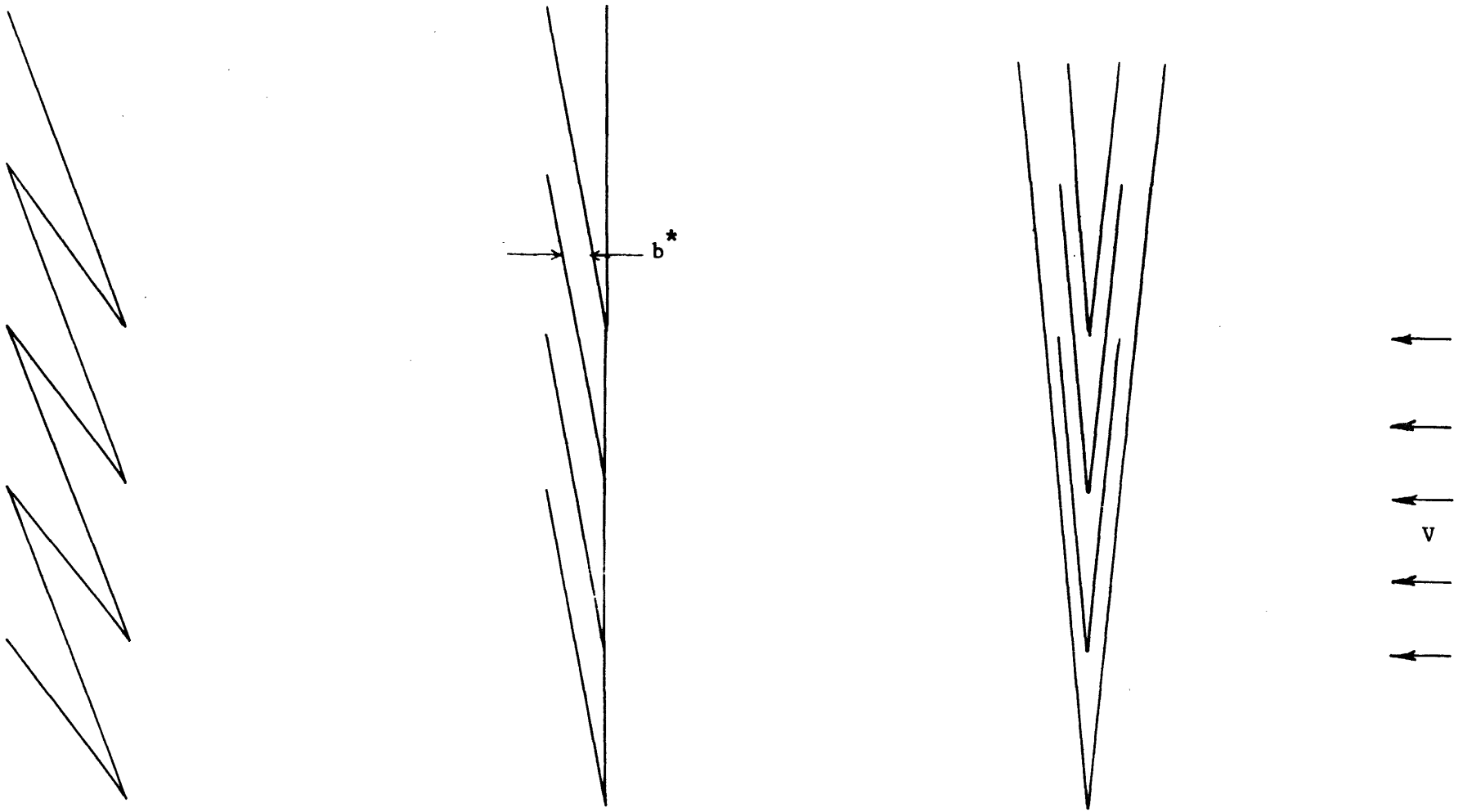

Figure 4-4 Schematic of Staged Diffuser Jets in a Crossflow for $\gamma_o = 0$

dilution is given by equation D-49. The exact value of this expression depends on several profile parameters. Depending on the choice of profiles the dilution is expected to fall in the range

$$S^* = C\,K = C\sqrt{\frac{sH}{a_o}} \tag{4.11}$$

$$.40 < C < .60$$

That this is comparable with the dilution obtained by viewing the diffuser as a collection of individual jets may be seen by rearranging equations 3.37 and 3.41 which describe the dilution for a single jet. In both the 3-D region and the 2-D region these expressions can be expressed as a function of jet crossectional area A_c rather than x. For the 3-D regions the result is

$$S^* = 1.45\sqrt{\frac{A_c}{a_o}} \tag{4.12}$$

where

$$A_c = \pi b^2$$

while for the 2-D region the result is

$$S^* = \sqrt{1.23\,\frac{A_c}{a_o} - .13\,\frac{H^2}{a_o}} \tag{4.13}$$

where $A_c = 2bH$

For large b this latter result reduces to

$$S^* = 1.11\sqrt{\frac{A_c}{a_o}} \tag{4.14}$$

The difference between equations 4.12 and 4.14 rests only in the difference

in profiles between 3-D and 2-D jets. If a top-hat profile had been used, (i.e., had the velocity been assumed constant over the crossection) it is easy to show that the results in both cases would be

$$S^* = \sqrt{\frac{A_c}{a_o}} \tag{4.15}$$

While the situation depicted in Figure 4-4b does not correspond exactly to either the 3-D or the 2-D analysis, it is logical to define an equivalent crossectional area as

$$A_c = 2b^*H \tag{4.16}$$

where b^* is defined in the figure. Based on previous results it may be expected that

$$\frac{b^*}{s} = \text{constant} \tag{4.17}$$

where the constant spreading rate is of the order of 0.1. (The spreading rates for 3-D and 2-D jets are 0.11 and 0.16 as defined in equations 3.35 and 3.39, while the spreading rate for a diffuser as a whole has been shown by Almquist and Stolzenbach (1976) to be about one-half the spreading rate for 2-D jet or about 0.08). Using a value of 0.1 and substituting equations 4.16 and 4.17 into equation 4.15, yields

$$S^* = .45 \sqrt{\frac{sH}{a_o}} \tag{4.18}$$

which is quite comparable with equation 4.11.

When the ambient current is identically zero, as in Figure 4-4c, or when γ_o does not equal 0, and the velocity is nearly zero, we would not

expect the overall dilution to change radically despite the interactions which take place. Experiments, such as those of Stolzenbach et al.(1976), bear this out, suggesting for instance that the peak surface temperatures in a staged diffuser in stagnant water are slightly higher for $\gamma_o = 0$ than for $\gamma_o \neq 0$. However, in computing the exposure history of entrained organisms (as is done in the following section) account should be taken of the background temperature rise which an individual jet feels due to the upstream jets. While this situation might more accurately be described by solving for the properties of a co-flowing jet, it will merely be assumed that a constant background temperature, given by the slot diffuser analysis, is added to the temperature rise induced by the individual jet. Thus for a jet in the 3-D region (i.e. before interaction with surface or bottom boundaries) the temperature would be given by

$$\frac{T - T_b}{T_o - T_b} = \frac{6.2\ D_o}{x} \tag{4.19}$$

where the background temperature T_b is obtained from equation 4.11. To be conservative, the constant C in equation 4.11 is taken as 0.40 making

$$\frac{T_b - T_a}{T_o - T_a} = \frac{1}{S^*} = \frac{2.5}{K} \tag{4.20}$$

where T_a is the ambient temperature

E. TIME - TEMPERATURE - SHEAR STRESS - VOLUME RELATIONSHIPS FOR A STAGED DIFFUSER

By using the Eulerian description of individual jets in a staged diffuser that was developed in the last section together with simple assumptions about particle trajectories in jets, we can find Lagrangian equations for temperature and shear stress following a moving particle.

In situations with an ambient crossflow, the procedure is:

1) Use equation 4.10 to determine the trajectory of the jet into which the particle is entrained. If this jet intersects a second jet, determine the trajectory of the second jet. If the second jet intersects a third jet, determine the trajectory of the third jet, and so on.
2) Assume that the particle travels along the centerline of each jet that it enters.
3) Use the Lagrangian equations developed in Chapter III, with appropriate values of x_e and t_e for each jet that the particle enters, to determine position, shear stress, and temperature as functions of time for the moving particle.
4) Plot the cumulative flowrate associated with each position that the particle passes through so that estimates of the rate of particles (number per time) that experience a particular exposure history can be made.

For stagnant water the procedure is similar except that account is taken of the background temperature rise defined by equation 4.20. For non-zero γ_o this is the only "interaction" which is considered, i.e. an individual jet is not considered to "intersect" with any downstream jets. For $\gamma_o = 0$ it is logical to assume that each jet intersects with the adjacent jet immediately downstream.

As an example, suppose we have a diffuser with $\frac{s}{D_o} = 20$, $\gamma_o = \pm 20°$ and a steady crossflow ratio $\frac{V}{D_o} = 0.03$. By using the jet trajectory equation 4.10, we find that $\frac{y}{D_o} = 0$ at $\frac{x}{D_o} = 20 = \frac{s}{D_o}$, for a jet on the

upstream side of the diffuser. (See Figure 4-5.) Suppose we are interested in the temperature history of a particle entrained at the point indicated on the figure. By using equations in Chapter III, we can develop the time-temperature-volume curves shown in Figure 4-5. These curves can be interpreted in the same way as the similar curves presented in Chapters II and III.

Clearly, direct interaction among jets increases the exposure impact felt by entrained organisms. Therefore it is worthwhile to examine equation 4.10 to see how the nature of this interaction varies as a function of the current speed V and the diffuser parameters D_o, γ_o, s and u_o. Let x_c be defined as the distance along the axis of the diffuser at which an upstream pointing jet crosses the diffuser axis. (x_c was also defined in Appendix G and was used as a basis for establishing equation 4.10.) Rearranging equation 4.10

$$\frac{x_c}{D_o} = \frac{\tan|\gamma_o|u_o}{.6V} \tag{4.21}$$

It is clear that for $x_c > 2s$, multiple interactions would occur as an entrained particle becomes successively re-entrained into every other downstream jet. The number of interactions which a particular organism might experience depends on the diffuser length L; for the most upstream jet, approximately $\frac{L}{x_c}$ interactions might be expected. For $x_c < 2s$ at most one interaction takes place while in the limit $x_c << 1$, no significant interaction takes place. However, this last regime amounts to a collection of totally independent jets which is not really a diffuser. In order to minimize the probability of interaction it is desireable to maintain

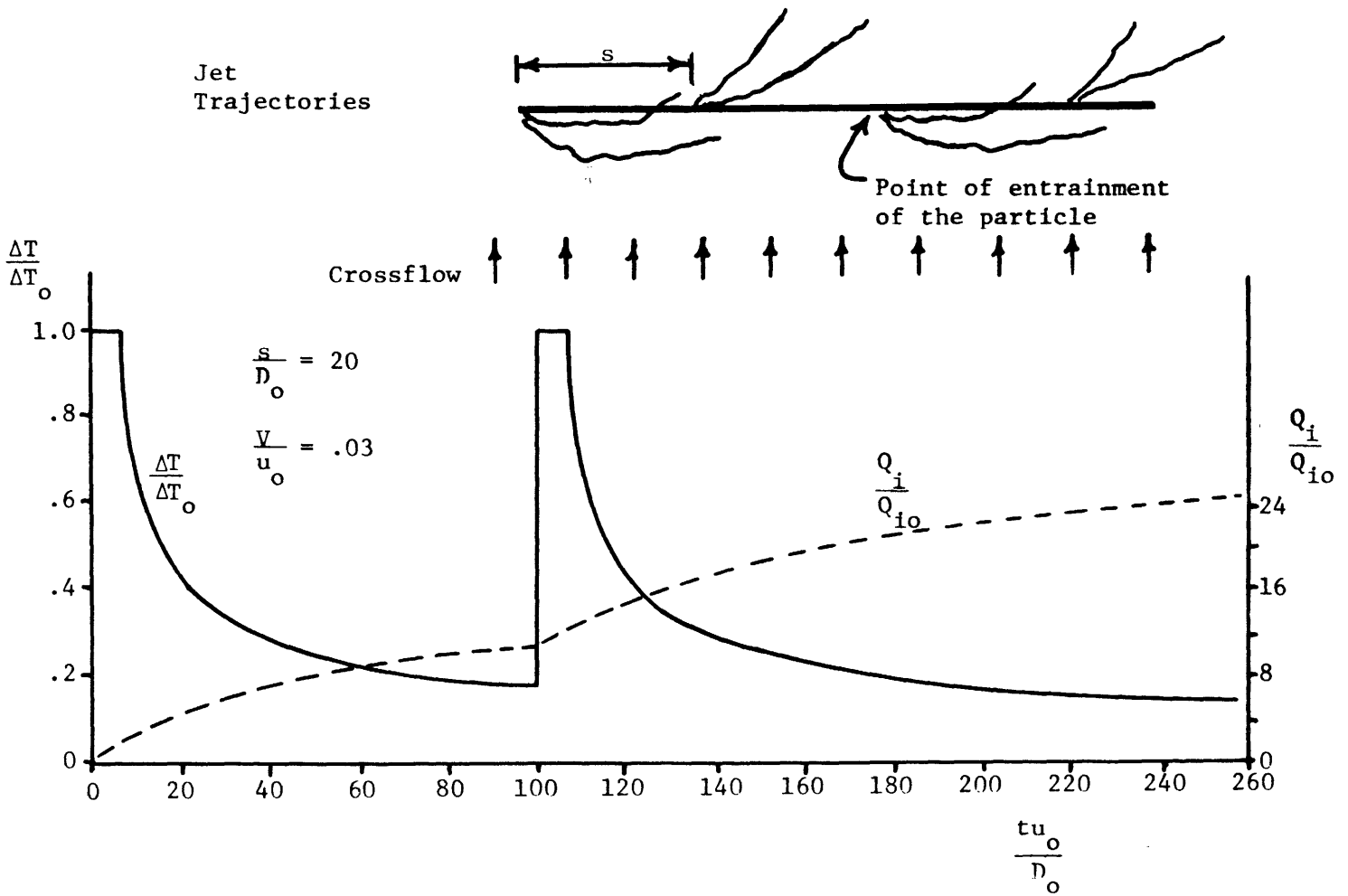

Figure 4-5 Lagrangian Description of a Staged Diffuser
(Based on the individual jet approach)

$x_c < 2s$ by satisfying

$$\frac{D_o}{s} \tan|\gamma_o| < 1.2 \frac{V}{u_o} \tag{4.22}$$

For a given range of ambient current speeds V, this criterion can be satisfied most often by the choice of small values of γ_o, D_o and u_o or a large value of s. However, in the limit as crossflow speed drops to zero, the criterion cannot be met. When the criterion cannot be met, the maximum number of interactions is proportional to L/x_c which is given by

$$\frac{L}{x_c} = \frac{.6}{\tan|\gamma_o|} \frac{V}{u_o} \frac{N}{D_o}$$

$$\approx \frac{s\, Q_o}{x_c D_o^2\, u_o} \tag{4.23}$$

Thus it is apparent that while small values of D_o or u_o, or a high value of s decrease the probability of interaction they also increase the extent of interactions in those cases where interactions does occur because they lead to longer diffuser lengths. In other words they increase the worst case impact. The choice of γ_o does not affect diffuser length so clearly $\gamma_o = 0$ minimizes the probability of interaction. However the combination of $\gamma = 0$ and $V = 0$ results in maximum re-entrainment. In order to lessen the worst case impact it appears that a small $\pm$ value of γ_o would be desireable.

F. SUMMARY

We began this chapter with a qualitative discussion of the factors that affect individual jet behavior in a staged diffuser. These

factors include jet interaction, ambient crossflow, finite water depth and buoyancy. Dimensional analysis and insight gained from experiments reduced the problem of individual jet behavior to the functional form of equation 4.8. For the case of a staged diffuser in a significant crossflow, which probably includes most real situations, it was concluded that individual jet trajectories could be determined approximately by the empirical equation 4.10 and that individual jet dilutions, temperatures, velocities and shear stresses could be determined approximately by using the results of Chapter III. Using this Eulerian description, a solution technique for Lagrangian equations was outlined in this chapter.

In using the Eulerian equation summarized here, it should be remembered that they are based on limited experimental evidence. The Lagrangian equations that are outlined in this chapter are based on these approximate Eulerian equations as well as on the assumption of very simplified particle trajectories.

V. SUMMARY AND CONCLUSIONS

A. DESIGN CONSIDERATIONS BASED ON ANALYSIS ON PREVIOUS CHAPTERS

The preceding chapters have analysed staged diffusers from several perspectives for the purpose of assessing thermal and shear stress related impacts. Chapter II analysed the diffuser as a line source (equivalent slot) of momentum in stagnant water. Both Eulerian and Lagrangian descriptions were obtained and solutions for the external flow field were also derived. Chapter III then repeated the analysis for a single diffuser jet. Finally Chapter IV considered the interaction which takes place among individual jets of a diffuser and compares the results with those obtained in Chapter III. The results of these three chapters can be used to show some general conclusions regarding the sensitivity of discharge impact to diffuser parameters.

For an overall description of diffuser performance in stagnant water (the condition of lowest dilution for a staged diffuser) the analysis of Chapter II is most appropriate. For the case of a horizontal bottom the diffuser performance depends on the variables Q_o, ΔT_o, u_o, L and H. In particular the dilution is proportional to the parameter

$$\mathbb{K} = \sqrt{\frac{sH}{a_o}} = \sqrt{\frac{LH\ u_o}{Q_o}} \tag{5.1}$$

For a constant value of the heat rejection $J_o = Q_o \Delta T_o$, near field temperature rises ΔT are scaled by

$$\Delta T \sim \frac{\Delta T_o}{S^*} \sim \frac{\text{constant}}{\sqrt{Q_o u_o LH}} \tag{5.2}$$

and thus the general level of excess temperature decreases as the square root of each of the four terms in the denominator and increases as the square root of the discharge temperature rise.

A similar expression can be written for shear stress by noting that shear stresses are proportional to the square of the longitudinal velocity which in turn is inversely proportional to the square of the dilution. Thus the magnitude of shear stress is expected to scale as

$$\tau \sim \frac{u_o^2}{S^{*2}} \sim \frac{u_o Q_o}{LH} \tag{5.2}$$

and thus the general level of stress increases with increasing flow rate or exit velocity and decreases with increasing diffuser length or water depth.

The slot diffuser analysis cannot easily be extended to treat the case of an ambient crossflow. However, arguments made in Chapter IV relating the slot jet analysis to the single jet analysis suggest that overall diffuser dilution increases substantially with ambient current velocity because of the increased length of the undisturbed individual jet trajectories. Experimental model studies bear this out. Thus an increase in V should result in generally lower values of both excess temperature and shear stress.

The above Eulerian description of diffuser performance was used to obtain a Lagrangian description of the exposure history which an entrained organism would experience if entrained into various portions of the plume. However, because the exposure history is sensitive to jet interactions, it was felt that a more detailed picture could be obtained

by examining the individual jets which comprise the diffuser. Thus Chapter III analyses an individual jet, first from an Eulerian and then from a Lagrangian perspective. Designs considerations pertinent to the latter analysis are graphed in Figure 3-4. Chapter IV then discusses the effects of jet interaction which pertain to jets in the context of a staged diffuser. The design considerations deduced from these two chapters are discussed below with emphasis on how the conclusions differ from those obtained from the slot diffuser analysis of Chapter II.

Increasing the number of jets N (by decreasing their diameter, while fixing jet velocity, condenser flow rate and temperature rise) decreases both temperature related and shear stress related impact from an individual jet because the duration of exposure is reduced. While this observation was derived for a single jet, it should hold for those diffuser arrangements (combination of γ_o and s) for which there is either no interaction between jets or the trajectory of a given jet intersects with only one additional jet (i.e. $\frac{x_c}{s} < 2$). Because the slot jet concept does not consider individual jets this conclusion supplements those possible from the analysis of Chapter II.

Temperature related impacts decrease with increasing jet velocity u_o (for fixed number of nozzles, condenser flow rate and temperature rise) since the duration of exposure decreases. Conversely the shear stress related impacts increase with increasing discharge velocity because the intensity, duration and exposure rates all increase. These conclusions based on exposure history agree qualitatively with the conclusions based on the Eulerian analysis of Chapter II.

For a fixed heat rejection, temperature-related impacts in the discharge zone increase with increasing condenser temperature rise ΔT_o because the duration and the intensity of exposure increase. Conversely, shear stress-related impacts decrease with increasing ΔT_o since duration of exposure and exposure rate (number of organisms entrained per unit time) both decrease. These conclusions based on exposure history also both agree with the conclusions based on the Eulerian analysis in Chapter II.

The spacing and horizontal orientation of diffuser jets, s and γ_o, affect mainly jet interaction; they have only minor effects on diffuser performance as a whole and no effect on the exposure history of an individual jet. For a given range of current speeds V, decreasing s or increasing $|\gamma_o|$ increases the probability of jet interaction but decreases the extent of interaction (number of times an entrained particle could be re-entrained) when interaction does occur. Increasing jet velocity u_o, or jet diameter D_o (or decreasing the number of jets N) has a similar effect. Designs for which $\gamma_o = 0$ have the least likelihood of re-entrainment (i.e. the jets will become independent of one another at the lowest threshold velocity V) but for stagnant situations this design will suffer the most re-entrainment. Model studies also suggest that in stagnant water dilution is slightly worse for $\gamma_o = 0$ than for $|\gamma_o| > 0$. Thus the selection of non-zero values for γ_o such as the ± 20 values selected for NEP-1 and 2 appears to decrease the worst case (stagnant ambient) impact by both increasing dilution and minimizing re-entrainment.

It should be emphasized that the above conclusions pertain to impacts associated with the discharge plume and do not consider impacts such as impingement or entrainment associated with the condenser water

intake. While these intake impacts are not sensitive to most of the diffuser design variables discussed above, they are very much related to the choice of Q_o and ΔT_o. In particular, the number of organisms exposed to intake impacts decreases with an increase in condenser ΔT_o due to the corresponding decrease in condenser flow rate Q_o. The duration and intensity of any non-thermal impact would be insensitive to the choice of ΔT_o, while the intensity of thermal impacts would clearly increase. While the optimal ΔT_o is not clear from the standpoint of thermal impacts, it is apparent that non-thermal impacts are minimized by maximizing ΔT_o.

B. COMPARISON OF STAGED DIFFUSERS WITH OTHER DIFFUSER TYPES

Before concluding, it is worthwhile to compare briefly the behavior of staged diffusers with other types of diffusers in terms of the analysis discussed in this report. Adams and Stolzenbach (1977) compared various diffuser types which might be utilized in shallow coastal regions including staged, tee, co-flowing and alternating diffusers. See Figure 1-1. Comparison was based on characteristic temperature rises using, for each diffuser, an analysis based on an equivalent slot concept similar to the analysis of Chapter II. A copy of this paper is included as Appendix H of this report.

A general conclusion of this comparison is that a staged diffuser is most effective in ambient crossflows because its orientation allows it to intercept crossflow in either direction, thus increasing dilution. Dilution is lowest under stagnant conditions, but because of the concentration of offshore momentum, an acceptable dilution can still be achieved. Furthermore this (minimum) dilution exceeds the minimum dilution obtained under worst case conditions for other diffuser types (e.g., for a strong

crossflow in the case of a tee diffuser, or a strong counterflow for a co-flowing diffuser). Thus the staged diffuser appears to be a versatile choice at sites which experience a wide range of current speeds in both alongshore directions.

Since all diffusers consist of a collection of individual jets, the analysis of Chapter III applies essentially to any diffuser type. Differences in exposure history come about as a result of differences in interaction among the jets. A qualitative idea of this interaction can be obtained by examining the flow fields sketched in Figure 2 of Appendix H. From the standpoint of minimizing re-entrainment, the tee diffuser appears preferable. Although a crossflow deflects the individual jets, thus shortening their unobstructed trajectories and decreasing overall dilution, the interaction among jets takes place at some distance downstream from the individual jet origins and each jet can interact with at most the two adjacent jets; i.e. there is little possibility for successive re-entrainment. For designs in which jet nozzles point into a crossflow (e.g., for an oblique or co-flowing diffuser facing a counterflow, some re-entrainment is inevitable and is usually correlated with decreased dilution.

An alternating diffuser is somewhat different from the other diffuser types since it imparts no horizontal momentum. Instead dilution is effected largely by horizontal density currents. In most shallow water situations, these currents are very unstable near the diffuser resulting in significant re-entrainment. This fact, coupled with the

relatively low dilutions and the relatively slow speed of density currents, suggests that organisms will be exposed to elevated temperatures for significantly longer times than in momentum diffuser. Because dilution in an alternating diffuser is not dependent on several of the parameters (e.g., flow rates or discharge velocity) which influence the performance of momentum diffuser, these parameters would likely be chosen on the basis of different objectives such as minimizing intake impact, or pumping costs. These measures both suggest decreased flow rate and discharge velocity which at the same time would minimize shear stresses within the plume.

C. CONCLUDING REMARKS

It should be emphasized that the relative impacts discussed above, and which distinguish among different diffuser designs, depend highly on site-specific information concerning organism tolerance to temperature and shear stress. Thus only general conclusions have been made. Although biological assessments are clearly beyond the scope of this study, it is hoped that this analysis can provide a physical framework for such study.

REFERENCES

Adams, E.E., "Submerged Multiport Diffusers in Shallow Water with Current," S.M. Thesis, R.M. Parsons Laboratory for Water Resources and Hydrodynamics, Department of Civil Engineering, MIT, (1972).

Adams, E.E., and K.D. Stolzenbach, "Comparison of Alternative Diffuser Designs for the Discharge of Heated Water into Shallow Receiving Water," R.M. Parsons Laboratory for Water Resources and Hydrodynamics, Department of Civil Engineering, MIT, (1977).

Almquist, C.W., and K.D. Stolzenbach, "Staged Diffusers in Shallow Water," R.M. Parsons Laboratory for Water Resources and Hydrodynamics, Department of Civil Engineering, MIT, Technical Report No. 213, (1976).

Brocard, D.N., "Hydrothermal Studies of Staged Diffuser Discharge in the Coastal Environment Charlestown Site,"Alden Research Lab. Report No. 136-77/M296EF, (1977).

Brocard, D.N., and Hsu, S.-D., "Transient Analytical Temperature Predictions for Heated Diffuser Discharge, NEP 1 and 2, Charlestown Site,"Alden Research Laboratory, Report No. 111-78/M14KF, (1978).

Chan, T.L., and J.F. Kennedy, "Turbulent Non-buoyant or Buoyant Jets Discharged into Flowing or Quiescent Fluids," Iowa Institute of Hydraulic Research, Iowa City, Iowa (1972).

Jirka, G., and D.R.F. Harleman, "The Mechanics of Submerged Multiport Diffusers in Shallow Water," R.M. Parsons Laboratory for Water Resources and Hydrodynamics, Department of Civil Engineering, MIT, Technical Report No. 169, (1973).

Lee, J.H., G.H. Jirka, and D.R.F. Harleman, "Modeling of Unidirectional Thermal Diffusers in Shallow Water," R.M. Parsons Laboratory for Water Resources and Hydrodynamics, Department of Civil Engineering, MIT, Technical Report No. 228, (1977).

Rajaratnam, N., Turbulent Jets, New York: American Elsevier Publishing Company, Inc., (1976).

Schubel, J.R., and B.C. Marcy (editors), Power Plant Entrainment, New York: Academic Press, Inc., (1978).

Stolzenbach, K.D., C.W. Almquist, E.E. Adams, and S.A. Freudberg, "Analytical and Experimental Studies of Discharge Designs for the Cayuga Station at the Somerset Alternate Site," R.M. Parsons Laboratory for Water Resources and Hydrodynamics, Department of Civil Engineering, MIT, Technical Report No. 211, (1976).

Streeter, V.L., Fluid Mechanics, New York: McGraw-Hill, Inc., (1971).

Tennekes, H., and J.L. Lumley, A First Course in Turbulence, Cambridge, Massachusetts: The MIT Press, (1972).

List of Symbols

Symbol	Definition
A_c	jet cross section area
C	shear stress coefficient
C_D	drag coefficient
D	duration of organism exposure
D_o	jet diameter
D_T	duration of organism exposure to thermal impact
D_τ	duration of organism exposure to shear stress impact
$\mathbb{F}_D$	drag force per unit jet length
$\mathbb{F}_E$	entrainment "force" per unit jet length
$\mathbb{F}_o$	discharge densimetric Froude number
H	water depth
H_o	water depth at $x = x_o$
I	intensity of organism exposure
I_T	intensity of organism exposure to thermal impact
I_τ	intensity of organism exposure to shear stress impact
J_i	individual jet kinematic thermal energy flux
J_{io}	initial individual jet kinematic thermal energy flux
$\mathbb{K}$	discharge parameter
$\mathbb{K}_o$	value of $\mathbb{K}$ based on H_o
L	diffuser length
M_o	initial kinematic momentum flux
M_i	individual jet kinematic momentum flux
M_{io}	initial individual jet kinematic flux
N	number of ports
Q_E	entrained flow rate
Q_i	individual jet flow rate
Q_{io}	individual discharge flow rate
Q_o	discharge flow rate
S^*	dilution
T_a	ambient temperature
T_b	background temperature
T_{max}	maximum temperature
ΔT	temperature rise
ΔT_c	centerline temperature use
ΔT_o	discharge temperature rise
V	ambient current velocity

List of Symbols

Symbol	Definition
a_o	port area
b	plume width
b^*	characteristic jet width in diffuser
f	lateral profile of mean velocity
g	lateral profile of shear stress
g	acceleration of gravity
h	port elevation above bottom
n	rate of organism exposure
n_T	rate of organism exposure to thermal impact
n_τ	rate of organism exposure to shear stress impact
r	radial coordinate
q_E	entrained flow rate per unit jet length
s	port spacing
t	time
$t_{e,f}$	time at which a particle enters the zone of flow establishment
$t_{e,3}$	time at which a particle enters the 3-D region
$t_{e,2}$	time at which a particle enters the 2-D region
u	longitudinal mean velocity
u_c	centerline jet velocity
u_o	jet discharge velocity
u'	fluctuating velocity component
v	lateral mean velocity
v_e	entrainment velocity
v'	fluctuating velocity component
x	longitudinal coordinate
x_c	value of x where a jet trajectory crosses diffuser axis
$x_{e,f}$	position at which a particle enters zone of flow establishment
$x_{e,3}$	position at which a particle enters the 3-D region
$x_{e,2}$	position at which a particle enters the 2-D region
x_o	upstream coordinate of diffuser
x_T	transition distance between 3-D and 2-D momentum region in slot jet analysis
y	lateral coordinate
z	vertical coordinate

List of Symbols

Symbol	Definition
α	vertical jet angle
α	entrainment coefficient
β	"crossflow" entrainment coefficient
β	coefficient of thermal expansion
γ_o	horizontal jet angle
ν	kinematic viscosity
ν_T	turbulent kinematic viscosity
ξ	centerline coordinate
π	3.14159
ρ	density
τ	shear stress
ψ	stream function

APPENDIX A

DETERMINATION OF THE STRAIGHT LINE PATH (RAY) IN A ROUND, TURBULENT JET FOR WHICH THE THERMAL IMPACT IS GREATEST

We wish to determine the straight line path in a turbulent jet for which the thermal impact on a moving organism is greatest. We will consider a round jet. The problem for a plane jet is analogous.

A definition sketch of a round jet is shown in Figure A-1. The jet is described by circular cylindrical coordinates (x,r,θ). It is assumed that there is no variation in the θ direction. We assume that entrained particles move along lines of constant η, where $\eta = r/b$, at the local mean fluid velocity. The problem reduces to finding the value of η for which the thermal impact is greatest. We will consider motion of a particle only in the zone of established flow.

In the zone of established flow of a round, turbulent jet, we have

$$\frac{u_c}{u_o} = C_1 \frac{D_o}{x}$$

$$\frac{u}{u_c} = f(\eta) \qquad \text{(A-1)}$$

where C_1 is a constant equal to 6.2 and $f(\eta)$ describes the velocity profile at a given jet cross-section (see Tennekes and Lumley, 1972). The function $f(\eta)$ must satisfy

$$f(0) = 1$$

$$f'(0) = 0 \qquad \text{(A-2)}$$

$$f(\infty) = 0$$

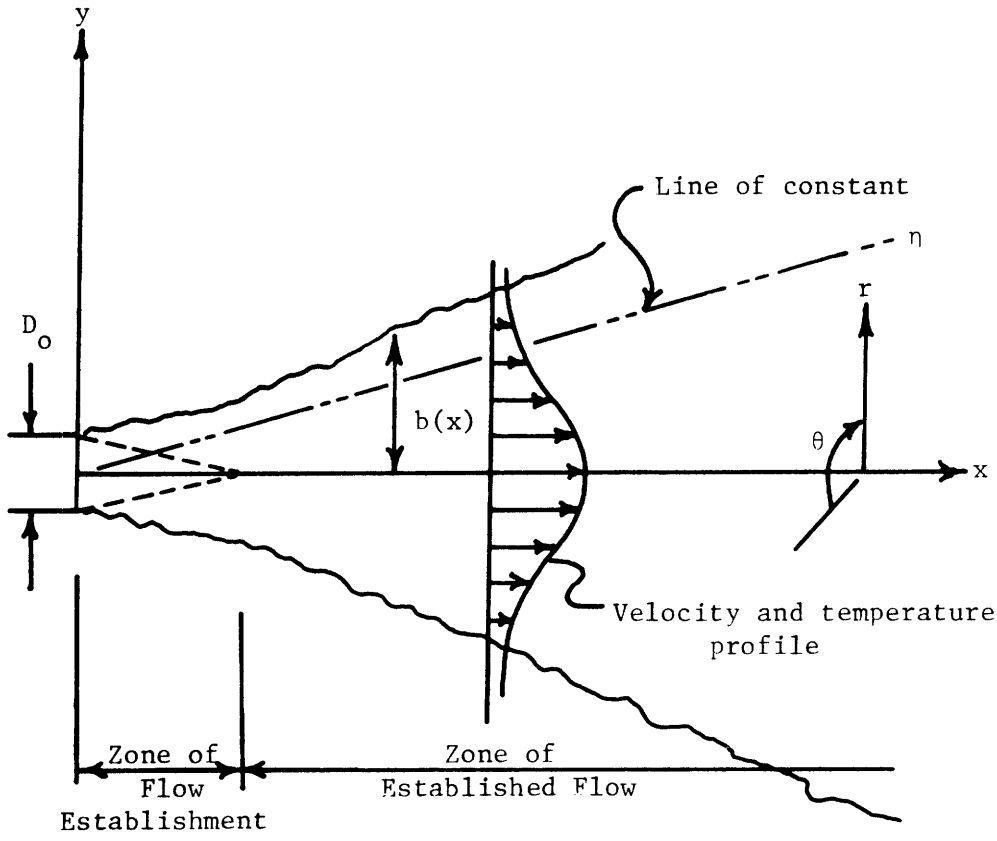

b = nominal jet width

T_a = ambient temperature

ΔT = temperature excess = $\Delta T(x,r)$

ΔT_c = centerline temperature excess = $\Delta T_c(x)$

ΔT_o = discharge temperature excess

u = mean x-component of velocity = $u(x,r)$

u_c = mean centerline x-velocity = $u_c(x)$

u_o = discharge velocity

$\eta = \frac{r}{b}$

Figure A-1 Definition Sketch of a Round Jet

and it reaches a maximum at $\eta = 0$. Assuming that momentum and heat diffuse in nearly the same manner (the Reynolds analogy) we have

$$\frac{\Delta T_c}{\Delta T_o} = C_1 \frac{D_o}{x}$$

$$\frac{\Delta T}{\Delta T_c} = f(\eta) \tag{A-3}$$

For particle motion along a ray, we have

$$\eta = \text{constant}$$

$$f(\eta) = \text{constant}. \tag{A-4}$$

The equation describing the motion of a particle moving along a ray is

$$\frac{dx}{dt} = u = C_1 \, u_o \frac{D_o}{x} f(\eta) \tag{A-5}$$

This expression can be integrated to give

$$\frac{x}{D_o} = \left[\left(\frac{x_e}{D_o}\right)^2 + 2f(\eta) \, C_1 \left(\frac{tu_o}{D_o} - \frac{t_e u_o}{D_o}\right)\right]^{1/2} \tag{A-6}$$

where

x_e = position at which the particle began its motion

t_e = time at which the particle began its motion.

Equation A-6 is a Lagrangian equation giving particle position as a function of time. It can be combined with equation A-3 to yield a Lagrangian expression giving the temperature excess experienced by the moving particle as a function of time:

$$\frac{\Delta T}{\Delta T_o} = C_1 f(\eta) \left[\left(\frac{x_e}{D_o}\right)^2 + 2f(\eta) C_1 \left(\frac{tu_o}{D_o} - \frac{t_e u_o}{D_o}\right)\right]^{-1/2} \tag{A-7}$$

This equation can be written

$$\frac{\Delta T}{\Delta T_o} = \frac{C_1}{\sqrt{\left(\frac{1}{f(\eta)}\right)^2 \left(\frac{x_e}{D_o}\right)^2 + \frac{2C_1}{f(\eta)} \left(\frac{tu_o}{D_o} - \frac{t_e u_o}{D_o}\right)}} \qquad \text{(A-8)}$$

Examination of equation A-8 shows that for given values of x_e, t_e and t, the maximum temperature excess is experienced where $f(\eta)$ is a maximum. As was discussed above, this occurs at $\eta = 0$, which is the jet centerline. Therefore, we conclude that the straight line path along which the thermal stress on a moving particle is greatest is the jet centerline.

APPENDIX B

LAGRANGIAN DESCRIPTION OF A STAGED DIFFUSER IN SHALLOW WATER OF CONSTANT DEPTH BASED ON THE CONCEPT OF A LINE SOURCE OF MOMENTUM

In this appendix we will develop a Langrangian description of a staged diffuser plume, based on the Eulerian equations of Almquist and Stolzenbach (1976). Our work is based on the following assumptions:

(1) An entrained particle moves directly to the plume centerline, and then moves along the centerline at the mean centerline velocity.

(2) The particle experiences temperatures equal to the mean centerline temperatures.

(3) The particle experiences shear stresses given by $\tau = C\rho u_c^2$, where ρ = water density, u_c = plume centerline velocity, and C = constant of order .05.

The assumptions made by Almquist and Stolzenbach in their analysis of staged diffusers are also implicitly made here. Dropping negligible terms the Eulerian equations they obtained are:

3-D region $(0 \leq x \leq x_T)$

$$\frac{u_c}{u_o} = \frac{\Delta T_c}{\Delta T_o} = \frac{3}{2\sqrt{\pi}} \frac{I_1}{\sqrt{I_2}} \frac{1}{\alpha_3} \frac{1}{\mathbb{K}} \left(\frac{H}{x}\right)^{1/2} \tag{B-1}$$

$$\frac{u_c}{u_o}, \frac{\Delta T_c}{\Delta T_o} \leq 1 \tag{B-2}$$

2-D momentum region ($x_T \leq x \leq L$)

$$\frac{u_c}{u_o} = \frac{\Delta T_c}{\Delta T_o} = \left(\frac{1}{2\alpha_2}\frac{I_3}{I_4}\right)^{1/2} \frac{1}{\mathbb{K}} \tag{B-3}$$

2-D jet region ($L \leq x$)

$$\frac{u_c}{u_o} = \frac{\Delta T_c}{\Delta T_o} = \frac{1}{\mathbb{K}} \left[4\alpha_j \frac{I_6}{I_5}\frac{H}{L}\frac{x}{H} + 2\eta\right]^{-1/2} \tag{B-4}$$

$$\eta = \left(\frac{I_6}{I_5}\right)^2 \frac{I_3}{I_4}\alpha_2 - 2\alpha_j \frac{I_6}{I_5} \tag{B-5}$$

where

I = constant depending on the velocity profile

α = entrainment coefficient.

To find Lagrangian equations, we integrate the expressions for velocity to get position of the moving particle as a function of time. The equations for position as a function of time are then combined with the Eulerian expressions for temperature and shear stress to give these quantities as functions of time for the moving particle.

3-D region ($0 \leq x \leq x_T$)

In the 3-D region we have

$$\frac{dx}{dt} = u_c = u_o \frac{3}{2\sqrt{\pi}} \frac{I_1}{\sqrt{I_2}} \frac{1}{\alpha_3} \frac{1}{\mathbb{K}} \left(\frac{H}{x}\right)^{1/2} \tag{B-6}$$

Integration of this equation gives

$$\frac{x}{H} = \left[\left(\frac{x_{e,3}}{H}\right)^{3/2} + \frac{9}{4\sqrt{\pi}} \frac{I_1}{\sqrt{I_2}} \frac{1}{\alpha_3} \frac{1}{\mathbb{K}} \left(\frac{tu_o}{H} - \frac{t_{e,3}u_o}{H}\right)\right]^{2/3} \tag{B-7}$$

where

$x_{e,3}$ = point at which the particle enters the 3-D region

$t_{e,3}$ = time at which the particle enters the 3-D region

Substituting equation B-7 into equation B-1, we get

$$\frac{\Delta T}{\Delta T_o} = \left[\frac{2}{3}\pi \frac{I_2}{I_1^2}\alpha_3^2 \mathbb{K}^2\left(\frac{tu_o}{H} - \frac{t_{e,3}u_o}{H}\right) + \frac{8\pi\sqrt{\pi}}{27}\frac{I_2\sqrt{I_2}}{I_1^3}\alpha_3^3 \mathbb{K}^3 \left(\frac{x_{e,3}}{H}\right)^{3/2}\right]^{-1/3} \qquad \text{(B-8)}$$

where equation B-2 must apply. Using equations B-1 and B-7, we can also get

$$\frac{\tau}{C\rho u_o^2} = \left[\frac{2}{3}\pi \frac{I_2}{I_1^2}\alpha_3^2 \mathbb{K}^2 \left(\frac{tu_o}{H} - \frac{t_{e,3}u_o}{H}\right) + \frac{8\pi\sqrt{\pi}}{27}\frac{I_2\sqrt{I_2}}{I_1^3}\alpha_3^3 \mathbb{K}^3 \left(\frac{x_{e,3}}{H}\right)^{3/2}\right]^{-2/3} \qquad \text{(B-9)}$$

where

$$\frac{\tau}{C\rho u_o^2} \leq 1 \ . \qquad \text{(B-10)}$$

2-D momentum region $(x_T \leq x \leq L)$

In the 2-D momentum region we have

$$\frac{dx}{dt} = u_c = u_o \left(\frac{1}{2\alpha_2}\frac{I_3}{I_4}\right)^{1/2}\frac{1}{\mathbb{K}} \ . \qquad \text{(B-11)}$$

Integration of this equation gives

$$\frac{x}{H} = \frac{x_{e,2}}{H} + \left(\frac{1}{2\alpha_2}\frac{I_3}{I_4}\right)^{1/2}\frac{1}{\mathbb{K}}\left(\frac{tu_o}{H} - \frac{t_{e,2}u_o}{H}\right) \qquad \text{(B-12)}$$

where

$x_{e,2}$ = point at which the particle enters the 2-D momentum region

$t_{e,2}$ = time at which the particle enters the 2-D momentum region.

The Lagrangian temperature and shear stress equations are simply

$$\frac{\Delta T}{\Delta T_o} = \left(\frac{1}{2\alpha_2}\frac{I_3}{I_4}\right)^{1/2} \mathbb{K} \tag{B-13}$$

$$\frac{\tau}{C\rho u_o^2} = \frac{1}{2\alpha_2}\frac{I_3}{I_4}\frac{1}{\mathbb{K}^2} \tag{B-14}$$

2-D jet region ($L \leq x$)

In the 2-D jet region we have

$$\frac{dx}{dt} = u_c = \frac{u_o}{\mathbb{K}}\left[4\alpha_j \frac{I_6}{I_5}\frac{H}{L}\frac{x}{H} + 2\eta\right]^{-1/2} \tag{B-15}$$

Integration of this equation gives

$$\frac{x}{H} = \frac{L}{H} - \frac{1}{2}\frac{I_6}{I_5}\frac{I_3}{I_4}\frac{\alpha_2}{\alpha_j}\frac{L}{H} + \left\{\left[\frac{x_{e,j}}{H} + \frac{1}{2}\frac{\alpha_2}{\alpha_j}\frac{I_6}{I_5}\frac{I_3}{I_4}\frac{L}{H} - \frac{L}{H}\right]^{3/2} + \frac{3}{4\sqrt{\alpha_j}}\sqrt{\frac{I_5}{I_6}}\sqrt{\frac{L}{H}}\frac{1}{\mathbb{K}}\left(\frac{tu_o}{H} - \frac{t_{e,j}u_o}{H}\right)\right\}^{2/3} \tag{B-16}$$

where

$x_{e,j}$ = point at which the particle enters the 2-D jet region

$t_{e,j}$ = time at which the particle enters the 2-D jet region

Combining equations B-16 and B-4, we get

$$\frac{\Delta T}{\Delta T_o} = \{6\alpha_j \frac{I_6}{I_5}\frac{H}{L}\,\mathbb{K}^2\,(\frac{tu_o}{H} - \frac{t_{e,j}u_o}{H}) + \mathbb{K}^3[4\alpha_j \frac{I_6}{I_5}\frac{H}{L}\frac{x_{e,j}}{H} + 2\eta]^{3/2\ -1/3}\} \qquad \text{(B-17)}$$

$$\frac{\tau}{C\rho u_o^{\,2}} = \{6\alpha_j \frac{I_6}{I_5}\frac{H}{L}\,\mathbb{K}^2\,(\frac{tu_o}{H} - \frac{t_{e,j}u_o}{H}) + \mathbb{K}^3[4\alpha_j \frac{I_6}{I_5}\frac{H}{L}\frac{x_{e,j}}{H} + 2\eta]^{3/2\ -2/3}\} \qquad \text{(B-18)}$$

A summary of the Lagrangian equations is given below.

3-D region ($0 \le x \le x_T$)

$$\frac{x}{H} = [(\frac{x_{e,3}}{H})^{3/2} + \frac{9}{4\sqrt{\pi}}\frac{I_1}{\sqrt{I_2}}\frac{1}{\alpha_3}\frac{1}{\mathbb{K}}\,(\frac{tu_o}{H} - \frac{t_{e,3}u_o}{H})]^{2/3}$$

$$\frac{\Delta T}{\Delta T_o} = [\frac{2}{3}\pi\frac{I_2}{I_1^{\,2}}\alpha_3^{\,2}\,\mathbb{K}^2\,(\frac{tu_o}{H} - \frac{t_{e,3}u_o}{H}) + \frac{8\pi\sqrt{\pi}}{27}\frac{I_2\sqrt{I_2}}{I_1^{\,3}}\alpha_3^{\,3}\,\mathbb{K}^3\,(\frac{x_{e,3}}{H})^{3/2\ -1/3}] \qquad \text{(B-19)}$$

$$\frac{\tau}{C\rho u_o^{\,2}} = [\frac{2}{3}\pi\frac{I_2}{I_1^{\,2}}\alpha_3^{\,2}\,\mathbb{K}^2\,(\frac{tu_o}{H} - \frac{t_{e,3}u_o}{H}) + \frac{8\pi\sqrt{\pi}}{27}\frac{I_2\sqrt{I_2}}{I_1^{\,3}}\alpha_3^{\,3}\,\mathbb{K}^3\,(\frac{x_{e,3}}{H})^{3/2\ -2/3}]$$

$$\frac{\Delta T}{\Delta T_o}\ ,\ \frac{\tau}{C\rho u_o^{\,2}} \le 1$$

2-D momentum region $(x_T \leq x \leq L)$

$$\frac{x}{H} = \frac{x_{e,2}}{H} + \left(\frac{1}{2\alpha_2}\frac{I_3}{I_4}\right)^{1/2} \frac{1}{\mathbb{K}} \left(\frac{tu_o}{H} - \frac{t_{e,2}u_o}{H}\right)$$

$$\frac{\Delta T}{\Delta T_o} = \left(\frac{1}{2\alpha_2}\frac{I_3}{I_4}\right)^{1/2} \frac{1}{\mathbb{K}} \tag{B-20}$$

$$\frac{\tau}{C\rho u_o^2} = \frac{1}{2\alpha_2}\frac{I_3}{I_4}\frac{1}{\mathbb{K}^2}$$

2-D jet region $(L \leq x)$

$$\frac{x}{H} = \frac{L}{H} - \frac{1}{2}\frac{I_6}{I_5}\frac{I_3}{I_4}\frac{\alpha_2}{\alpha_j}\frac{L}{H} + \left\{\left[\frac{x_{e,j}}{H} + \frac{1}{2}\frac{\alpha_2}{\alpha_j}\frac{I_6}{I_5}\frac{I_3}{I_4}\frac{L}{H} - \frac{L}{H}\right]^{3/2} + \frac{3}{4\sqrt{\alpha_j}}\sqrt{\frac{I_5}{I_6}}\sqrt{\frac{L}{H}}\frac{1}{\mathbb{K}}\left(\frac{tu_o}{H} - \frac{t_{e,j}u_o}{H}\right)\right\}^{2/3}$$

$$\frac{\Delta T}{\Delta T_o} = \left\{6\alpha_j \frac{I_6}{I_5}\frac{H}{L}\mathbb{K}^2\left(\frac{tu_o}{H} - \frac{t_{e,j}u_o}{H}\right) + \mathbb{K}^3\left[4\alpha_j \frac{I_6}{I_5}\frac{H}{L}\frac{x_{e,j}}{H} + 2\eta\right]^{3/2}\right\}^{-1/3} \tag{B-21}$$

$$\frac{\tau}{C\rho u_o^2} = \left\{6\alpha_j \frac{I_6}{I_5}\frac{H}{L}\mathbb{K}^2\left(\frac{tu_o}{H} - \frac{t_{e,j}u_o}{H}\right) + \mathbb{K}^3\left[4\alpha_j \frac{I_6}{I_5}\frac{H}{L}\frac{x_{e,j}}{H} + 2\eta\right]^{3/2}\right\}^{-2/3}$$

If we assume Gaussian velocity profiles in the diffuser plume, we have

$$I_1 = \frac{1}{2}$$

$$I_2 = \frac{1}{4}$$

$$I_3 = I_5 = \frac{\sqrt{\pi}}{2}$$

$$I_4 = I_6 = \sqrt{\frac{\pi}{8}}$$

$$\alpha_3 = .057$$

$$\alpha_2 = .069$$

$$\alpha_j = .069$$

(see Almquist and Stolzenbach (1976)). Using these constants in equations B-19 through B-21, we have

3-D region $(0 \leq x \leq x_T)$

$$\frac{x}{H} = \left[\left(\frac{x_{e,3}}{H}\right)^{3/2} + \frac{22.3}{\mathbb{K}}\left(\frac{tu_o}{H} - \frac{t_{e,3}u_o}{H}\right)\right]^{2/3}$$

$$\frac{\Delta T}{\Delta T_o} = \left[\left(\frac{\mathbb{K}}{12.1}\right)^2 \left(\frac{tu_o}{H} - \frac{t_{e,3}u_o}{H}\right) + \left(\frac{\mathbb{K}}{14.8}\right)^3 \left(\frac{x_{e,3}}{H}\right)^{3/2}\right]^{-1/3}$$

$$\frac{\tau}{C\rho u_o^2} = \left[\left(\frac{\mathbb{K}}{12.1}\right)^2 \left(\frac{tu_o}{H} - \frac{t_{e,3}u_o}{H}\right) + \left(\frac{\mathbb{K}}{14.8}\right)^3 \left(\frac{x_{e,3}}{H}\right)^{3/2}\right]^{-2/3}$$

$$\frac{\Delta T}{\Delta T_o}, \frac{\tau}{C\rho u_o^2} \leq 1 \qquad \text{(B-22)}$$

2-D momentum region $(x_T \leq x \leq L)$

$$\frac{x}{H} = \frac{x_{e,2}}{H} + \frac{3.20}{\mathbb{K}} \left(\frac{tu_o}{H} - \frac{t_{e,2}u_o}{H}\right)$$

$$\frac{\Delta T}{\Delta T_o} = \frac{3.20}{\mathbb{K}} \qquad \text{(B-23)}$$

$$\frac{\tau}{C\rho u_o^2} = \frac{10.3}{\mathbb{K}}$$

2-D jet region $(L \leq x)$

$$\frac{x}{H} = \frac{1}{2}\frac{L}{H} + \left\{\left[\frac{x_{e,j}}{H} - \frac{1}{2}\frac{L}{H}\right]^{3/2} + \frac{3.40}{\mathbb{K}}\sqrt{\frac{L}{H}}\left(\frac{tu_o}{H} - \frac{t_{e,j}u_o}{H}\right)\right\}^{2/3}$$

$$\frac{\Delta T}{\Delta T_o} = \left\{.293\,\frac{H}{L}\,\mathbb{K}^2\left(\frac{tu_o}{H} - \frac{t_{e,j}u_o}{H}\right) + \mathbb{K}^3\left[.195\,\frac{H}{L}\,\frac{x_{e,j}}{H} - .0976\right]^{3/2}\right\}^{-1/3} \qquad \text{(B-24)}$$

$$\frac{\tau}{C\rho u_o^2} = \left\{.293\,\frac{H}{L}\,\mathbb{K}^2\left(\frac{tu_o}{H} - \frac{t_{e,j}u_o}{H}\right) + \mathbb{K}^3\left[.195\,\frac{H}{L}\,\frac{x_{e,j}}{H} - .0976\right]^{3/2}\right\}^{-2/3}$$

It should be noted that each of the expressions summarized above is valid only in the region for which it was derived. For example, if a particle is entrained into the 3-D region, the equations derived

for the 3-D region (equations B-19 or B-22) should be used to describe the particle's history until it reaches the point $x=x_T$, which is the beginning of the 2-D momentum region. From here the equations for the 2-D momentum region (equations B-20 or B-23) should be used until the particle reaches x=L, which is the beginning of the 2-D jet region. After this point, the equations derived for the 2-D jet region (equations B-21 or B-24) should be used.

APPENDIX C

THE ENTRAINMENT FLOWFIELD SURROUNDING A STAGED DIFFUSER IN WATER OF CONSTANT DEPTH

We wish to solve for the flow field induced by a staged diffuser in water of constant depth. We assume a stagnant, semi-infinite receiving body of water, that the flow outside of the turbulent diffuser plume can be adequately described using potential flow theory, and that the diffuser plume can be treated as a line sink for entrained water. The entrainment demand at each point along the diffuser is determined using the analysis of Almquist and Stolzenbach (1976). This problem is illustrated in Figure C-1a.

We assume that the flow field in the potential flow region is two dimensional. If u is the x component of fluid velocity and v is the y component, we can define a velocity potential ϕ such that

$$u = \frac{\partial \phi}{\partial x} \tag{C-1}$$

$$v = \frac{\partial \phi}{\partial y} \tag{C-2}$$

and a stream function ψ such that

$$u = -\frac{\partial \psi}{\partial y} \tag{C-3}$$

$$v = \frac{\partial \psi}{\partial x} \tag{C-4}$$

The irrotational flow condition is that

$$\nabla^2 \psi = 0 \tag{C-5}$$

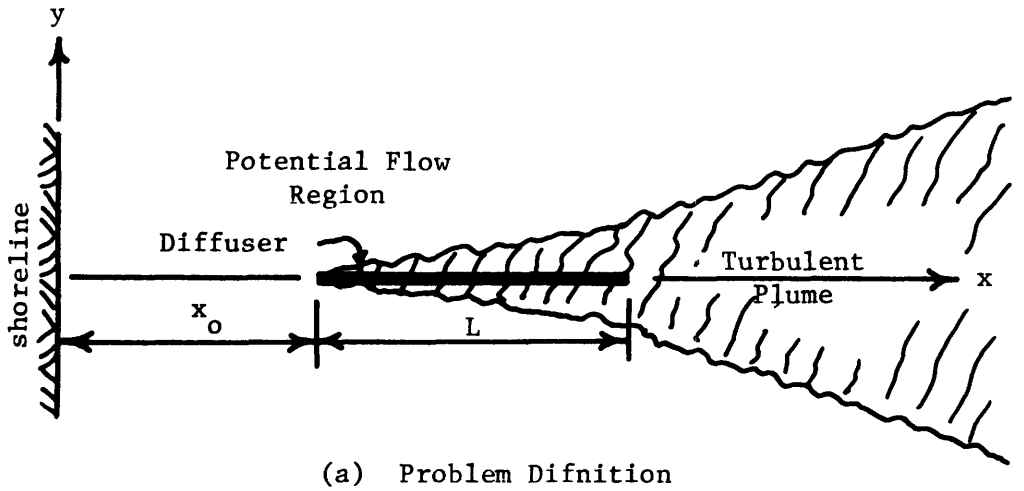

(a) Problem Difnition

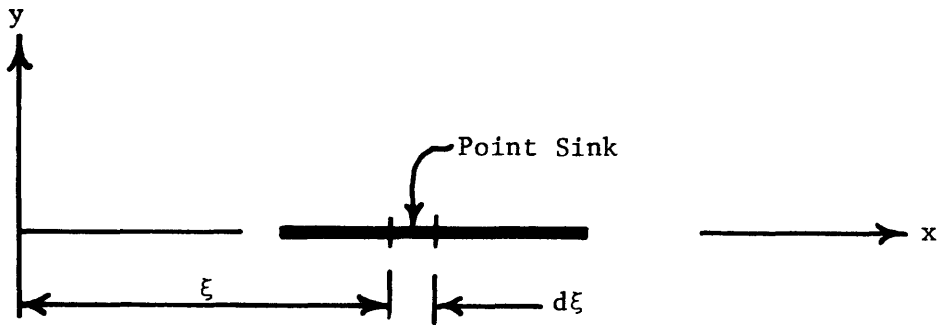

(b) Staged Diffuser as a Series of Point Sinks

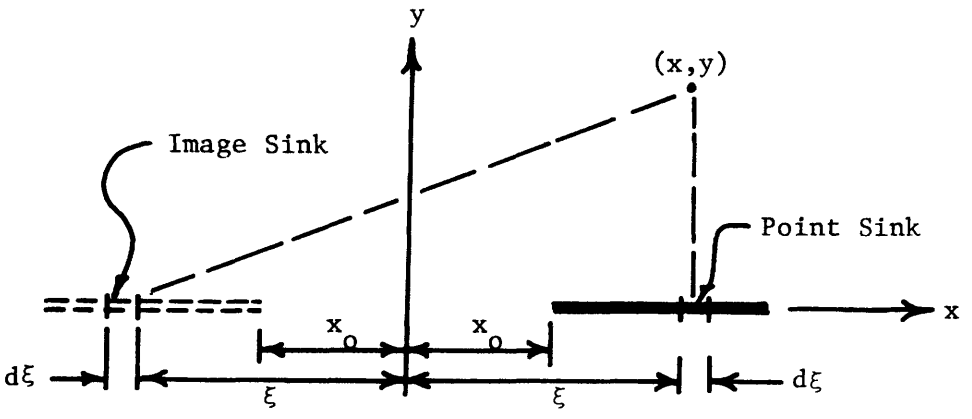

(c) Treatment of the Shore Boundary Using an Image Diffuser

Figure C-1 Definition Sketches for the Potential Flow Solution to the Entrainment Flowfield (Horizontal Bottom Case)

and continuity requires

$$\nabla^2\phi = 0 \tag{C-6}$$

Along the shoreline, the boundary condition is

$$\frac{\partial\phi}{\partial x} = 0 \tag{C-7}$$

$$\psi = \text{constant} \tag{C-8}$$

Along the x-axis, the boundary condition is

$$\frac{\partial\phi}{\partial y} = -v_e(x) \tag{C-9}$$

$$\frac{\partial\psi}{\partial x} = -v_e(x) \tag{C-10}$$

where $v_e(x)$ is the entrainment velocity induced by the diffuser at the point x. We seek functions ϕ and ψ that satisfy the governing equations C-5 and C-6 and the boundary conditions C-7 through C-10.

We can treat the diffuser as a series of point sinks, each with length $d\xi$ and intensity

$$dQ(\xi) = 2v_e(\xi)d\xi \tag{C-11}$$

where ξ is the location of the point sink. (See Figure C-1b.) Each point sink induces a flow at every point in the x-y plane, which is described by

$$d\psi(x,y,\xi) = \frac{dQ(\xi)}{2\pi H} \tan^{-1}\left(\frac{x-\xi}{y}\right) \tag{C-12}$$

$$d\phi(x,y\xi) = \frac{dQ(\xi)}{2\pi H} \ell n \sqrt{(x-\xi)^2 + y^2} \tag{C-13}$$

(see Streeter, 1971). Since the governing equations C-5 and C-6 are linear, we can find $\psi(x,y)$ and $\phi(x,y)$ by summing the contributions of all of the point sinks. We deal with the shore boundary condition by placing an "image" diffuser as shown in Figure C-1c. The contribution to $\phi(x,y)$ and $\psi(x,y)$ of a point source at ξ and its image at $-\xi$ is found by superposition to be

$$d\psi(x,y,\xi) = \frac{dQ(\xi)}{2\pi H}\left[\tan^{-1}\left(\frac{x-\xi}{y}\right) + \tan^{-1}\left(\frac{x+\xi}{y}\right)\right] \qquad \text{(C-14)}$$

$$d\phi(x,y,\xi) = \frac{dQ(\xi)}{2\pi H}\left[\ell n\sqrt{(x-\xi)^2 + y^2} + \ell n\sqrt{(x+\xi)^2 + y^2}\right] \qquad \text{(C-15)}$$

To solve for (x,y) and (x,y), we integrate $d\psi$ and $d\phi$ over the whole length of the diffuser plume:

$$\psi(x,y) = \int_{x_o}^{\infty} \frac{dQ(\xi)}{d\xi}\frac{1}{2\pi H}\left[\tan^{-1}\left(\frac{x-\xi}{y}\right) + \tan^{-1}\left(\frac{x+\xi}{y}\right)\right]d\xi \qquad \text{(C-16)}$$

$$\phi(x,y) = \int_{x_o}^{\infty} \frac{dQ(\xi)}{d\xi}\frac{1}{2\pi H}\left[\ell n\sqrt{(x-\xi)^2+y^2} + \ell n\sqrt{(x+\xi)^2+y^2}\right]d\xi \qquad \text{(C-17)}$$

The function $dQ(\xi)$ is found from equation C-11 and $v_e(\xi)$ is determined from the analysis of Almquist and Stolzenbach (1976).

We chose to use ψ to describe the entrainment flowfield. No analytical solution is easily obtained and we evaluated equation C-16 numerically at chosen points in the xy plane to determine the flowfield. A listing of the computer program we used to perform this operation is given below.

```
C     PROGRAM COMPUTES THE FLOWFIELD AROUND A STAGED DIFFUSER
C     ON A HORIZONTAL BOTTOM
C     BASED ON ALMQUIST'S 1976 THEORY
C
C     OUTPUT AT A POINT = 100*H/K/QO*PSI
C     H=WATER DEPTH, K=ALMQUIST'S DIFFUSER PARAMETER
C     QO=TOTAL DIFFUSER DISCHARGE
C     PSI=AMOUNT OF WATER FLOWING BETWEEN THE POINT AND
C     THE SHORE PER UNIT DEPTH
C
C     M=NUMBER OF GRID POINTS ALONG DIFFUSER AXIS
C     N=NUMBER OF GRID POINTS PERPENDICULAR TO DIFFUSER AXIS
C     L=OUTPUT INTERVAL
C     K=NUMBER OF INTERVALS THAT THE DIFFUSER IS DIVIDED INTO
C     FOR NUMERICAL INTEGRATION
C     XO=DISTANCE OFFSHORE/H
C     XL=(DIFFUSER LENGTH)/H
C     XS=(GRID SPACING ALONG DIFFUSER AXIS)/H
C     YS=(GRID SPACING PERPENDICULAR TO DIFFUSER AXIS)/H
C
      REAL PSI(31,21),XO,XL,XS,YS,XI,YJ,X,DELX,DELPSI
      INTEGER M,N,L,K,ML,JJ,II,KL
      READ (5,1000) M,N,L,K
1000  FORMAT(4I5)
      READ(5,2000) XO,XL,XS,YS
2000  FORMAT(4F10.4)
      WRITE(6,1000) M,N,L,K
      WRITE(6,2000) XO,XL,XS,YS
C
      ML=M-1
      DELX=(FLOAT(ML)*XS-XO)/FLOAT(K)
C
      DO 100 I=1,M
      J=1
      II=I-1
      X=(FLOAT(II))*XS
      IF(X-XO.GT.XL) GO TO 120
      IF(X-XO.GT.10.5) GO TO 110
      IF(X-XO.GT.0.0) GO TO 105
      PSI(I,J)=0.0
      GO TO 100
105   PSI(I,J)=(0.0674)/XL*(X-XO)*SQRT(X-XO)*100.0*2.0*0.5
      GO TO 100
110   PSI(I,J)=(.221)/XL*(X-XO)*100.0
      GO TO 100
120   PSI(I,J)=SQRT((.0976)/XL*(X-XO)-(.0488))*100.0
100   CONTINUE
C
```

```
      DO 3000 I=1,M
      DO 3000 J=2,N
      PSI(I,J)=0.0
      II=I-1
      JJ=J-1
      XI=(FLOAT(II))*XS
      YI=(FLOAT(JJ))*YS
C
      DO 50 KL=1,K
      X=(FLOAT(KL)-0.5)*DELX+XO
C
      IF(X-XO.GT.XL) GO TO 20
```

```
      IF(X-XO.GT.10.5) GO TO 10
C
C     3-D REGION
      DELPSI=1.0/62.0/XL*SQRT(X-XO)*DELX*
     1(ATAN((X+XI)/YI)-ATAN((X-XI)/YI))*200.0
      GO TO 45
C
C     2-D MOMENTUM REGION
10    DELPSI=1.0/28.5/XL*DELX*(ATAN((X+XI)/YI)-ATAN((X-XI)/YI))*200.0
      GO TO 45
C
C     2-D JET REGION
20    DELPSI=1.0/91.1/XL/SQRT(0.195/XL*(X-XO)-0.0976)*DELX*
     1(ATAN((X+XI)/YI)-ATAN((X-XI)/YI))*200.0
C
45    PSI(I,J)=PSI(I,J)+DELPSI
50    CONTINUE
C
3000  CONTINUE
C
      WRITE(6,3500)
3500  FORMAT(1H1)
      WRITE(6,4000)((PSI(I,J),J=1,N,L),I=1,M,L)
4000  FORMAT('-',13F5.1)
      WRITE(6,3500)
      STOP
      END
```

APPENDIX D

EULERIAN DESCRIPTION OF A STAGED DIFFUSER ON A SLOPING BOTTOM

In this appendix, we develop Eulerian equations describing the near field of a staged diffuser on a sloping bottom. The analysis is very similar to that of Almquist and Stolzenbach (1976) for water of constant depth. We assume a stagnant ambient body of water with semi-infinite lateral dimensions. The diffuser is treated as a line source of momentum and the near field is divided into an initial region, a momentum region and a jet region (see Figure 2-6). In the initial region, the plume does not intersect the water surface and it is assumed to behave like a round jet with continuous momentum input. The plume in the momentum region is assumed to be vertically well mixed and it is treated as a confined jet with continuous momentum input. The plume in the jet region is also assumed to be fully mixed, and it is treated as a confined jet with no additional momentum input. Velocity and temperature profiles in each region are assumed to be similar, and an entrainment hypothesis is used that relates plume centerline velocity and entrainment velocity. Buoyancy is neglected.

Assuming that momentum and heat diffuse in nearly the same manner (the Reynolds analogy) we can express the similarity assumption as

$$\frac{\Delta T}{\Delta T_c} = \frac{u}{u_c} = f_i(\eta) \qquad \text{initial region}$$

$$\frac{\Delta T}{\Delta T_c} = \frac{u}{u_c} = f_m(\eta) \qquad \text{momentum region} \qquad \text{(D-1)}$$

$$\frac{\Delta T}{\Delta T_c} = \frac{u}{u_c} = f_j(\eta) \qquad \text{jet region}$$

where

$$\eta = \frac{r}{b} \qquad \text{initial region}$$

$$\eta = \frac{y}{b} \qquad \text{momentum and jet regions.}$$

We define the kinematic momentum flux M as

$$M = \int_A u^2 dA_c$$

where A_c is the plume cross-sectional area. The entrained flowrate and the kinematic momentum flux can be written as

$$\left.\begin{aligned} Q_E &= \pi b^2 u_c I_1 \\ M &= \pi b^2 u_c^2 I_2 \end{aligned}\right\} \quad \text{initial region}$$

$$\left.\begin{aligned} Q_E &= 2bHu_c I_3 \\ M &= 2bHu_c^2 I_4 \end{aligned}\right\} \quad \text{momentum region} \qquad \text{(D-2)}$$

$$\left.\begin{aligned} Q_E &= 2bHu_c I_5 \\ M &= 2bHu_c^2 I_6 \end{aligned}\right\} \quad \text{jet region}$$

where

$$I_1 = \int_o^\infty f_i(\eta)\eta d\eta$$

$$I_2 = \int_o^\infty f_i^2(\eta)\eta d\eta$$

$$I_3 = \int_o^\infty f_m(\eta) d\eta$$

$$I_4 = \int_o^\infty f_m^2(\eta) d\eta$$

$$I_5 = \int_o^\infty f_j(\eta)d\eta$$

$$I_6 = \int_o^\infty f_j^2(\eta)d\eta \qquad \text{(D-3)}$$

The entrainment hypothesis is

$$v_e = \alpha_i u_c \quad \text{initial region}$$

$$v_e = \alpha_m u_c \quad \text{momentum region} \qquad \text{(D-4)}$$

$$v_e = \alpha_j u_c \quad \text{jet region}$$

where

v_e = entrainment velocity at the width b

α = entrainment coefficient, assumed constant.

Having defined these terms, we can now proceed with the analysis.

Initial region $(x_o \leq x \leq x_T)$

Since the plume does not intersect the water surface in the initial region, the varying depth has no effect on the plume behavior. The equations describing this region are essentially the same as those describing the 3-D region of Almquist and Stolzenbach, with x replaced by $x-x_o$, H replaced by H_o, and $\mathbb{K}$ replaced by $\mathbb{K}_o$. The equations are easily found to be

$$\frac{u_c}{u_o} = \frac{3}{2\sqrt{\pi}} \frac{I_1}{\sqrt{I_2}} \frac{1}{\alpha_i} \frac{1}{\mathbb{K}_o} \left(\frac{x}{H_o} - \frac{x_o}{H_o}\right)^{-1/2} \qquad \text{(D-5)}$$

$$\frac{b}{H_o} = \frac{2}{3} \frac{\alpha_i}{I_1} \left(\frac{x}{H_o} - \frac{x_o}{H}\right) \qquad \text{(D-6)}$$

$$\frac{Q_E}{Q_o} = \frac{2\sqrt{\pi}}{3} \frac{\alpha_i}{\sqrt{I_2}} \mathbb{K}_o \left(\frac{H_o}{L}\right)\left(\frac{x}{H_o} - \frac{x_o}{H_o}\right)^{3/2} \qquad \text{(D-7)}$$

Momentum region $(x_T \leq x \leq x_o + L)$

The governing equations in the momentum region are

$$\text{continuity:} \quad \frac{dQ_E}{dx} = 2 \frac{H_o}{x_o} \alpha_m \, x \, u_c \tag{D-8}$$

$$\text{momentum:} \quad \frac{dM}{dx} = \frac{Q_o u_o}{L} \tag{D-9}$$

with

$$Q_E = 2 \frac{H_o}{x_o} I_3 x b u_c \tag{D-10}$$

$$M = 2 \frac{H_o}{x_o} I_4 x b u_c^2 \tag{D-11}$$

from equations D-2.

To solve these governing equations, first combine equations D-8 and D-10 to get

$$\frac{d}{dx} (x b u_c) = \frac{\alpha_m}{I_3} x u_c \tag{D-12}$$

Integration of equation D-9, with the boundary condition that M=0 at $x=x_o$ yields

$$M = \frac{Q_o u_o}{L} (x - x_o) \tag{D-13}$$

Combining this result with equation D-11 one finds

$$x u_c = \frac{1}{2 \frac{H_o}{x_o} I_4} \frac{Q_o u_o}{L} \left(\frac{x - x_o}{b u_c}\right) \tag{D-14}$$

Substituting equation D-14 into equation D-12, we have

$$\frac{d}{dx} (x b u_c) = \frac{\alpha_m}{I_3} \frac{1}{2 \frac{H_o}{x_o} I_4} \frac{Q_o u_o}{L} \left(\frac{x - x_o}{b u_c}\right) \tag{D-15}$$

After integration and some rearrangement, equation D-15 becomes

$$\frac{x}{H_o}\frac{b}{H_o}\frac{u_c}{u_o} = \sqrt{\frac{\alpha_m}{I_3 I_4}}\sqrt{\frac{x_o}{H_o}}\ \frac{1}{\mathbb{K}_o}\left\{\frac{1}{3}\left(\frac{x}{H_o}\right)^3 - \frac{1}{2}\left(\frac{x_o}{H_o}\right)\left(\frac{x}{H_o}\right)^2 + C_1\right\}^{1/2} \tag{D-16}$$

where C_1 is an arbitrary constant of integration. Equation D-14 can be written

$$\frac{b}{H_o}\frac{u_c}{u_o} = \frac{u_o}{u_c}\frac{1}{2I_4}\frac{1}{\mathbb{K}_o^2}\left(\frac{x_o}{H_o}\right)\left(\frac{H_o}{x}\right)\left(\frac{x}{H_o} - \frac{x_o}{H_o}\right) \tag{D-17}$$

and combinined with equations D-16 to solve for $\frac{u_c}{u_o}$:

$$\frac{u_c}{u_o} = \frac{1}{2}\sqrt{\frac{I_3}{\alpha_m I_4}}\sqrt{\frac{x_o}{H_o}}\ \frac{1}{\mathbb{K}_o}\left(\frac{x}{H_o} - \frac{x_o}{H_o}\right)\left\{\frac{1}{3}\left(\frac{x}{H_o}\right)^3 - \frac{1}{2}\left(\frac{x_o}{H_o}\right)\left(\frac{x}{H_o}\right)^2 + C_1\right\}^{-1/2} \tag{D-18}$$

Using this result in equation D-17, we get

$$\frac{b}{H_o} = \frac{2\alpha_m}{I_3}\frac{1}{\frac{x}{H_o}\left(\frac{x}{H_o} - \frac{x_o}{H_o}\right)}\left\{\frac{1}{3}\left(\frac{x}{H}\right)^3 - \frac{1}{2}\left(\frac{x_o}{H_o}\right)\left(\frac{x}{H_o}\right)^2 + C_1\right\} \tag{D-19}$$

Equations D-18 and D-19 can now be combined in the definition of Q_E, equation D-10, to find

$$\frac{Q_E}{Q_o} = 2\sqrt{\frac{\alpha_m I_3}{I_4}}\sqrt{\frac{H_o}{x_o}}\left(\frac{H_o}{L}\right)\ \mathbb{K}_o\left\{\frac{1}{3}\left(\frac{x}{H_o}\right)^3 - \frac{1}{2}\left(\frac{x_o}{H_o}\right)\left(\frac{x}{H_o}\right)^2 + C_1\right\}^{1/2} \tag{D-20}$$

In order to find the constant C_1, we match the equation for $\frac{Q_E}{Q_o}$ in the initial region with the equation for $\frac{Q_E}{Q_o}$ in the momentum region at $x=x_T$. That is, we require $\frac{Q_E}{Q_o}$ to be continuous at $x=x_T$. By so doing, we find that

$$C_1 = \frac{\pi}{9} \frac{I_4}{I_2 I_3} \frac{\alpha_i^2}{\alpha_m} \frac{x_o}{H_o} \left(\frac{x_T}{H_o} - \frac{x_o}{H_o}\right)^3$$

$$+ \frac{1}{2} \left(\frac{x_o}{H_o}\right)\left(\frac{x_T}{H_o}\right)^2 - \frac{1}{3} \left(\frac{x_T}{H_o}\right)^3 \qquad \text{(D-21)}$$

Note that the choice of x_T is left orbitrary. One reasonable choice is the value of x at which the plume intersects the surface, as determined from the expression for b in the initial region.

Jet region $\quad x_o + L \leq x$

The governing equations in the jet region are

$$\text{continuity:} \quad \frac{dQ_E}{dx} = 2 \frac{H_o}{x_o} \alpha_j \, x u_c \qquad \text{(D-22)}$$

$$\text{momentum:} \quad \frac{dM}{dx} = 0 \qquad \text{(D-23)}$$

and we have the definitions

$$Q_E = 2 \frac{H_o}{x_o} I_5 \, b x u_c \qquad \text{(D-24)}$$

$$M = 2 \frac{H_o}{x_o} I_6 \, b x u_c^2 \qquad \text{(D-25)}$$

from equations D-2.

To solve these equations, equations D-22 and D-24 are combined to yield

$$\frac{d}{dx}(xbu_c) = \frac{\alpha_j}{I_5} xu_c \tag{D-26}$$

The integrated momentum equation is simply

$$M = Q_o u_o \tag{D-27}$$

which may be combined with equation D-25 to find

$$xu_c = \frac{1}{2\frac{H_o}{x_o} I_6} Q_o u_o \left(\frac{1}{u_c b}\right) \tag{D-28}$$

Equations D-28 and D-26 may be combined to obtain

$$xbu_c \frac{d}{dx}(xbu_c) = \frac{1}{2I_5 I_6} \frac{\frac{\alpha_j}{H_o}}{\frac{}{x_o}} Q_o u_o x$$

which can be integrated and rearranged to give

$$\left(\frac{x}{H_o}\frac{b}{H_o}\frac{u_c}{u_o}\right)^2 = \frac{\alpha_j}{2I_5 I_6}\frac{x_o}{H_o}\frac{1}{\mathbb{K}_o^2}\frac{L}{H_o}\left[\left(\frac{x}{H_o}\right)^2 + C_2\right] \tag{D-29}$$

where C_2 is an arbitrary constant of integration. Equations D-29 and D-24 are now combined to give

$$\frac{Q_E}{Q_o} = \sqrt{\frac{2I_5}{I_6}}\sqrt{\frac{H_o}{x_o}}\sqrt{\alpha_j}\ \mathbb{K}_o\sqrt{\frac{H_o}{L}}\left\{\left(\frac{x}{H_o}\right)^2 + C_2\right\}^{1/2} \tag{D-30}$$

The constant C_2 is found by matching $\frac{Q_E}{Q_o}$ in the jet region with $\frac{Q_E}{Q_o}$ in the momentum region at x=L. This boundary condition gives

$$C_2 = 2\frac{I_3}{I_4}\frac{I_6}{I_5}\frac{\alpha_m}{\alpha_j}\left(\frac{H_o}{L}\right)\left\{\frac{1}{3}\left[\left(\frac{x_o+L}{H_o}\right)^3 - \left(\frac{x_T}{H_o}\right)^3\right]\right.$$

$$- \frac{1}{2}\frac{x_o}{H_o}\left[\left(\frac{x_o+L}{H_o}\right)^2 - \left(\frac{x_T}{H_o}\right)^2\right] \qquad \text{(D-31)}$$

$$\left. + \frac{\pi}{9}\frac{I_4}{I_2 I_3}\frac{\alpha_i^2}{\alpha_m}\frac{x_o}{H_o}\left(\frac{x_T}{H_o} - \frac{x_o}{H_o}\right)^3\right\} - \left(\frac{x_o+L}{H_o}\right)^2$$

Equations D-28 and D-29 can be combined to find

$$\frac{u_c}{u_o} = \sqrt{\frac{I_5}{2I_6}}\frac{1}{\sqrt{\alpha_j}}\sqrt{\frac{x_o}{H_o}}\sqrt{\frac{L}{H_o}}\frac{1}{\mathbb{K}_o}\left\{\left(\frac{x}{H_o}\right)^2 + C_2\right\}^{-1/2} \qquad \text{(D-32)}$$

Finally this result can be put in equation D-29 to give

$$\frac{b}{H_o} = \frac{\alpha_j}{I_5}\left(\frac{H_o}{x}\right)\left\{\left(\frac{x}{H_o}\right)^2 + C_2\right\} . \qquad \text{(D-33)}$$

Summary

Initial region $(x_o \leq x \leq x_T)$

$$\frac{u_c}{u_o} = \frac{3}{2\sqrt{\pi}}\frac{I_1}{\sqrt{I_2}}\frac{1}{\alpha_i}\frac{1}{\mathbb{K}_o}\left(\frac{x}{H_o} - \frac{x_o}{H_o}\right)^{-1/2}$$

$$\frac{b}{H_o} = \frac{2}{3}\frac{\alpha_i}{I_1}\left(\frac{x}{H_o} - \frac{x_o}{H_o}\right) \qquad \text{(D-34)}$$

$$\frac{Q_E}{Q_o} = \frac{2\sqrt{\pi}}{3}\frac{2i}{\sqrt{I_2}}\mathbb{K}_o\left(\frac{H_o}{L}\right)\left(\frac{x}{H_o} - \frac{x_o}{H_o}\right)^{3/2}$$

Momentum region $(x_T \leq x \leq x_o + L)$

$$\frac{u_c}{u_o} = \frac{1}{2}\sqrt{\frac{I_3}{\alpha_m I_4}}\sqrt{\frac{x_o}{H_o}}\ \frac{1}{\mathbb{K}_o}\left(\frac{x}{H_o} - \frac{x_o}{H_o}\right)\left\{\frac{1}{3}\left(\frac{x}{H_o}\right)^3 - \frac{1}{2}\left(\frac{x_o}{H_o}\right)\left(\frac{x}{H_o}\right)^2 + C_1\right\}^{-1/2}$$

$$\frac{b}{H_o} = \frac{2\alpha_m}{I_3}\frac{1}{\frac{x}{H_o}\left(\frac{x}{H_o} - \frac{x_o}{H_o}\right)}\left\{\frac{1}{3}\left(\frac{x}{H_o}\right)^3 - \frac{1}{2}\left(\frac{x_o}{H_o}\right)\left(\frac{x}{H_o}\right)^2 + C_1\right\} \qquad \text{(D-35)}$$

$$\frac{Q_E}{Q_o} = 2\sqrt{\frac{\alpha_m I_3}{I_4}}\sqrt{\frac{H_o}{x_o}}\left(\frac{H_o}{L}\right)\ \mathbb{K}_o\left\{\frac{1}{3}\left(\frac{x}{H_o}\right)^3 - \frac{1}{2}\left(\frac{x_o}{H_o}\right)\left(\frac{x}{H_o}\right)^2 + C_1\right\}^{1/2}$$

$$C_1 = \frac{\pi}{9}\frac{I_4}{I_2 I_3}\frac{\alpha_i^2}{\alpha_m}\frac{x_o}{H_o}\left(\frac{x_T}{H_o} - \frac{x_o}{H_o}\right)^3$$

$$+ \frac{1}{2}\left(\frac{x_o}{H_o}\right)\left(\frac{x_T}{H_o}\right)^2 - \frac{1}{3}\left(\frac{x_T}{H_o}\right)^3$$

Jet region $(x_o + L \leq x)$

$$\frac{u_c}{u_o} = \sqrt{\frac{I_5}{2I_6}}\ \frac{1}{\sqrt{\alpha_j}}\sqrt{\frac{x_o}{H_o}}\sqrt{\frac{L}{H_o}}\ \frac{1}{\mathbb{K}_o}\left\{\left(\frac{x}{H_o}\right)^2 + C_2\right\}^{-1/2}$$

$$\frac{b}{H_o} = \frac{\alpha_j}{I_5}\frac{H_o}{x}\ \left(\frac{x}{H_o}\right)^2 + C_2\}$$

$$\frac{Q_E}{Q_o} = \sqrt{\frac{2I_5}{I_6}}\ \sqrt{\alpha_j}\ \sqrt{\frac{H_o}{x_o}}\sqrt{\frac{H_o}{L}}\ \mathbb{K}_o\left\{\left(\frac{x}{H_o}\right)^2 + C_2\right\}^{1/2}$$

$$C_2 = 2\frac{I_3}{I_4}\frac{I_6}{I_5}\frac{\alpha_m}{\alpha_j}\frac{H_o}{L}\left\{\frac{1}{3}\left[\left(\frac{x_o+L}{H_o}\right)^3 - \left(\frac{x_T}{H_o}\right)^3\right]\right.$$

$$- \frac{1}{2}\frac{x_o}{H_o}\left[\left(\frac{x_o+L}{H_o}\right)^2 - \left(\frac{x_T}{H_o}\right)^2\right]$$

$$\left. + \frac{\pi}{9}\frac{I_4}{I_2 I_3}\frac{\alpha_i^2}{\alpha_m}\frac{x_o}{H_o}\left(\frac{x_T}{H_o} - \frac{x_o}{H_o}\right)^3\right\} - \left(\frac{x_o+L}{H_o}\right)^2 \qquad \text{(D-36)}$$

Profile Parameters

If we assume Gaussian velocity and temperature profiles, the similarity functions are

$$f_i = f_m = f_j = e^{-\eta^2} \quad .$$

The corresponding values of the various constants are

$$I_1 = \frac{1}{2}$$

$$I_2 = \frac{1}{4}$$

$$I_3 = I_5 = \sqrt{\frac{\pi}{4}}$$

$$I_4 = I_6 = \sqrt{\frac{\pi}{8}}$$

$$\alpha_i = .057$$

$$\alpha_m = \alpha_j = .069 \quad .$$

where we have used the accepted value of α for round jets in the initial region and the accepted value of α for plane jets in the momentum and jet regions. Using these values, the equations become

Initial region $(x_o \leq x \leq x_T)$

$$\frac{u_c}{u_o} = \frac{14.9}{\mathbb{K}_o} \left(\frac{x}{H_o} - \frac{x_o}{H_o}\right)^{-1/2}$$

$$\frac{b}{H_o} = .076 \left(\frac{x}{H_o} - \frac{x_o}{H_o}\right) \qquad \text{(D-37)}$$

$$\frac{Q_E}{Q_o} = .135 \ \mathbb{K}_o \frac{H_o}{L} \left(\frac{x}{H_o} - \frac{x_o}{H_o}\right)^{3/2}$$

Momentum region $(x_T \leq x \leq x_o + L)$

$$\frac{u_c}{u_o} = 2.26 \frac{1}{\mathbb{K}_o} \sqrt{\frac{x_o}{H_o}} \left(\frac{x}{H_o} - \frac{x_o}{H_o}\right) \left\{\frac{1}{3}\left(\frac{x}{H_o}\right)^3 - \frac{1}{2}\left(\frac{x_o}{H_o}\right)\left(\frac{x}{H_o}\right)^2 + C_1\right\}^{-1/2}$$

$$\frac{b}{H_o} = (.156) \frac{1}{\frac{x}{H_o}\left(\frac{x}{H_o} - \frac{x_o}{H_o}\right)} \left\{\frac{1}{3}\left(\frac{x}{H_o}\right)^3 - \frac{1}{2}\left(\frac{x_o}{H_o}\right)\left(\frac{x}{H_o}\right)^2 + C_1\right\} \qquad \text{(D-38)}$$

$$\frac{Q_E}{Q_o} = .625 \sqrt{\frac{H_o}{x_o}} \left(\frac{H_o}{L}\right) \mathbb{K}_o \left\{\frac{1}{3}\left(\frac{x}{H_o}\right)^3 - \frac{1}{2}\left(\frac{x_o}{H_o}\right)\left(\frac{x}{H_o}\right)^2 + C_1\right\}^{1/2}$$

$$C_1 = .0465 \frac{x_o}{H_o}\left(\frac{x_T}{H_o} - \frac{x_o}{H_o}\right)^3 + \frac{1}{2}\left(\frac{x_o}{H_o}\right)\left(\frac{x_T}{H_o}\right)^2 - \frac{1}{3}\left(\frac{x_T}{H_o}\right)^3$$

Jet region $(x_o + L \leq x)$

$$\frac{u_c}{u_o} = \frac{3.20}{\mathbb{K}_o} \sqrt{\frac{x_o}{H_o}} \sqrt{\frac{L}{H_o}} \left\{ \left(\frac{x}{H_o}\right)^2 + C_2 \right\}^{-1/2}$$

$$\frac{b}{H_o} = .078 \frac{H_o}{x} \left\{ \left(\frac{x}{H_o}\right)^2 + C_2 \right\}$$

$$\frac{Q_E}{Q_o} = .442 \sqrt{\frac{H_o}{x_o}} \sqrt{\frac{H_o}{L}} \; \mathbb{K}_o \left\{ \left(\frac{x}{H_o}\right)^2 + C_2 \right\}^{1/2} \qquad \text{(D-39)}$$

$$C_2 = -\frac{H_o}{L} \left\{ \frac{1}{3} \left[\left(\frac{x_o+L}{H_o}\right)^3 - \left(\frac{x_T}{H_o}\right)^3 \right] \right.$$

$$- \frac{1}{2} \frac{x_o}{H_o} \left[\left(\frac{x_o+L}{H_o}\right)^2 - \left(\frac{x_T}{H_o}\right)^2 \right]$$

$$\left. + .0465 \frac{x_o}{H_o} \left(\frac{x_T}{H_o} - \frac{x_o}{H_o}\right)^3 \right\} - \left(\frac{x_o+L}{H_o}\right)^2$$

Asymptotic values of the solution

In the limit as x_o approaches infinity, the bottom slope becomes zero and the water depth is a constant value H_o. If we evaluate equations D-34 through D-36 under these limiting conditions, we can show that these equations approach the solution of Almquist and Stolzenbach (1976) for water of constant depth. We will show that this is true for the dilution, S^*. The procedure is similar for the other variables. In order to proceed, we define

$$x' = x - x_o \qquad \text{(D-40)}$$

$$x_T' = x_T - x_o \qquad \text{(D-41)}$$

so that x' has its origin at the upstream end of the diffuser. This corresponds to the origin of x in the analysis of Almquist and Stolzenbach (1976).

In the initial region, we have

$$\frac{Q_E}{Q_o} = \frac{2\sqrt{\pi}}{3} \frac{\alpha_i}{\sqrt{I_2}} \mathbb{K}_o \frac{H_o}{L} \left(\frac{x}{H_o} - \frac{x_o}{H_o}\right)^{3/2} \tag{D-42}$$

$$S^* = \frac{Q_E}{Q_o \left(\frac{x-x_o}{L}\right)} \quad .$$

Combining equations D-41 and D-42, we get

$$S^* = \frac{2\sqrt{\pi}}{3} \frac{\alpha_i}{\sqrt{I_2}} \mathbb{K}_o \left(\frac{x'}{H_o}\right)^{1/2} \tag{D-43}$$

As x_o approaches infinity and the water depth approaches a constant value H, equation D-43 becomes

$$S^* = \frac{2\sqrt{\pi}}{3} \frac{\alpha_i}{\sqrt{I_2}} \mathbb{K} \left(\frac{x'}{H}\right)^{1/2} \tag{D-44}$$

which is the expression obtained by Almquist and Stolzenbach (1976) for the 3-D region.

In the momentum region, we have

$$\frac{Q_E}{Q_o} = 2\sqrt{\frac{\alpha_m I_3}{I_4}} \sqrt{\frac{H_o}{x_o}} \left(\frac{H_o}{L}\right) \mathbb{K}_o \left\{\frac{1}{3}\left(\frac{x}{H_o}\right)^3 - \frac{1}{2}\left(\frac{x_o}{H_o}\right)\left(\frac{x}{H_o}\right)^2 + \frac{\pi}{9} \frac{I_4}{I_2 I_3} \frac{\alpha_i^2}{\alpha_m} \frac{x_o}{H_o} \left(\frac{x_T}{H_o} - \frac{x_o}{H_o}\right)^3\right.$$

$$+ \frac{1}{2}\left(\frac{x_o}{H_o}\right)\left(\frac{x_T}{H_o}\right)^2 - \frac{1}{3}\left(\frac{x_T}{H_o}\right)^3 \Big\}^{1/2}$$

$$S^* = \frac{Q_E}{Q_o\left(\frac{x-x_o}{L}\right)} \qquad \text{(D-45)}$$

Combining equations D-45 and D-40, we obtain

$$S^* = 2\sqrt{\frac{\alpha_m I_3}{I_4}}\sqrt{\frac{H_o}{x_o}}\left(\frac{H_o}{L}\right) \mathbb{K}_o\left(\frac{L}{x'}\right)\left\{\frac{1}{3}\left(\frac{x'+x_o}{H_o}\right)^3\right.$$

$$- \frac{1}{2}\frac{x_o}{H_o}\left(\frac{x'+x_o}{H_o}\right)^2 + \frac{\pi}{9}\frac{I_4}{I_2 I_3}\frac{\alpha_i^2}{\alpha_m}\frac{x_o}{H_o}\left(\frac{x_T'}{H_o}\right)^3 \qquad \text{(D-46)}$$

$$\left. + \frac{1}{2}\left(\frac{x_o}{H_o}\right)\left(\frac{x_T'+x_o}{H_o}\right)^2 - \frac{1}{3}\left(\frac{x_T'+x_o}{H_o}\right)^3 \right\}^{1/2}$$

Equation D-46 can be simplified to yield

$$S^* = 2\sqrt{\frac{\alpha_m I_3}{I_4}}\sqrt{\frac{H_o}{x_o}}\,\frac{H_o}{L}\,\mathbb{K}_o\,\frac{L}{x'}\left\{\frac{1}{3}\left(\frac{x'}{H_o}\right)^3\right.$$

$$+ \frac{1}{2}\left(\frac{x'}{H_o}\right)^2\left(\frac{x_o}{H_o}\right) + \frac{\pi}{9}\frac{I_4}{I_2 I_3}\frac{\alpha_i^2}{\alpha_m}\frac{x_o}{H_o}\left(\frac{x_T'}{H_o}\right)^3 \qquad \text{(D-47)}$$

$$\left. - \frac{1}{2}\frac{x_o}{H_o}\left(\frac{x_T'}{H_o}\right)^2 - \frac{1}{3}\left(\frac{x_T'}{H_o}\right)^3 \right\}^{1/2}$$

As x_o becomes very large and the depth approaches a constant value H, equation D-47 becomes

$$S^* = 2\sqrt{\frac{\alpha_m I_3}{I_4}}\sqrt{\frac{H}{x_o}}\left(\frac{H}{L}\right) \mathbb{K} \frac{L}{x'}\left\{\frac{1}{2}\left(\frac{x'}{H}\right)^2\left(\frac{x_o}{H}\right)\right.$$

$$\left. + \frac{\pi}{9}\frac{I_4}{I_2 I_3}\frac{\alpha_i^2}{\alpha_m}\frac{x_o}{H}\left(\frac{x_T'}{H}\right)^3 - \frac{1}{2}\frac{x_o}{H}\left(\frac{x_T'}{H}\right)^2\right\}^{1/2} \qquad \text{(D-48)}$$

or

$$S^* = \frac{I_3}{I_4} \mathbb{K} \left\{2\alpha_m \frac{I_4}{I_3} + \left(\frac{x_T'}{H}\right)^2\left[\frac{4\pi}{9}\frac{I_4^2}{I_3^2 I_2}\alpha_i^2\frac{x_T'}{H}\right.\right.$$

$$\left.\left. -2\alpha_m\frac{I_4}{I_3}\right]\left(\frac{H}{x'}\right)^2\right\}^{1/2} \qquad \text{(D-49)}$$

which is the expression obtained by Almquist and Stolzenbach (1976) for the 2-D momentum region.

In the jet region, we have

$$\frac{Q_E}{Q_o} = \sqrt{\frac{2I_5}{I_6}}\sqrt{\alpha_j}\sqrt{\frac{H_o}{x_o}}\sqrt{\frac{H_o}{L}} \mathbb{K}_o \left\{\left(\frac{x}{H_o}\right)^2 + C_2\right\}^{1/2}$$

$$C_2 = 2\frac{I_3}{I_4}\frac{I_6}{I_5}\frac{\alpha_m}{\alpha_j}\frac{H_o}{L}\left\{\frac{1}{3}\left[\left(\frac{x_o+L}{H_o}\right)^3 - \left(\frac{x_T}{H_o}\right)^3\right]\right.$$

$$- \frac{1}{2}\frac{x_o}{H_o}\left[\left(\frac{x_o+L}{H_o}\right)^2 - \left(\frac{x_T}{H_o}\right)^2\right] \qquad \text{(D-50)}$$

$$\left. + \frac{\pi}{9}\frac{I_4}{I_2 I_3}\frac{\alpha_i^2}{\alpha_m}\frac{x_o}{H_o}\left(\frac{x_T}{H_o} - \frac{x_o}{H_o}\right)^3\right\} - \left(\frac{x_o+L}{H_o}\right)^2$$

$$S^* = \frac{Q_E}{Q_o}$$

The expression $\left(\frac{x}{H_o}\right)^2 + C_2$ can be put in terms of the definitions D-40 and D-41:

$$\left(\frac{x}{H_o}\right)^2 + C_2 = \left(\frac{x_o+x'}{Ho}\right)^2 + 2\,\frac{I_3}{I_4}\,\frac{I_6}{I_5}\,\frac{\alpha_m}{\alpha_j}\,\frac{Ho}{L}\,\left\{\frac{1}{3}\left[\left(\frac{x_o+L}{Ho}\right)^3 - \left(\frac{x_T'+x_o}{Ho}\right)^3\right] - \frac{1}{2}\,\frac{x_o}{Ho}\left[\left(\frac{x_o+L}{Ho}\right)^2 - \left(\frac{x_T'+x_o}{Ho}\right)^2\right] + \frac{\pi}{9}\,\frac{I_4}{I_2 I_3}\,\frac{\alpha_i^2}{\alpha_m}\,\frac{x_o}{Ho}\left(\frac{x_T'}{Ho}\right)^3\right\} - \left(\frac{x_o+L}{Ho}\right)^2 \qquad \text{(D-51)}$$

This equation can be simplified to yield

$$\left(\frac{x}{Ho}\right)^2 + C_2 = \left(\frac{x'}{Ho}\right)^2 + 2\,\frac{x_o}{Ho}\left(\frac{x'}{Ho} - \frac{L}{Ho}\right) - \left(\frac{L}{Ho}\right)^2 + 2\,\frac{I_3}{I_4}\,\frac{I_6}{I_5}\,\frac{\alpha_m}{\alpha_j}\,\frac{Ho}{L}\left\{\frac{1}{2}\,\frac{x_o}{Ho}\left(\frac{L}{Ho}\right)^2 - \frac{1}{2}\,\frac{x_o}{Ho}\left(\frac{x_T'}{Ho}\right) + \frac{\pi}{9}\,\frac{I_4}{I_2 I_3}\,\frac{\alpha_i^2}{\alpha_m}\,\frac{x_o}{Ho}\left(\frac{x_T'}{Ho}\right)^3\right\} \qquad \text{(D-52)}$$

As x_o becomes very large and as the depth approaches a constant value H, equation D-52 becomes

$$\left(\frac{x}{Ho}\right)^2 + C_2 = 2\,\frac{x_o}{Ho}\left(\frac{x'}{Ho} - \frac{L}{Ho}\right) + 2\,\frac{I_3}{I_4}\,\frac{I_6}{I_5}\,\frac{\alpha_m}{\alpha_j}\,\frac{Ho}{L}\,\frac{x_o}{Ho}\left\{\frac{1}{2}\left(\frac{L}{Ho}\right)^2 - \frac{1}{2}\left(\frac{x_T'}{Ho}\right)^2 + \frac{\pi}{9}\,\frac{I_4}{I_2 I_3}\,\frac{\alpha_i^2}{\alpha_m}\left(\frac{x_T'}{Ho}\right)^3\right\} \qquad \text{(D-53)}$$

Under these conditions, the expression for S^* becomes

$$S^* = \frac{I_5}{I_6} 1K \{4\alpha_j \frac{I_6}{I_5}\frac{x'}{L} + 2(\frac{I_6}{I_5}\frac{I_3}{I_4})^2 [\alpha_m \frac{I_4}{I_3}$$

$$+ (\frac{x_T'}{L})^2 (\frac{2\pi}{9} \frac{I_4^2}{I_3^2 I_2} \alpha_i^2 \frac{x_T'}{H} - \alpha_m \frac{I_4}{I_3})]$$

$$-4\alpha_j \frac{I_6}{I_5}\}^{1/2}$$

which is the expression obtained by Almquist and Stolzenbach (1976) for the 2-D jet region.

APPENDIX E

LAGRANGIAN DESCRIPTION OF A STAGED DIFFUSER ON A SLOPING BOTTOM

In this appendix we will develop a Lagrangian description of a staged diffuser plume on a sloping bottom, based on the Eulerian equations presented in Appendix E. Our work is based on the following assumptions:

(1) An entrained particle moves directly to the plume centerline, and then moves along the centerline at the mean centerline velocity.

(2) The particle experiences temperatures equal to the mean centerline temperatures.

(3) The particle experiences shear stresses given by $\tau = C\rho u_c^2$, where ρ = water density, u_c = plume centerline velocity, and C = constant of order .05.

The assumptions made in Appendix D are also implicitly made here.

To find Lagrangian equations, we integrate the expressions for velocity to get position of the moving particle as a function of time. The equations for position as a function of time are then combined with the Eulerian expressions for temperature and shear stress to give these quantities as functions of time for the moving particle. In the initial region we have (see Appendix D)

$$\frac{dx}{dt} = u_c = u_o \frac{3}{2\sqrt{\pi}} \frac{I_1}{\sqrt{I_2}} \frac{1}{\alpha_i} \frac{1}{\mathbb{K}_o} \left(\frac{x}{H_o} - \frac{x_o}{H_o}\right)^{-1/2} \qquad \text{(E-1)}$$

Integration of this expression gives

$$\frac{x}{H_o} = \frac{x_o}{H_o} + \left\{\left(\frac{x_{e,i}}{H_o} - \frac{x_o}{H_o}\right)^{3/2} + \frac{9}{4\sqrt{\pi}} \frac{I_1}{\sqrt{I_2}} \frac{1}{\alpha_i} \frac{1}{\mathbb{K}_o} \left(\frac{tu_o}{H_o} - \frac{t_{e,i}u_o}{H_o}\right)\right\}^{2/3} \qquad \text{(E-2)}$$

where

$x_{e,i}$ = point at which the particle enters the initial region

$t_{e,i}$ = time at which the particle enters the initial region

Substituting equation E-2 into the expressions for $\frac{\Delta T}{\Delta T_o}$ and $(\frac{u_c}{u_o})^2$ (see Appendix D) we obtain

$$\frac{\Delta T}{\Delta T_o} = \{\frac{8\pi\sqrt{\pi}}{27} \frac{I_2\sqrt{I_2}}{I_1^3} \alpha_i^3 \mathbb{K}_o^3 (\frac{x_{e,i}}{H_o} - \frac{x_o}{H_o})^{3/2} + \frac{2}{3}\pi \frac{I_2}{I_1^2} \alpha_i^2 \mathbb{K}_o^2 (\frac{tu_o}{H_o} - \frac{t_{e,i}u_o}{H_o})\}^{-1/3} \quad \text{(E-3)}$$

$$\frac{\tau}{C\rho u_o^2} = \{\frac{8\pi\sqrt{\pi}}{27} \frac{I_2\sqrt{I_2}}{I_1^3} \alpha_i^3 \mathbb{K}_o^3 (\frac{x_{e,i}}{H_o} - \frac{x_o}{H_o})^{3/2} + \frac{2}{3}\pi \frac{I_2}{I_1^2} \alpha_i^2 \mathbb{K}_o^2 (\frac{tu_o}{H_o} - \frac{t_{e,i}u_o}{H_o})\}^{-2/3} \quad \text{(E-4)}$$

The equations in the momentum region must be simplified to allow an analytical solution. We do this by setting $x_T = x_o$; that is, we assume that the existence of the initial region has little effect over most of the momentum region. This assumption is similar to the simplifications made in the 2-D momentum region in Appendix B. Using this simplification, we have in the momentum region (see Appendix D).

$$\frac{u_c}{u_o}, \frac{\Delta T_c}{\Delta T_o} \simeq \frac{\sqrt{3}}{2} \sqrt{\frac{I_3}{\alpha_m I_4}} \sqrt{\frac{x_o}{H_o}} \frac{1}{\mathbb{K}_o} (2\frac{x}{H_o} + \frac{x_o}{H_o})^{-1/2} \quad \text{(E-5)}$$

Integrating the expression

$$\frac{dx}{dt} = u_c$$

we get

$$\frac{x}{H_o} = -\frac{1}{2}\frac{x_o}{H_o} + \frac{1}{2}\left\{\left(2\frac{x_{e,m}}{H_o} + \frac{x_o}{H_o}\right)^{3/2} + 3\sqrt{\frac{3}{2}}\sqrt{\frac{I_3}{\alpha_m I_4}}\sqrt{\frac{x_o}{H_o}}\frac{1}{\mathbb{K}_o}\left(\frac{tu_o}{H_o} - \frac{t_{e,m}u_o}{H_o}\right)\right\}^{2/3} \tag{E-6}$$

where

$x_{e,m}$ = point at which the particle enters the momentum region

$t_{e,m}$ = time at which the particle enters the momentum region

Combining equations E-6 and E-5, we get

$$\frac{\Delta T}{\Delta T_o} = \left\{\frac{2}{3}\sqrt{\frac{2}{3}}\left(\frac{\alpha_m I_4}{I_3}\right)^{3/2}\left(\frac{H_o}{x_o}\right)^{3/2}\mathbb{K}_o{}^3\left(2\frac{x_{e,m}}{H_o} + \frac{x_o}{H_o}\right)^{3/2} + 2\frac{\alpha_m I_4}{I_3}\frac{H_o}{x_o}\mathbb{K}_o{}^2\left(\frac{tu_o}{H_o} - \frac{t_{e,m}u_o}{H_o}\right)\right\}^{-1/3} \tag{E-7}$$

$$\frac{\tau}{c\rho u_o{}^2} = \left\{\left(\frac{2}{3}\frac{\alpha_m I_4}{I_3}\frac{H_o}{x_o}\right)^{3/2}\mathbb{K}_o{}^3\left(2\frac{x_{e,m}}{H_o} + \frac{x_o}{H_o}\right)^{3/2} + 2\frac{\alpha_m I_4}{I_3}\frac{H_o}{x_o}\mathbb{K}_o{}^2\left(\frac{tu_o}{H_o} - \frac{t_{e,m}u_o}{H_o}\right)\right\}^{-2/3} \tag{E-8}$$

Integrating the expression

$$\frac{dx}{dt} = u_c$$

in the jet region, we get (see Appendix D)

$$C_2 \ln\left\{\frac{\frac{x}{Ho} + \sqrt{\left(\frac{x}{Ho}\right)^2 + C_2}}{\frac{x_{e,j}}{Ho} + \sqrt{\left(\frac{x_{e,j}}{Ho}\right)^2 + C_2}}\right\} + \frac{x}{H_o}\sqrt{C_2 + \left(\frac{x}{H_o}\right)^2} - \frac{x_{e,j}}{H_o}\sqrt{C_2 + \left(\frac{x_{e,j}}{H_o}\right)^2} \tag{E-9}$$

$$= \frac{\sqrt{2I_5}}{I_6} \frac{1}{\sqrt{\alpha_j}} \sqrt{\frac{x_o}{H_o}} \sqrt{\frac{L}{H_o}} \frac{1}{\mathbb{K}_o} \left(\frac{tu_o}{H_o} - \frac{t_{e,j}u_o}{H_o}\right)$$

where

$x_{e,j}$ = point at which the particle enters the jet region

$t_{e,j}$ = time at which the particle enters the jet region

No explicit solution of equation E-9 for x as a function of t appears to be possible, and there are no reasonable approximations that will simplify the equation sufficiently. Lagrangian equations for position, temperature exposure and shear stress exposure in the jet region must be obtained implicitly from equations E-9 and D-36. It should be noted that to be consistent with the simplifications made in the momentum region, x_T should be set equal to x_o in using these implicit Lagrangian expressions in the jet region. The Lagrangian equations developed in this appendix are summarized below.

Initial region ($x_o \leq x \leq x_T$)

$$\frac{x}{H_o} = \frac{x_o}{H_o} + \left\{\left(\frac{x_{e,i}}{H_o} - \frac{x_o}{H_o}\right)^{3/2} + \frac{9}{4\sqrt{\pi}} \frac{I_1}{\sqrt{I_2}} \frac{1}{\alpha_i} \frac{1}{\mathbb{K}_o} \left(\frac{tu_o}{H_o} - \frac{t_{e,i}u_o}{H_o}\right)\right\}^{2/3}$$

$$\frac{\Delta T}{\Delta T_o} = \left\{\frac{8\pi\sqrt{\pi}}{27} \frac{I_2\sqrt{I_2}}{I_1^3} \alpha_i^3 \mathbb{K}_o^3 \left(\frac{x_{e,i}}{H_o} - \frac{x_o}{H_o}\right)^{3/2} + \frac{2}{3}\pi \frac{I_2}{I_1^2} \alpha_i^2 \mathbb{K}_o^2 \left(\frac{tu_o}{H_o} - \frac{t_{e,i}u_o}{H_o}\right)\right\}^{-1/3} \tag{E-10}$$

$$\frac{\tau}{C\rho u_o} = \left\{\frac{8\pi\sqrt{\pi}}{27} \frac{I_2\sqrt{I_2}}{I_1^3} \alpha_i^3 \mathbb{K}_o^3 \left(\frac{x_{e,i}}{H_o} - \frac{x_o}{H_o}\right)^{3/2} + \frac{2}{3}\pi \frac{I_2}{I_1^2} \alpha_i^2 \mathbb{K}_o^2 \left(\frac{tu_o}{H_o} - \frac{t_{e,i}u_o}{H_o}\right)\right\}^{-2/3}$$

Momentum region ($x_T \leq x \leq x_o + L$)

$$\frac{x}{H_o} = -\frac{1}{2}\frac{x_o}{H_o} + \frac{1}{2}\left\{\left(2\ \frac{x_{e,m}}{H_o} + \frac{x_o}{H_o}\right)^{3/2} + 3\sqrt{\frac{3}{2}}\ \sqrt{\frac{I_3}{\alpha_m I_4}}\sqrt{\frac{x_o}{H_o}}\ \frac{1}{\mathbb{K}_o}\left(\frac{tu_o}{H_o} - \frac{t_{e,m}u_o}{H_o}\right)^{2/3}\right.$$

$$\frac{\Delta T}{\Delta T_o} = \left\{\left(\frac{2}{3}\frac{\alpha_m I_4}{I_3}\frac{H_o}{x_o}\right)^{3/2}\ \mathbb{K}_o^3\ \left(2\ \frac{x_{e,m}}{H_o} + \frac{x_o}{H_o}\right)^{3/2} + 2\ \frac{\alpha_m I_4}{I_3}\frac{H_o}{x_o}\ \mathbb{K}_o^2\ \left(\frac{tu_o}{H_o} - \frac{t_{e,m}u_o}{H_o}\right)\right\}^{-1/3} \qquad \text{(E-11)}$$

$$\frac{\tau}{C\rho u_o^2} = \left\{\left(\frac{2}{3}\frac{\alpha_m I_4}{I_3}\frac{H_o}{x_o}\right)^{3/2}\ \mathbb{K}_o^3\ \left(2\ \frac{x_{e,m}}{H_o} + \frac{x_o}{H_o}\right)^{3/2} + 2\ \frac{\alpha_m I_4}{I_3}\frac{H_o}{x_o}\ \mathbb{K}_o^2\ \left(\frac{tu_o}{H_o} - \frac{t_{e,m}u_o}{H_o}\right)\right\}^{-2/3}$$

Jet region ($x_o + L \leq x$)

$$C_2 \ln\left\{\frac{\sqrt{C_2 + \left(\frac{x}{H_o}\right)^2} + \frac{x}{H_o}}{\sqrt{C_2 + \left(\frac{x_{e,j}}{H_o}\right)} + \frac{x_{e,j}}{H_o}}\right\}$$

$$+ \frac{x}{H_o}\ \sqrt{C_2 + \left(\frac{x}{H_o}\right)^2} - \frac{x_{e,j}}{H_o} - \sqrt{C_2 + \left(\frac{x_{e,j}}{H_o}\right)^2}$$

$$= \sqrt{\frac{2I_5}{I_6}}\ \frac{1}{\sqrt{\alpha_j}}\ \sqrt{\frac{x_o}{H_o}}\sqrt{\frac{L}{H_o}}\ \frac{1}{\mathbb{K}_o}\left(\frac{tu_o}{H_o} - \frac{t_{e,j}u_o}{H_o}\right) \qquad \text{(E-12)}$$

$$\frac{\Delta T}{\Delta T_o} = \sqrt{\frac{I_5}{2I_6}}\ \frac{1}{\sqrt{\alpha_j}}\sqrt{\frac{x_o}{H_o}}\sqrt{\frac{L}{H_o}}\ \frac{1}{\mathbb{K}_o}\left\{\left(\frac{x}{H_o}\right)^2 + c_2\right\}^{-1/2}$$

$$\frac{\tau}{C\rho u_o^2} = \frac{I_5}{2I_6} \frac{1}{\alpha_j} \frac{x_o}{H_o} \frac{L}{H_o} \frac{1}{\mathbb{K}_o} \left\{\left(\frac{x}{H_o}\right)^2 + c_2\right\}^{-1}$$

$$c_2 = 2\frac{I_3}{I_4} \frac{I_6}{I_5} \frac{\alpha_m}{\alpha_j} \left[\frac{x_o}{H_o} \frac{L}{H_o} + \frac{2}{3} \left(\frac{L}{H_o}\right)^2\right] - \left(\frac{x_o + L}{H_o}\right)^2$$

where c_2 has been evaluated for $x_T = x_o$. If we assume Gaussian velocity and temperature profiles, we have

$$I_1 = \frac{1}{2}$$

$$I_2 = \frac{1}{4}$$

$$I_3 = I_5 = \frac{\sqrt{\pi}}{2}$$

$$I_4 = I_6 = \sqrt{\frac{\pi}{8}}$$

$$\alpha_i = .057$$

$$\alpha_m = \alpha_j = .069$$

and the equations become:

Initial region ($x_o \leq x \leq x_T$)

$$\frac{x}{H_o} = \frac{x_o}{H_o} + \left\{\left(\frac{x_{e,i}}{H_o} - \frac{x_o}{H_o}\right)^{3/2} + \frac{22.3}{\mathbb{K}_o} \left(\frac{tu_o}{H_o} - \frac{t_{e,i}u_o}{H_o}\right)\right\}^{2/3} \qquad \text{(E-13)}$$

$$\frac{\Delta T}{\Delta T_o} = \left\{\left(\frac{\mathbb{K}_o}{14.9}\right)^3 \left(\frac{x_{e,i}}{H_o} - \frac{x_o}{H_o}\right)^{3/2} + \left(\frac{\mathbb{K}_o}{12.1}\right)^2 \left(\frac{tu_o}{H_o} - \frac{t_{e,i}u_o}{H_o}\right)\right\}^{-1/3}$$

$$\frac{\tau}{C\rho u_o^2} = \left\{\left(\frac{\mathbb{K}_o}{14.9}\right)^3 \left(\frac{x_{e,i}}{H_o} - \frac{x_o}{H_o}\right)^{3/2} + \left(\frac{\mathbb{K}_o}{12.1}\right)^2 \left(\frac{tu_o}{H_o} - \frac{t_{e,i}u_o}{H_o}\right)\right\}^{-2/3}$$

Momentum region ($x_T \leq x \leq x_o + L$)

$$\frac{x}{H_o} = -\frac{1}{2} \frac{x_o}{H_o} + \frac{1}{2} \left\{\left(2 \frac{x_{e,m}}{H_o} + \frac{x_o}{H_o}\right)^{3/2}\right.$$

$$+ 16.6 \sqrt{\frac{x_o}{H_o}} \frac{1}{\mathbb{K}_o} \left(\frac{tu_o}{H_o} - \frac{t_{e,m} u_o}{H_o}\right)\}^{2/3}$$

$$\frac{\Delta T}{\Delta T_o} = \{\left(\frac{\mathbb{K}_o}{5.54}\right)^3 \left(\frac{H_o}{x_o}\right)^{3/2} \left(2 \frac{x_{e,m}}{H_o} + \frac{x_o}{H_o}\right)^{3/2}$$

$$+ \left(\frac{\mathbb{K}_o}{3.20}\right)^2 \frac{H_o}{x_o} \left(\frac{tu_o}{H_o} - \frac{t_{e,m} u_o}{H_o}\right)\}^{-1/3} \qquad \text{(E-14)}$$

$$\frac{\tau}{C\rho u_o^2} = \{\left(\frac{\mathbb{K}_o}{5.54}\right)^3 \left(\frac{H_o}{x_o}\right)^{3/2} \left(2 \frac{x_{e,m}}{H_o} + \frac{x_o}{H_o}\right)^{3/2}$$

$$+ \left(\frac{\mathbb{K}_o}{3.20}\right)^2 \frac{H_o}{x_o} \left(\frac{tu_o}{H_o} - \frac{t_{e,m} u_o}{H_o}\right)\}^{-2/3}$$

Jet region ($x_o + L \leq x$)

$$C_2 \ln \left\{ \frac{\sqrt{C_2 + \left(\frac{x}{H_o}\right)} + \frac{x}{H_o}}{\sqrt{C_2 + \left(\frac{x_{e,j}}{H_o}\right)^2} + \frac{x_{e,j}}{H_o}} \right\}$$

$$+ \frac{x}{H_o} \sqrt{C_2 + \left(\frac{x}{H_o}\right)^2} - \frac{x_{e,j}}{H_o} \sqrt{C_2 + \left(\frac{x_{e,j}}{H_o}\right)^2}$$

$$\frac{\Delta T}{\Delta T_o} = 6.40 \sqrt{\frac{x_o}{H_o}} \sqrt{\frac{L}{H_o}} \left\{\left(\frac{x}{H_o}\right)^2 + c_2\right\}^{-1/2} \qquad \text{(E-15)}$$

$$\frac{\tau}{C\rho u_o^2} = \frac{10.2}{\mathbb{K}_o} \frac{x_o}{H_o} \frac{L}{H_o} \left\{\left(\frac{x}{H_o}\right)^2 + c_2\right\}^{-1}$$

$$c_2 = -\left(\frac{x_o}{H_o}\right)^2 - \frac{1}{3} \left(\frac{L}{H_o}\right)^2$$

It should be noted that each of the expressions summarized above is valid only in the region for which it was derived. For example, if a particle is entrained into the initial region, the equations derived for the initial region (equations E-10 or E-13) should be used to describe the particle's history until it reaches the point $x = x_T$, which is the beginning of the momentum region. From here the equations for the momentum region (equations E-11 or E-14) should be used until the particle reaches $x = x_o + L$, which is the beginning of the jet region. After this point, the equations derived for the jet region (equations E-12 or E-15) should be used.

APPENDIX F

THE ENTRAINMENT FLOWFIELD SURROUNDING A STAGED DIFFUSER ON A SLOPING BOTTOM

We wish to solve for the flow field induced by a staged diffuser on a sloping bottom. We assume a stagnant, semi-infinite receiving body of water, and we assume that the flow outside of the turbulent diffuser plume can be described adequately using potential flow theory. The turbulent plume is assumed to be uniform over the water dpeth as illustrated in Figure F-1. Cylindrical coordinates (y,r,θ) are used to describe the potential flow region.

A velocity potential ϕ can be defined such that

$$u_y = \frac{\partial \phi}{\partial y}$$

$$u_r = \frac{\partial \theta}{\partial r} \qquad \text{(F-1)}$$

$$u_\theta = \frac{1}{r}\frac{\partial \phi}{\partial \theta}$$

where

u_y = y component of velocity

u_r = r component of velocity

u_θ = θ component of velocity.

Continuity requires

$$\nabla^2 \phi = 0 \qquad \text{(F-2)}$$

in the potential flow region. Since there can be no fluid velocity normal to the free surface or normal to the bottom, we have the boundary conditions

$$\frac{\partial \phi}{\partial \theta} = 0 \quad \text{at } \theta = 0$$

$$\frac{\partial \phi}{\partial \theta} = 0 \quad \text{at } \theta = -\theta_o \qquad \text{(F-3)}$$

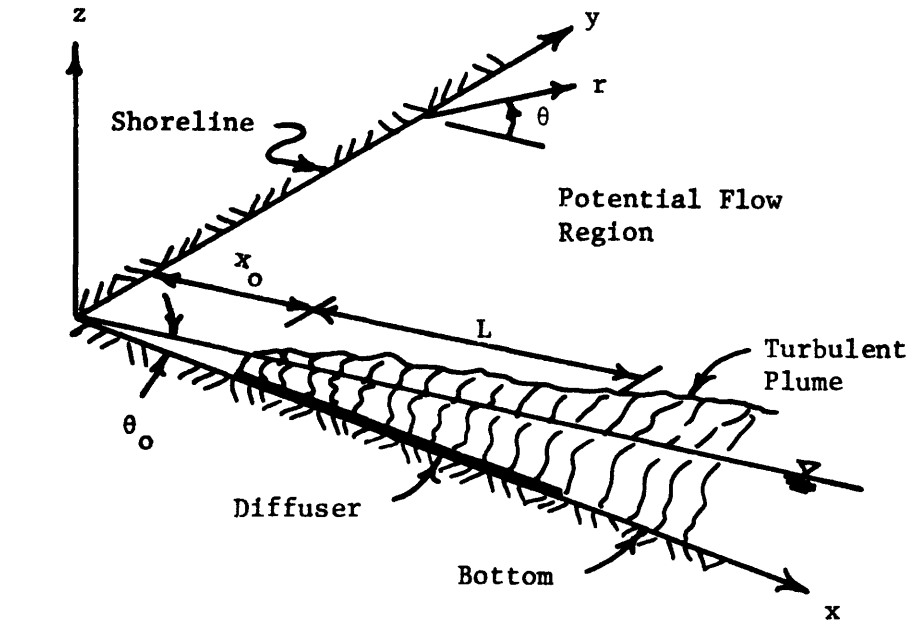

(a) Problem Definition

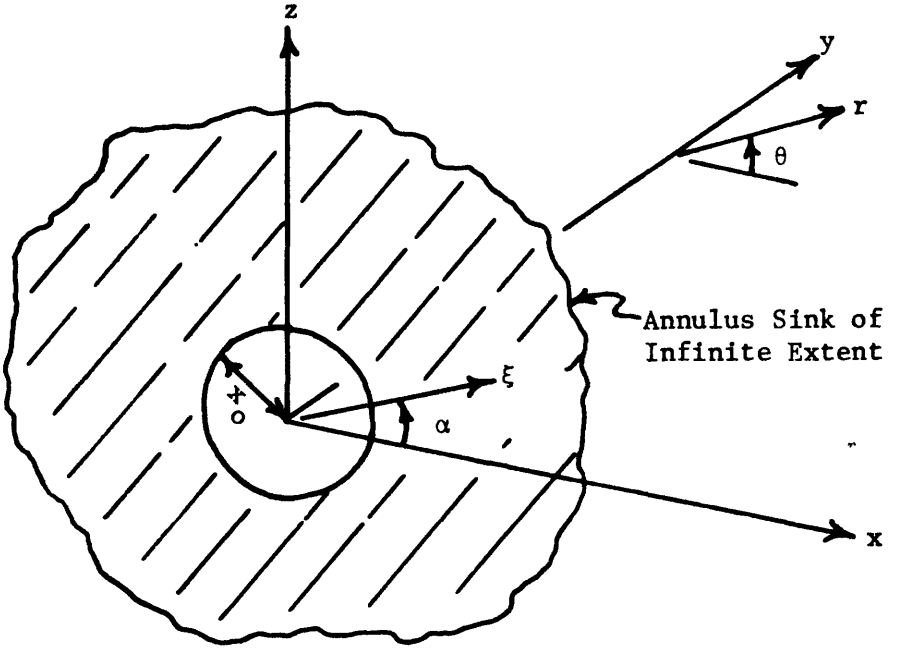

(b) Schematization of the Flow Field in Terms of an Annulus Sink

Figure F-1 Definition Sketches for the Potential Flow Solution to the Entrainment Flow Field (Sloping Bottom Case)

The boundary condition along the diffuser is

$$\frac{\partial \phi}{\partial y} = -v_e \quad \text{at} \quad y = 0 \tag{F-4}$$

where v_e is the entrainment velocity induced by the diffuser which may vary with x. We seek a solution to the governing equation F-2 that satisfies the boundary conditions F-3 and F-4.

We assume that there are no changes in the θ direction; that is

$$\frac{\partial}{\partial \theta} = 0 \quad \text{everywhere.} \tag{F-5}$$

This assumption is consistent with the small bottom slope and relatively shallow depths near the diffuser, and with the assumption that the turbulent plume is fully mixed over the water depth. Under equation F-5, the surface and bottom boundary conditions, equations F-3, are automatically satisfied. Another consequence of equation F-5 is that the original problem is essentially the same as the one shown in Figure F-2, in which an annulus sink of infinite extent is placed in an infinite body of fluid. The annulus sink is axially symmetrical, so that the sink intensity varies with ξ but not with α. In the original problem, the flow is confined to one small wedge defined by the angle θ_o. This small wedge is a subset of the flowfield induced by the annulus sink. The velocities and flowrates induced in the wedge are the same in both situations.

The problem therefore reduces to solving for the flowfield induced by the annulus sink, which, because of symmetry, is easier than solving the original problem shown in Figure F-1. Continuity requires that the governing equation in the fluid is equation F-2. The boundary

condition at the annulus sink is

$$\frac{\partial \phi}{\partial y} = -v_e(\xi) \quad \text{at } y = 0 \tag{F-6}$$

where v_e is entrainment velocity, as before. We can obtain a solution to equations F-2 and F-6 by treating the annulus as a collection of point sinks, each with intensity

$$dQ = v_e(\xi)\xi d\xi d\alpha$$

where (ξ,α) is the location of the point sink. At a point (y,r,θ), the value of the potential associated with such a sink located at (ξ,α) is given by

$$d\phi(\xi,\alpha,y,r,\theta) = -\frac{v_e(\xi)\xi d\xi d\alpha}{4\pi R(\xi,\alpha,y,r,\theta)} \tag{F-7}$$

where R is the distance between the points (ξ,α) and (y,r,θ). Since the governing equation F-2 and the boundary condition F-6 are linear in ϕ, we can find $\phi(y,r,\theta)$ by superposing the elements $d\phi(y,r,\theta,\xi,\alpha)$ induced by each point sink (ξ,α) in the annulus. We therefore have

$$\phi(y,r,\theta) = -\int_{x_o}^{\infty} d\xi \int_{o}^{2\pi} \frac{v_e(\xi)\xi d\alpha}{4\pi R(\xi,\alpha,y,r,\theta)} \tag{F-8}$$

This equation gives ϕ at any point in the infinite body of fluid. Since we are interested in the "wedge" shown in Figure F-1, we will compute ϕ only for points in the xy plane, where θ is zero. For these points

$$R(\xi,\alpha,y,r,\theta) = R(\xi,\alpha,x,y) = \sqrt{x^2+y^2+\xi^2-2x\xi\cos\alpha} \tag{F-9}$$

and we have

$$\phi(x,y) = -\int_{x_o}^{\infty} d\xi \int_{o}^{2\pi} \frac{v_e(\xi)\xi d\alpha}{4\pi\sqrt{x^2+y^2+\xi^2-2x\xi\cos\alpha}} \qquad \text{(F-10)}$$

In order to describe the flowfield in the "wedge" shown in Figure F-1 by means of streamlines, we define a stream function $\psi(x,y)$ such that

$\psi(x,y)$ = the amount of water flowing per unit time between the point (x,y) and the shore.

Using Equation F-1 and the assumption that θ_o is small, we have

$$\psi(x,y) \approx \int_{o}^{x} \left.\frac{\partial\phi}{\partial y}\right|_{(\eta,y)} \theta_o \eta d\eta \qquad \text{(F-11)}$$

where η is a dummy variable for integration. Combining Equations F-11 and F-10, we have

$$\psi(x,y) = -\int_{o}^{x} \frac{\partial}{\partial y}\left\{\int_{x_o}^{\infty} d\xi \int_{o}^{2\pi} \frac{v_e(\xi)\xi d\alpha}{4\pi\sqrt{\eta^2+y^2+\xi^2-2\eta\xi\cos\alpha}}\right\}\theta_o \eta d\eta \qquad \text{(F-12)}$$

or, moving the derivative inside the integrals

$$\psi(x,y) = \int_{o}^{x} \theta_o \eta d\eta \int_{x_o}^{\infty} d\xi \int_{o}^{2\pi} \frac{v_e(\xi)\xi y d\alpha}{4\pi R^3} \qquad \text{(F-13)}$$

where

$$R = \sqrt{\eta^2+y^2+\xi^2-2\eta\xi\cos\alpha} \qquad \text{(F-14)}$$

The continuity equation for a staged diffuser is

$$\frac{dQ_E}{d\xi} = 2v_e\theta_o\xi \qquad \text{(F-15)}$$

where Q_E is the entrained flowrate of the diffuser, written here as a function of ξ. Using equation F-15, equation F-13 can be put in the alternate form

$$\psi(x,y) = \int_o \eta d\eta \int_{x_o}^{\infty} d\xi \int_o^{2\pi} \frac{\frac{dQ_E}{d\xi} y d\alpha}{8\pi R^3} \qquad \text{(F-16)}$$

The quantity $\frac{dQ_E}{d\xi}$ is found from a near field analysis of the diffuser plume.

We have developed a computer program that evaluates equations F-14 and F-16 numerically at several points (x,y) to determine the flow field. In our program there is a choice in determining $\frac{dQ_E}{d\xi}$: it can be found using the theory of Almquist and Stolzenbach (1976) for a staged diffuser on a horizontal bottom, or it can be found using the theory for sloping bottom that was presented in Appendix D. Although the analysis of Appendix D seems more consistent, since it was developed specifically for the case of a sloping bottom, there are reasons for using the constant depth theory instead. Both theories are expected to be applicable for a distance of order one diffuser length past the end of the diffuser. Somewhere past this point, the plume lifts off of the bottom. It is expected that when the plume is detached from the bottom, its thickness in the vertical direction will remain relatively constant. It will therefore behave more like a plane jet, which has constant thickness, than like a jet which remains attached to the bottom, which has a thickness that increases with distance. Since the analysis of a staged diffuser on a horizontal bottom (Almquist and Stolzenbach (1976)) models the diffuser plume past

the end of the diffuser as a plane jet, it is expected to predict diffuser performance past the point of detachment better than the sloping bottom theory presented in Appendix D. Far from the diffuser, the theory for horizontal bottom predicts (see Equation 2.3)

$$\frac{dQ_e}{dx} \sim x^{-1/2}$$

while the theory for sloping bottom predicts (see Equation 2.9)

$$\frac{dQ_e}{dx} \sim \text{constant.}$$

Because the horizontal bottom theory predicts an entrainment demand that decays with distance, while the sloping bottom theory predicts an entrainment demand that stays constant, it makes a significant difference which theory is used when modeling the diffuser plume far from the diffuser. In describing the entrainment flow field surrounding a staged diffuser on a sloping bottom, it is felt that the analysis of Almquist and Stolzenbach describes the plume near the diffuser adequately, and that it describes the plume far from the diffuser better than the theory for sloping bottom. For these reasons, and for simplicity, it was decided to use the analysis of Almquist and Stolzenbach (1976) to find the entrainment demand along the entire diffuser plume.

A listing of the computer program used to find $\psi(x,y)$ is given below.

```
C     PROGRAM TO COMPUTE PSI FIELD NEAR A STAGED DIFFUSER
C     ON A SLOPING BOTTOM
C     BASED ON ALMQUIST'S THEORY MODIFIED TO ACCOUNT FOR A SMALL
C     BOTTOM SLOPE
C     OUTPUT AT A POINT = (100/KK)*(Q/QO)
C     KK=DIFFUSER PARAMETER = SQRT(S*HO/AO)
C     S = NOZZLE SPACING
C     HO = WATER DEPTH AT DIFFUSER ORIGIN
C     AO = NOZZLE AREA
C     Q = VOLUME FLUX BETWEEN SHORE AND THE POINT
C     QO = TOTAL DIFFUSER DISCHARGE
C     XO=DIFFUSER DISTANCE OFFSHORE
C     THETAO=BOTTOM SLOPE
C     M=NUMBER OF GRID POINTS IN X-DIRECTION
C     N=NUMBER OF GRID POINTS IN Y-DIRECTION
C     XDIST=EXTENT OF GRID IN X-DIRECTION
C     YDIST=EXTENT OF GRID IN Y-DIRECTION
C     ATEST=CONVERGENCE CRITERION
C     IFLAG=1 MEANS 'INNER SOLUTION'=ALMQUIST SOLUTION
C
      DIMENSION V(31,21), PSI(31,21)
C
C     READ IN DATA
      READ(5,5) IFLAG
5     FORMAT(I5)
      READ(5,10) M,N
10    FORMAT(2I5)
      READ(5,20) XO,XDIST,YDIST,THETAO,ATEST
20    FORMAT(5F10.5)
      WRITE(6,10) M,N
      WRITE(6,20) XO,XDIST,YDIST,THETAO,ATEST
C
      ML=M-1
      NL=N-1
      XSPACE=XDIST/FLOAT(ML)
      YSPACE=YDIST/FLOAT(NL)
      XL1=(XDIST-XO)/XSPACE*1.01
      L1=IFIX(XL1)
      L2=10
      IF(IFLAG.EQ.1) L2=5
      NR=10
      RHO=0.90
```

```
C
C       FIND AMAX=MAXIMUM XI
        IF(IFLAG.EQ.1) GO TO 170
        X=XDIST
        Y=YDIST
        AA=(X+XO+1.0)
        AB=SQRT((X+XO+1.0)**2+Y*Y)
        AC=(RHO+(1.0-RHO)*AA/AB)**2
        A=SQRT(AC/(1.0-AC))*Y-X
        AMAX=A
        WRITE(6,160) AMAX
160     FORMAT(F10.5)
170     IF(IFLAG.EQ.1) AMAX=2.0*XDIST
C
        L1I=L1
        L2I=L2
        NRI=NR
        AMAXI=AMAX


C
        L1O=L1I
        L2O=L2I
        NRO=NRI
        AMAXO=AMAXI
C
C       CONVERGENCE CHECKS
        DO 994 KTEST=1,10
C
C       CONVERGENCE CHECK---AMAX
        X=XDIST
        Y=YDIST
        DO 975 KOUNT=1,20
        KKOUNT=KOUNT-1
        AMAXT=AMAX+0.25*FLOAT(KKOUNT)*AMAXI
        VTEST=VEE(X,Y,L1,L2,NR,XO,XDIST,AMAXT,THETAO,IFLAG)
        IF(KOUNT.EQ.1) OLD=VTEST
        IF(KOUNT.EQ.1) GO TO 975
        TEST=ABS(1.0-VTEST/OLD)
        IF(TEST.LE.ATEST) GO TO 980
        OLD=VTEST
975     CONTINUE
980     AMAX=AMAXT-0.25*AMAXI
        WRITE(6,985) AMAX
985     FORMAT(F10.5)
```

```
C
C       CONVERGENCE CHECK---L2
        X=XDIST
        Y=YSPACE
        DO 200 KOUNT=1,10
        KKOUNT=KOUNT-1
        L2TEST=L2+FLOAT(KKOUNT)*L2I
        VTEST=VEE(X,Y,L1,L2TEST,NR,XO,XDIST,AMAX,THETAO,IFLAG)
        IF(KOUNT.EQ.1) OLD=VTEST
        IF(KOUNT.EQ.1) GO TO 200
        TEST=ABS(1.0-VTEST/OLD)
        IF(TEST.LE.ATEST) GO TO 300
        OLD=VTEST
200     CONTINUE
300     L2=L2TEST-L2I
        WRITE(6,400) L2
400     FORMAT(I5)
C
C       CONVERGENCE CHECK---L1
        X=XDIST
        Y=YSPACE
        DO 800 KOUNT=1,10
        KKOUNT=KOUNT-1
        L1TEST=L1+FLOAT(KKOUNT)*L1I
        VTEST=VEE(X,Y,L1TEST,L2,NR,XO,XDIST,AMAX,THETAO,IFLAG)
        IF(KOUNT.EQ.1) OLD=VTEST
        IF(KOUNT.EQ.1) GO TO 800
        TEST=ABS(1.0-VTEST/OLD)
        IF(TEST.LE.ATEST) GO TO 900
        OLD=VTEST
800     CONTINUE
900     L1=L1TEST-L1I
        WRITE(6,950) L1
950     FORMAT(I5)
C


C       CONVERGENCE CHECK---NR
        X=XDIST
        Y=YSPACE
        DO 500 KOUNT=1,50
        KKOUNT=KOUNT-1
        NRTEST=NR+FLOAT(KKOUNT)*NRI
        VTEST=VEE(X,Y,L1,L2,NRTEST,XO,XDIST,AMAX,THETAO,IFLAG)
        IF(KOUNT.EQ.1) OLD=VTEST
        IF(KOUNT.EQ.1) GO TO 500
        TEST=ABS(1.0-VTEST/OLD)
        IF(TEST.LE.ATEST) GO TO 600
        OLD=VTEST
500     CONTINUE
600     NR=NRTEST-NRI
        WRITE(6,700) NR
700     FORMAT(I5)
C
```

```
      T=ABS(1.0-AMAX/AMAXO)
      IF(T.GT.ATEST) GO TO 993
      IF(L1.GT.L1O) GO TO 993
      IF(L2.GT.L2O) GO TO 993
      IF(NR.GT.NRO) GO TO 993
      GO TO 995
993   AMAXO=AMAX
      L1O=L1
      L2O=L2
      NRO=NR
994   CONTINUE
995   WRITE(6,996)
996   FORMAT(1H1)
      WRITE(6,985) AMAX
      WRITE(6,400) L1
      WRITE(6,400) L2
      WRITE(6,400) NR
C
C
C     COMPUTE V FOR POINTS ON DIFFUSER AXIS
      DO 100 I=1,M
      J=1
      II=I-1
      XI=XSPACE*FLOAT(II)
      V(I,J)=0.0
      IF(IFLAG.EQ.1) GO TO 50
      IF (XI.GE.XO-XSPACE/10.0) V(I,J)=0.765/THETAO/SQRT(XO)/
     1SQRT(2.0*XI+XO)*0.5
      IF(XI.GT.XO+1.0) V(I,J)=0.765/THETAO/SQRT(XO)/SQRT(3.0*XI*XI
     1-1.0-3.0*XO-3.0*XO*XO)*0.5
      GO TO 100
50    IF(XI.GE.XO-XSPACE/10.0) V(I,J)=0.44/THETAO/XI*0.5
      IF(XI.GE.XO+1.0) V(I,J)=0.195/THETAO/XI/SQRT(0.39*(XI-XO)
     1-0.195)*0.5
100   CONTINUE
C
C     COMPUTE V FOR REMAINING GRID POINTS
      DO 1000 I=1,M
      DO 1000 J=2,N
      II=I-1
      JJ=J-1
      X=XSPACE*FLOAT(II)
      Y=YSPACE*FLOAT(JJ)
```

```
      V(I,J)=VEE(X,Y,L1,L2,NR,XO,XDIST,AMAX,THETAO,IFLAG)
1000  CONTINUE
      WRITE(6,2000)
2000  FORMAT(1H1)
      WRITE(6,4000)((V(I,J),J=1,N),I=1,M)
4000  FORMAT('-',13F5.2)
C
C     COMPUTE PSI
C     POINTS ALONG SHORE
      DO 5000 J=1,N
      I=1
      PSI(I,J)=0.0
5000  CONTINUE
C     REMAINING POINTS
      DO 6000 I=2,M
      DO 6000 J=1,N
      II=I-1
      X=XSPACE*FLOAT(II)
      IF(J.GT.1) GO TO 5500
      IF(X.GT.XO) GO TO 5500
      PSI(I,J)=0.0
      GO TO 6000
5500  AREA=0.5*THETAO*(2.0*X-XSPACE)*XSPACE
      VBAR=(V(I,J)+V(I-1,J))/2.0
      DPSI=VBAR*AREA*100.0
      PSI(I,J)=PSI(I-1,J)+DPSI
6000  CONTINUE
      WRITE(6,2000)
      WRITE(6,7000)((PSI(I,J),J=1,N),I=1,M)
7000  FORMAT('-',13F5.1)
      WRITE(6,2000)
C
C     CHECK KNOWN VALUES OF PSI ALONG DIFFUSER AXIS
      DO 8000 I=1,M
      II=I-1
      X=XSPACE*FLOAT(II)
      PSIC=0.0
      IF(IFLAG.EQ.1) GO TO 7300
      IF(X.GE.XO) PSIC=0.5*0.255/SQRT(XO)*(X-XO)*SQRT(2.0*X+XO)*100.(
      IF(X.GE.XO+1.0) PSIC=0.5*0.255/SQRT(XO)*SQRT(3.0*X*X-1.0
     1-3.0*XO-3.0*XO*XO)*100.0
      GO TO 7400
7300  IF(X.GE.XO) PSIC=0.44*(X-XO)*50.0
      IF(X.GE.XO+1.0) PSIC=SQRT(0.39*(X-XO)-0.195)*50.0
7400  WRITE(6,7500) PSIC
7500  FORMAT(F5.1)
8000  CONTINUE
C
      WRITE(6,2000)
```

```
      STOP
      END
      FUNCTION VEE(XF,YF,L1F,L2F,NRF,XOF,XDISTF,AMAXF,T8F,IFLAGF)
      DTHETA=2.0*3.14/FLOAT(NRF)
      DXI1=(XDISTF-XOF)/FLOAT(L1F)
      DXI2=(AMAXF-XDISTF)/FLOAT(L2F)
      VEE=0.0
C
C     XI-INTEGRATION
      LXI=L1F+L2F


      DO 9000 L=1,LXI
      IF(L.GT.L1F) GO TO 8200
      XI=XOF+DXI1*(FLOAT(L)-0.5)
      IF(XI.GT.XOF+1.0) GO TO 8100
      DQ=0.765*XI/SQRT(XOF)/SQRT(2.0*XI+XOF)*DXI1
      IF(IFLAGF.EQ.1) DQ=0.44*DXI1
      GO TO 8300
8100  DQ=0.765*XI/SQRT(XOF)/SQRT(3.0*XI*XI-1.0-3.0*XOF-3.0*XOF*XOF)*DXI1
      IF(IFLAGF.EQ.1) DQ=0.195/SQRT(0.39*(XI-XOF)-0.195)*DXI1
      GO TO 8300
8200  LL1=L-L1F
      XI=XDISTF+DXI2*(FLOAT(LL1)-0.5)
      DQ=0.765*XI/SQRT(XOF)/SQRT(3.0*XI*XI-1.0-3.0*XOF-3.0*XOF*XOF)*DXI2
      IF(IFLAGF.EQ.1) DQ=0.195/SQRT(0.39*(XI-XOF)-0.195)*DXI2
C
C     RADIAL INTEGRATION
8300  DELV=0.0
      DO 8400 LR=1,NRF
      THETA=DTHETA*(FLOAT(LR)-0.5)
      DV=DTHETA/(XF*XF+YF*YF+XI*XI-2.0*XF*XI*COS(THETA))**1.5
      DELV=DELV+DV
8400  CONTINUE
C
      DELTAV=YF/4.0/3.14/T8F*DQ*DELV
      VEE=VEE+DELTAV
9000  CONTINUE
      RETURN
      END
```

APPENDIX G

EXPERIMENTAL PROGRAM

INTRODUCTION

In this appendix we will discuss the experimental program that was carried out to obtain a qualitative idea of the nature of jet interaction in a staged diffuser and to obtain quantitative results about individual jet trajectories.

EXPERIMENTAL SETUP

The experiments were conducted in a rectangular 36' x 18' basin on the first floor of the Ralph M. Parsons Laboratory for Water Resources and Hydrodynamics. The experimental equipment is shown in Figure G-1.

In order to produce a crossflow, water was pumped up from a reservoir in the laboratory basement through the crossflow manifolds at the upstream end of the basin. Six rotameters in parallel measured the crossflow rate. A slotted weir with a layer of horsehair matting was used to even out the crossflow nonuniformities near the upstream end of the basin. At the downstream end of the basin, water flowed over a sharp-crested weir whose height could be adjusted to set the water depth. Water was drained from the basin by gravity.

Water for the diffuser was pumped from beneath the floor up to a constant head tank. Its temperature was essentially the same as that used for the crossflow. From the head tank, water flowed through a rotameter and into a series of two manifolds. The diffuser consisted of 13 copper 90° ells spaced at 6" and mounted on a frame above the water surface. Jet inside diameters of 1/4" and 1/8" were available. The

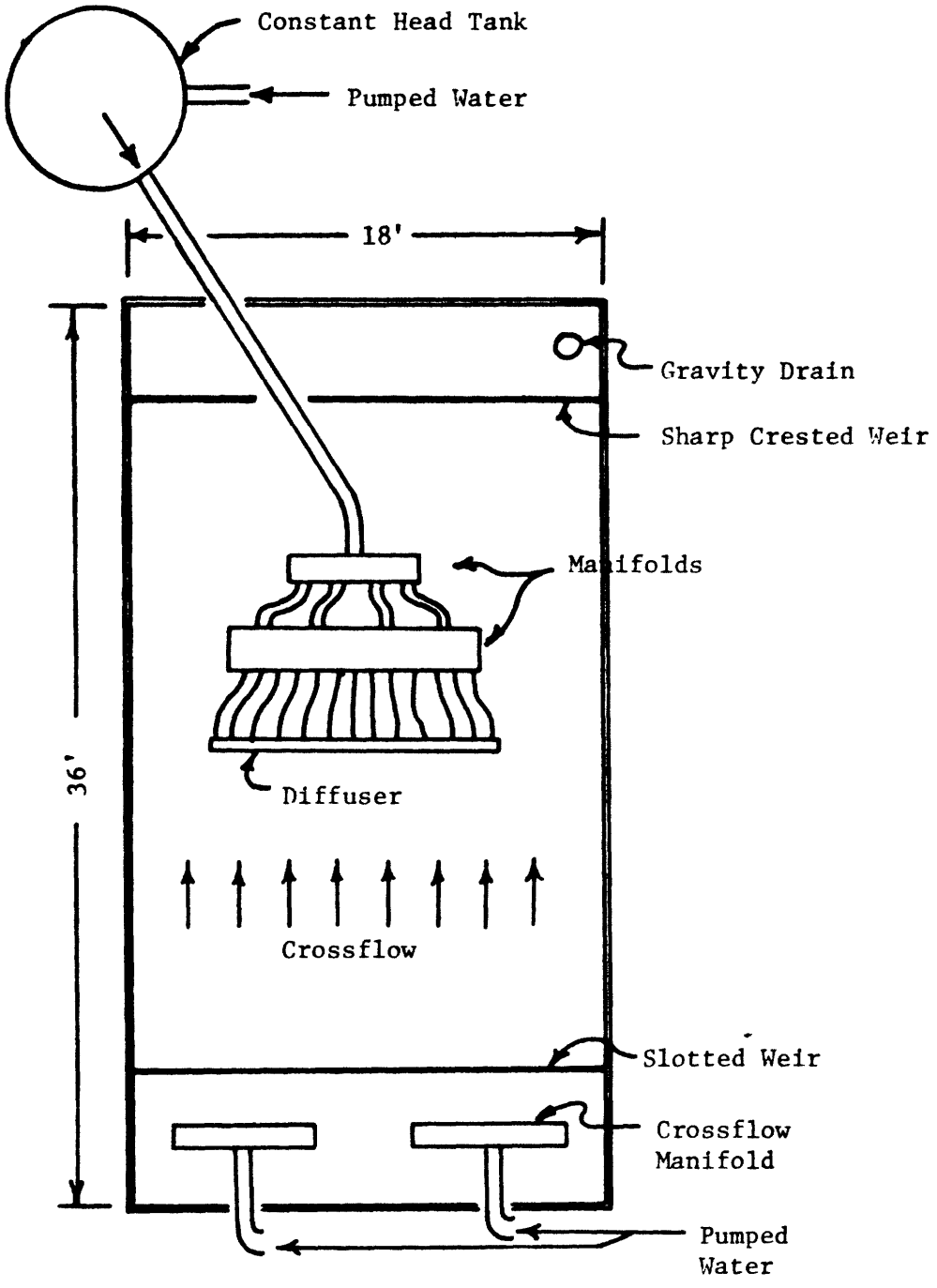

Figure G-1 Experimental Set Up

discharge angle and the height of the jets above the floor were adjustable although the latter was adjusted to a constant value of one jet diameter. Dye could be fed into one or more of the jets, and a Polaroid land camera mounted above the diffuser was used to photograph the trajectories of jets that were made visible with the dye.

For experiments that required stagnant receiving water, the basin was filled and left to still for about one hour. In experiments with a crossflow, the basin was filled and the crossflow was allowed to run for about 1/2 hour. A stream of dye was sprayed into the basin to test visually for lateral crossflow uniformity. After the diffuser was turned on, a series of photographs of jet trajectories was taken for different values of the diffuser parameters $\frac{H}{D_o}$, $\sqrt{\frac{sH}{a_o}}$, $\frac{V}{u_o}$ and γ_o. The diffuser was allowed to run for 20 minutes between photographs. For the stagnant water experiments, it was necessary to drain the basin periodically to keep the water level constant.

After a series of photographs was taken, the photographs were traced and enlarged by hand, and centerline trajectories were determined by plotting a line which was equidistant between the two visible jet edges.

RESULTS

Two sets of experiments were conducted - one with a crossflow and one with a stagnant receiving water. The details of the experiments, including a characterization of the observed trajectories, are included in Tables G-1 and G-2. Because it is expected that in most real situations crossflow will be strong enough to dominate jet trajectories, only the

experiments in Table G-1 are discussed.

An obvious first consideration in analyzing the observed jet trajectories is to compare them with the trajectories of jets in infinite surroundings - for example, as predicted by Rajaratnam's (1976) empirical equation for a jet oriented along the x-axis:

$$\frac{y}{D_o} = 0.077\left(\frac{V}{D_o}\right)^{2.6}\left(\frac{x}{D_o}\right)^{3.6} \qquad \text{(G-1)}$$

This can be modified to account for a small discharge angle, γ_o

Table G-1 Summary of the Experimental Data for the Crossflow Case*

Run	$\frac{V}{u_o}$	$\frac{SH}{a_o}$	$\frac{H}{D_o}$	γ_o	$\frac{x_c}{D_o}$
1	$\frac{1}{80}$	428	14	±27°	54
2	$\frac{1}{60}$	↓	↓	↓	34
3	$\frac{1}{40}$	↓	↓	↓	38
4	$\frac{1}{30}$	↓	↓	↓	24
5	$\frac{1}{30}$	↓	↓	±14°	18
6	$\frac{1}{40}$	↓	↓	↓	15
7	$\frac{1}{60}$	↓	↓	↓	17
8	$\frac{1}{80}$	↓	↓	↓	24

*The trajectory of the 7th (middle) jet in the series of 13 jets was measured. The jet being observed discharged in the upstream direction (i.e. $\gamma_o < o$). x_c is the point at which the jet centerline crossed the diffuser centerline.

Table G-1 (continued)

Run	$\frac{V}{u_o}$	$\frac{SH}{a_o}$	$\frac{H}{D_o}$	γ_o	$\frac{x_c}{D_o}$
9	$\frac{1}{106}$	199	6.5	±14°	54
10	$\frac{1}{80}$	↓	↓	↓	20
11	$\frac{1}{53}$	↓	↓	↓	21
12	$\frac{1}{40}$	↓	↓	↓	24
13	$\frac{1}{40}$	↓	↓	±27°	28
14	$\frac{1}{53}$	↓	↓	↓	50
15	$\frac{1}{80}$	↓	↓	↓	72
16	$\frac{1}{106}$	↓	↓	↓	80
17	$\frac{1}{110}$	611	20	±27°	76
18	$\frac{1}{83}$	↓	↓	↓	50
19	$\frac{1}{55}$	↓	↓	↓	40
20	$\frac{1}{41}$	↓	↓	↓	27
21	$\frac{1}{41}$	↓	↓	±14°	26
22	$\frac{1}{55}$	↓	↓	↓	36
23	$\frac{1}{83}$	↓	↓	↓	24
24	$\frac{1}{110}$	↓	↓	↓	80

Table G-2 Summary of the Experimental Data for the Stagnant Case*

Run	$\frac{SH}{a_o}$	$\frac{H}{D_o}$	γ_o	$\frac{y_c}{D_o}$
25	199	6.5	±14°	5
26	↓	↓	±14°	-1
27			±14°	7
28			±27°	9
29			±27°	7
30			±27°	8
31	428	14	±27°	13
32	↓	↓	±27°	16
33			±27°	15
34			±14°	8
35			±14°	6
36			±14°	7
37	611	20	±14°	7
38	↓	↓	±14°	8
39			±14°	8
40			±27°	23
41			±27°	16
42			±27°	15

*The trajectory of the 7th (middle) jet in the series of 13 jets was measured. y_c is the distance between the jet centerline and the diffuser centerline at x=2s.

$$\frac{y}{D_o} = 0.077\left(\frac{V}{u_o}\right)^{2.6}\left(\frac{x}{D_o}\right)^{3.6} + \left(\frac{x}{D_o}\right)\tan\gamma_o \qquad \text{(G-2)}$$

To test the success of equation (G-2) in predicting the experimentally observed jet trajectories, we have plotted $\left(\frac{y}{D_o} - \frac{x}{D_o}\tan\gamma_o\right)$ against $\left(0.077\left(\frac{V}{u_o}\right)^{2.6}\left(\frac{x}{D_o}\right)^{3.6}\right)$ in Figure G-2. The observed deflections are substantially larger than Rajaratnam's equation predicts. Further, his equation does not appear to have the correct functional form, since it plots as a straight line in Figure G-2 while the observed trajectories are curved.

In order to arrive at a different relationship, let us define x_c as the distance at which a jet discharging in the upstream direction (i.e. $\gamma_o < 0$) crosses the diffuser centerline. (x_c is tabulated in Table G-1). We can present the experimental data by plotting $\frac{x_c}{D_o}$ against various combinations of diffuser parameters. It was found that a fairly consistent straight line results if we plot $\frac{x_c}{D_o}$ against $\frac{u_o}{V}\tan|\gamma_o|$. (See Figure G-3) No consistent dependence on $\frac{H}{D_o}$ was apparent. Also, it appeared that jet trajectories are not affected significantly by adjacent jets, since the same functional relationship, $\frac{x_c}{D_o} \sim \frac{u_o}{V}\tan|\gamma_o|$ fits the data whether the jet intersects the diffuser centerline several port spacings away from its origin or less than one port spacing away from its origin. This point is further substantiation of the fact that the straight line relationship holds even for values of $\frac{V}{u_o}$ as low as $\frac{1}{100}$, indicating that ambient crossflow, rather than the effects of upstream jets. is the dominant influence on jet trajectory.

A jet trajectory equation of the form

$$\frac{y}{D_o} = c\left(\frac{V}{u_o}\right)\left(\frac{x}{D_o}\right)^2 + \left(\frac{x}{D_o}\right)\tan\gamma_o \qquad \text{(G-3)}$$

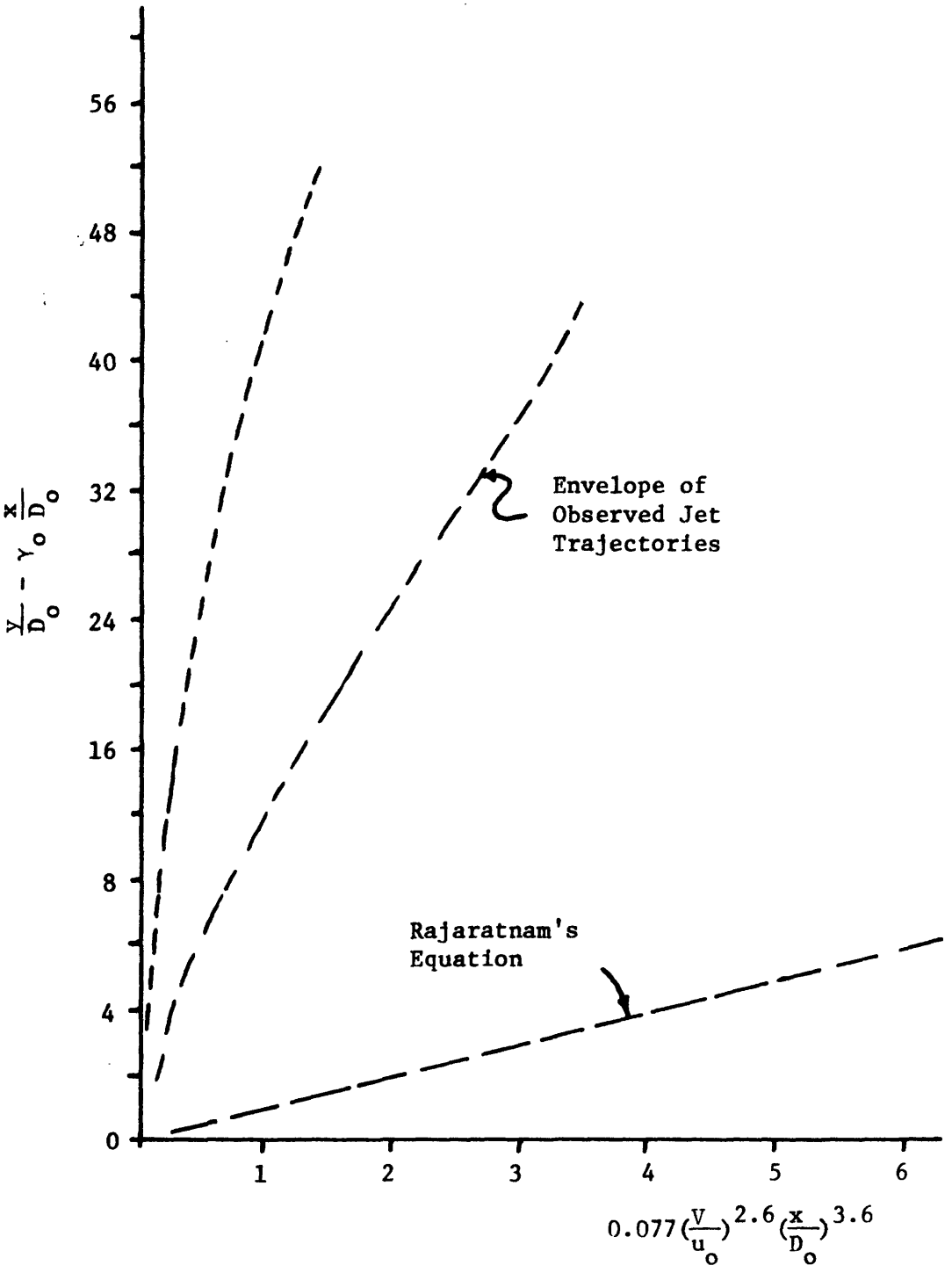

Figure G-2 Comparison of Experimental Data with Rajaratnam's Empirical Jet Trajectory Equation

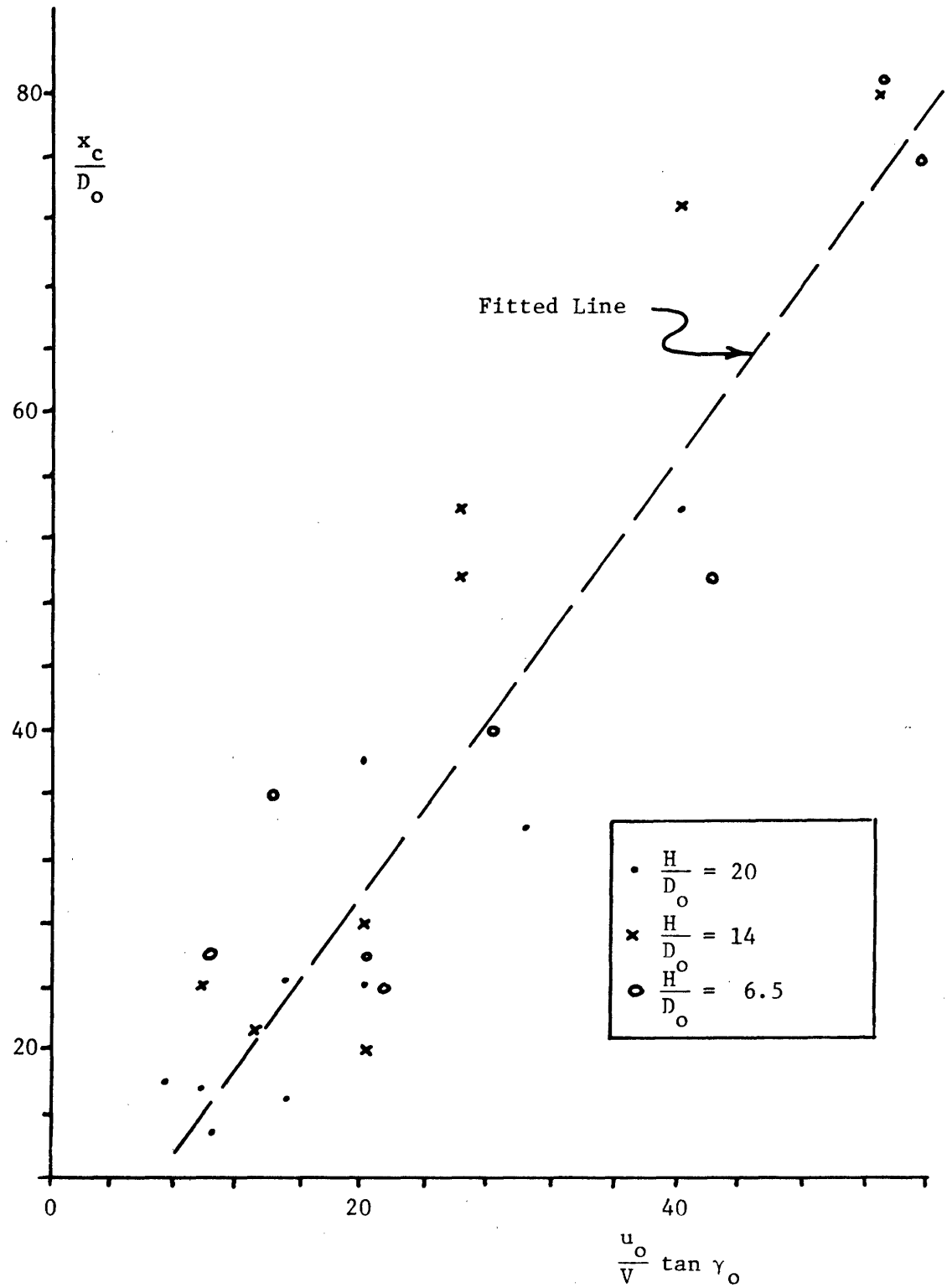

Figure G-3 Observed $\frac{x_c}{D_o}$ vs. $\frac{u_o}{V}$ tan γ_o

is consistent with the observed functional relationship, $\frac{x_c}{D_o} \sim \frac{u_o}{V} \tan |\gamma_o|$. This can be seen by setting $\frac{y}{D_o} = 0$ at $\frac{x}{D_o} = \frac{x_c}{D_o}$ in equation G-3. To test equation G-3, we have plotted $(\frac{y}{D_o} - \frac{x}{D_o} \tan \gamma_o)$ against $(\frac{V}{u_o})(\frac{x}{D_o})^2$ in Figure G-4. There is substantial scatter in the data, but it seems to be fairly well represented by the jet trajectory equation:

$$\frac{y}{D_o} = 0.6(\frac{V}{u_o})(\frac{x}{D_o})^2 + (\frac{x}{D_o}) \tan \gamma_o \qquad \text{(G-4)}$$

which was the equation presented in Chapter IV.

DISCUSSION

To try to interpret this result, consider the jet shown in Figure G-5. If we assume that γ is small compared to 1, we can write the integrated x-momentum equation:

$$\begin{aligned} M_i &= \text{jet momentum in the x-direction} \\ &\simeq \text{constant} \\ &\simeq M_{oi} \qquad \text{(G-5)} \\ &\simeq \frac{\pi}{4} D_o^2 \rho u_o^2 \end{aligned}$$

and an integrated y - momentum (deflection) equation:

$$\begin{aligned} \frac{d}{dx}(M_{oi}\theta) &= F \\ M_{oi}\frac{d\theta}{dx} &= F \qquad \text{(G-6)} \\ \frac{d\theta}{dx} &= \frac{F}{M_{oi}} \end{aligned}$$

where F is the force per unit length on the jet due to crossflow. We know that

$$\frac{d\theta}{dx} \simeq \frac{d^2y}{dx^2}, \text{ so that:}$$

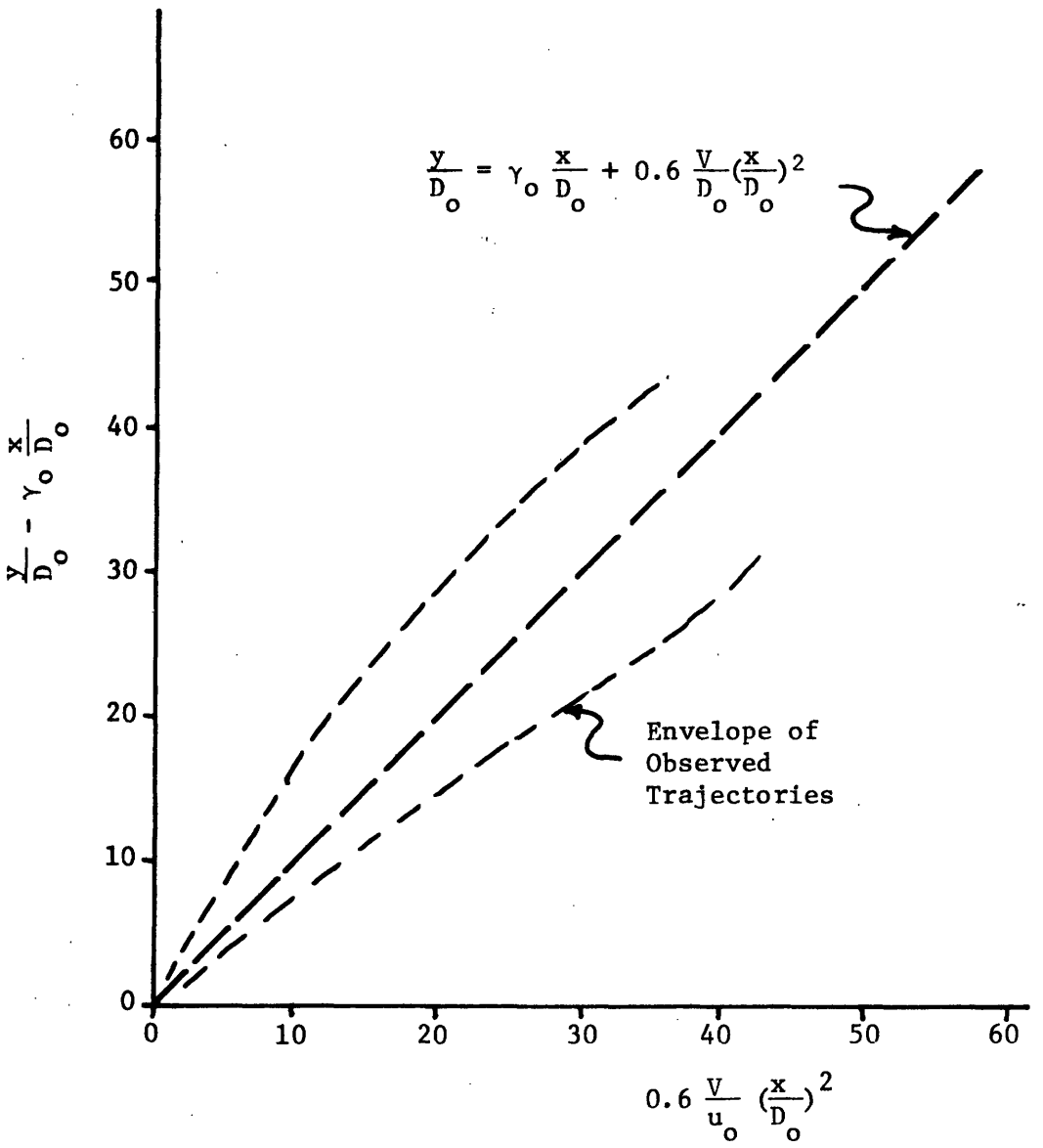

Figure G-4 Empirical Jet Trajectory Equation and Observed Trajectories

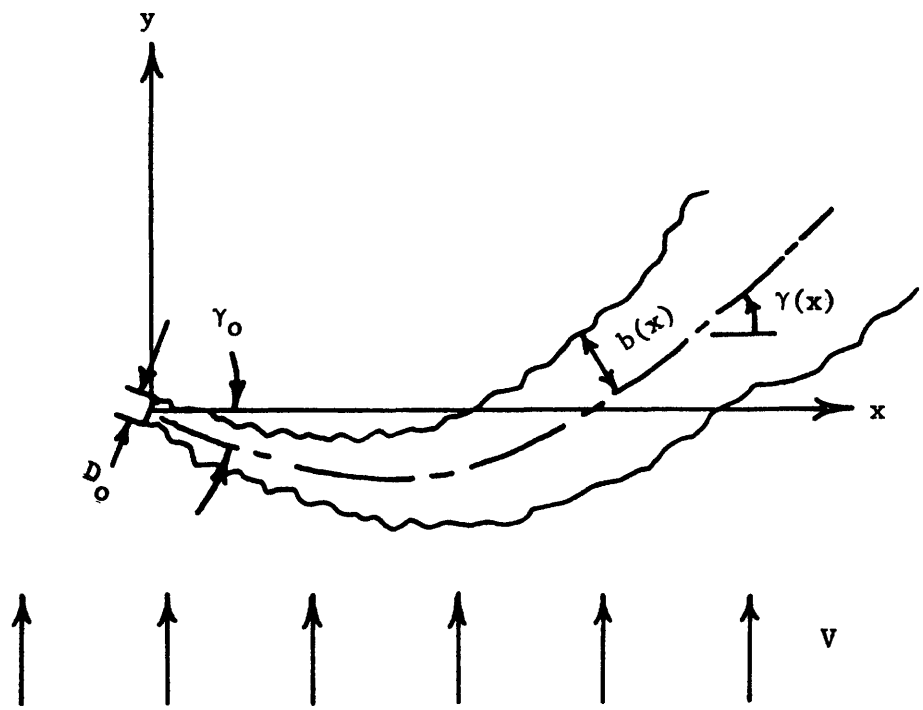

b = jet width

D_o = discharge diameter

M_{oi} = discharge momentum = $\frac{\pi}{4} D_o^2 \rho u_o^2$

u = jet velocity component parallel to the jet centerline

u_c = jet velocity at the centerline

u_o = discharge velocity

V = crossflow velocity

γ = jet inclination

γ_o = initial jet inclination

ρ = water density

Figure G-5 Definition Sketch of a Round Jet in Crossflow

$$\frac{d^2y}{dx} \simeq \frac{F}{M_{oi}}$$

$$\frac{d^2(\frac{y}{D_o})}{d(\frac{x}{D_o})^2} \simeq \frac{FD_o}{M_{oi}} \qquad \text{(G-7)}$$

From equation G-3, we see that $\frac{d^2(\frac{y}{D_o})}{d(\frac{x}{D_o})^2} \sim \frac{V}{u_o}$, and we have:

$$\frac{V}{u_o} \sim \frac{FD_o}{M_{oi}}$$

$$F \sim \frac{V}{u_o}\frac{M_{oi}}{D_o} \qquad \text{(G-8)}$$

$$F \sim \rho u_o D_o V$$

The fact that $F \sim V$ suggests an "entrainment" type of force, which was discussed in Chapter IV:

$$F_E = q_e \rho V \qquad \text{(G-9)}$$

Matching this with equation G-8, we find that $q_e \sim u_o D_o$, as is the case for a round jet in stagnant surroundings of infinite extent. For jets in deep, stagnant water, and using a value of c = .057,

$$F_E = 0.25\ u_o D_o \rho V \qquad \text{(G-10)}$$

Our data, on the other hand, gives:

$$F_E = u_o D_o \rho V \qquad \text{(G-11)}$$

the fact that the observed constant in the equation is much larger than that for deep, stagnant water can be explained by the increased entrainment due to crossflow effects. However, we might have expected that the

entrainment in this case would somehow increase with V, making F a function of V to some higher power than the value of unity which was observed.

The fact that the observed jet deflections are much larger than those predicted by Rajaratnam's equation could be explained by the relatively shallow water. However, it is intuitively expected that shallow water would increase "drag" forces, as opposed to "entrainment" forces, as was discussed in Chapter IV. Drag forces are expected to be proportional to V^2, while the observed force was proportional to V.

It is interesting that our data does not indicate that jet trajectory is a function of water depth, H. It is possible that shallow water affects trajectories a great deal, but that its effect over the range of H tested was obscured by scatter in the data.

APPENDIX H

COMPARISON OF ALTERNATIVE DIFFUSER DESIGNS FOR THE DISCHARGE OF HEATED WATER INTO SHALLOW RECEIVING WATER[1]

E.E. Adams and K.D. Stolzenbach
Massachusetts Institute of Technology
Cambridge, Massachusetts 02139

ABSTRACT

Submerged multi-port diffusers represent the most efficient means for rapidly dispersing large volumes of heated water from power plants into shallow waterbodies such as continental shelves, lakes or large rivers. An examination of existing diffuser designs reveals that the majority may be classified into one of four categories-- co-flowing, tee, staged and alternating-- characterized by the orientation of the diffuser nozzles, pipeline and local current. The first three employ horizontal momentum to induce an entrainment current and the preferred design for a given location depends on the predominant current speed and direction. The alternating diffuser does not induce any net momentum, and while a longer diffuser is generally required to achieve any level of mixing, several secondary advantages may accrue with this design. Formulas for the near field dilution under limiting conditions are presented for each diffuser type and an example design comparison shows the sensitivity of the diffusers' performance to various plant, cooling system and environmental variables.

INTRODUCTION

In the past five to ten years a number of submerged, multi-port diffusers have been designed to discharge heated water from large steam electric generating stations which employ once-through cooling systems. The basic principle in these diffusers is that by discharging the flow through a number of individual ports, the total area available for jet entrainment is increased and hence rapid dilution of the discharged water can be obtained. This is especially important when considering large generating stations which have substantial cooling water flow rates, and when considering shallow receiving water bodies where the quantity of water available for dilution is limited. In this paper, the near field mixing characteristics of several basic types of shallow water diffusers are summarized and the example calculations are used to compare their performance under a range of conditions.

The variables used to describe a multi-port diffuser are shown in the definition sketch of Figure 1. In this paper, diffuser performance will be based on a characteristic maximum surface temperature induced in the near field. To eliminate consideration of local hot spots caused by single jets, T_{max} will be loosely defined as the highest surface temperature

[1]presented at Waste Heat Management and Utilization Conference, Miami Beach, March 9-11, 1977.

for which a closed isotherm greater than a certain minimum size can be drawn. It must be noted that this is just one of many criteria which can be used to evaluate diffuser designs. Defining the near field dilution S in terms of T_{max} one can write

$$S = \frac{T_o - T_a}{T_{max} - T_a} = \frac{\Delta T_o}{\Delta T_{max}} = \text{function} \left[\mathbb{F}_o \ \frac{V}{u_o}, \ \frac{L}{H}, \ \frac{\ell}{H}, \ \frac{D_o}{H}, \frac{h}{H}, \ \alpha, \ \beta, \gamma \right] \quad (1)$$

where

$$\mathbb{F}_o = \frac{u_o}{\sqrt{\frac{\Delta\rho_o}{\rho_a} g D_o}}$$

and $\Delta\rho_o/\rho_a$ is the relative density difference associated with ΔT_o and T_a. For closely spaced ports, $\ell \lesssim H$, the influence of individual ports will not be felt, and for the purposes of analysis, the individual ports may be replaced by an equivalent slot diffuser having the same discharge and momentum flux per unit length [1], [2]. Thus the width B_o of an equivalent slot diffuser is $\pi D_o^2 / 4\ell$. In addition, in shallow water, the port elevation is of secondary significance as long as $h/H \lesssim .5$. With these assumptions the dilution may now be written

$$S = \text{function} \left[\mathbb{F}_s, \frac{V}{u_o}, \ \frac{L}{H}, \ \frac{H}{B_o}, \ \alpha, \ \beta, \ \gamma \right] \quad (2)$$

where

$$\mathbb{F}_s = \frac{u_o}{\sqrt{\frac{\Delta\rho_o}{\rho_a} g B_o}}$$

Whether or not the receiving water is shallow will depend on the type of diffuser under consideration but in general the condition will hold if H satisfies a relationship of the form

$$\frac{H}{B_o} < \text{function} \left[\mathbb{F}_s, \frac{V}{u_o}, \frac{L}{H}, \ \alpha, \ \beta, \ \gamma \right] \quad (3)$$

The above two functions have been evaluated for four basic types of diffusers distinguished by the values of the angles α, β, and γ. These types have been loosely referred to as co-flowing, tee, staged and alternating diffusers. While clearly not an exhaustive list, these types represent the range of shallow water diffusers which have been designed to date.

DISCUSSION OF INDIVIDUAL DESIGNS

The four types of diffusers, and typical flow fields which might be observed by the operation of the diffuser in a coastal area are shown in Figure 2. Salient features and near field dilution relationships for each design are discussed below and the relative advantages are summarized in Table 1. More discussion regarding the analyses can be found in the references noted or in reference [3].

Co-Flowing Diffusers ($\alpha \sim 0^o$, $\beta \sim 0^o$, $\gamma \sim 90^o$)

In this type of diffuser, the nozzles are oriented essentially horizontally (a small angle $\alpha \approx 20^o$ may be desirable to prevent bottom scour) and at right angles to the diffuser line as indicated in Figure 2(a). Flow is induced primarily from behind the diffuser with additional mixing caused by lateral entrainment at the ends of the diffuser. In a co-flowing situation, dilution is augmented by the flow of ambient water which would pass naturally over the diffuser. For long diffuser, $L/H \gtrsim 10$, end effects can be neglected and the flow entering the diffuser is proportional to the dilution S_c. An analysis based on continuity, one-dimensional momentum equations and the Bernoulli equation evaluated along a streamline gives [4]

$$S_c = \frac{1}{2}\left[\frac{VH}{u_o B_o} + \sqrt{\left(\frac{VH}{u_o B_o}\right)^2 + \frac{2H\cos\alpha\sin\gamma}{B_o}}\right] \tag{4}$$

In the limit of no current, the dilution is given by

$$S_c = \sqrt{\frac{H\cos\alpha\sin\gamma}{2B_o}} \tag{5}$$

while for a strong ambient current the dilution approaches the ratio of the flow which would pass over a dormant diffuser to the diffuser discharge flow, or

$$S_c = \frac{VH}{u_o B_o} \tag{6}$$

In Equation (4) it is noted that the parameter $\mathbb{F}_s$ does not appear. This is because, for shallow water, $\mathbb{F}_s$ is large and the influence of buoyancy for this diffuser type is relatively unimportant. A criterion for shallow water is that the heated flow away from the diffuser be attached to the bottom, or that the densimetric Froude number based on water depth and on the mixed flow velocity and density difference by greater than unity. For these conditions the criterion for shallow water is

$$\frac{H}{B} < \frac{1}{2}\,\mathbb{F}_s^{4/3} \tag{7}$$

In order that the temperature downstream be truly uniform over depth, a somewhat stricter relationship must hold.

A comparison of predicted dilutions with those observed in experimental model studies, for cases in which L/H > 10 and Equation (7) is satisfied, is presented in Figure 3. A comprehensive study of co-flowing diffusers including end effects, is in progress [5].

If the current opposes the diffuser nozzles ($\gamma \sim -90^o$), Equation (4) may be used as long as

$$\frac{VH}{u_o B_o} > \left| \frac{2H\cos\alpha \sin\gamma}{B_o} \right| \qquad (8)$$

If this inequality is not satisfied, direct re-entrainment of the plume will occur as depicted in Figure 2(b), and the effective dilution will decrease sharply causing T_{max} to rise. Because of the strongly asymmetrical performance with respect to current direction, co-flowing diffusers are most desirable in situations where the current flows in one predominant direction, such as in large rivers.

Tee Diffuser ($\alpha \sim 0^o$, $\beta \sim 90^o$, $\gamma \sim 90^o$)

One way to avoid the preferred direction of the co-flowing diffuser is to orient the diffuser pipe parallel to the predominant current direction ($\beta \sim 90^o$) resulting in a "tee" diffuser as shown in Figure 2(c). (The name is derived from the orientation of the diffuser pipe with respect to its feeder pipe.) In stagnant flow conditions the tee diffuser behaves much like a co-flowing diffuser with the major difference being the orientation. In coastal areas the fact that the momentum is directed offshore minimizes shoreline impact, but this advantage may be weighed against potential disadvantages associated with large induced currents.

In a crossflow, dilution decreases because of interaction among the individual jets and because the pressure distribution which is set up by the ambient flow limits the quantity of water which can enter from behind the diffuser. Furthermore, the temperature distribution along the diffuser is often very non-uniform making ΔT_{max} somewhat higher than the average induced temperature. A comprehensive theory for the performance of a tee diffuser in a crossflow is not available but experimental data from a number of studies has been compiled and is presented in Figure 4. The large scatter in the data can be attributed in part to differences in topography-- different bottom slopes mean different volumes of water behind the diffuser available for entrainment, while site specific coastal features can result in different local values of β -- and differences in the resolution of ΔT_{max}. (Dilutions in Figure 4 are based on the highest temperature isotherm which is plotted.) A relationship between the observed dilution in a crossflow, S_t, and the theoretical dilution in stagnant water, Equation (5) evaluated for $\alpha = 0$, $\gamma = 90$, is given by

$$\frac{\sqrt{H/2B_o}}{S_t} = \left[1 + \frac{5V^2H}{u_o^2 B_o}\right]^{1/2} \qquad (9)$$

A disadvantage of this type of diffuser is that dilution appears to decrease monotonically with crossflow velocity, V. Whereas with other basic designs the "worst case" situation is well-defined (V=0), the maximum current at a site can only be defined statistically, and the worst case performance of a tee diffuser depends on the statistical definition. For instance the maximum induced temperature associated with the current speed which is exceeded 10% of the time may differ significantly from the maximum temperature encountered with the (larger) current speed which is exceeded only 1% of the time. The fact that the greater turbulence associated with the higher ambient velocity will smooth out non-uniformities in the temperature distribution, and may eventually cause lower temperatures at positions downstream, points to one of the limitations inherent in using a single performance criterion (i.e., ΔT_{max}) to evaluate discharge designs. Another (minor) disadvantage of a tee diffuser is that in coastal areas with a sloping bottom, a somewhat longer feeder pipe is required.

Staged Diffuser ($\alpha \sim 0$, $\beta \sim 0$, $\gamma \sim 0$)

Another diffuser design which has no preferred orientation with respect to longshore current direction is the "staged" diffuser. Although early diffuser design studies apparently ignored this concept, several staged diffusers have been designed recently for coastal regions where significant longshore currents can occur in either direction. As indicated in Figure 2(d) the diffuser works by entraining water primarily along its sides and jetting it along the diffuser axis. Thus, like the tee diffuser, an offshore current is produced which helps keep heat away from the shoreline.

In stagnant situations the flow is symmetrical with respect to the diffuser axis with the maximum induced temperatures and velocities occuring along the axis. A theory to treat this situation has been developed by extending classical jet analysis (using integrated equations and assumed transverse profiles for velocity and excess temperatures) to treat the case of a continuous source of momentum [6]. For $L/H \gtrsim 15$, the theory predicts a constant centerline dilution near the end of the diffuser given by

$$S_s = 0.38\sqrt{\frac{H}{B_o}} \qquad (10)$$

where the factor of 0.38 reflects the choice of lateral entrainment coefficient as well as lateral velocity and excess temperature profiles. Equation (10) differs from Equation (5) for a uni-directional diffuser only by a constant and reflects the fact that both situations involve a directed

source of momentum. For short diffusers, $L/H \leq 15$, the flow is not fully developed and both observed and predicted dilutions are somewhat greater than those given by Equation (10). Beyond the diffuser, $y > L/2$ as defined in Figure 1, excess temperature decreases due to lateral entrainment; as with co-flowing and tee diffusers, this effect is greatest for small L/H.

Also in analogy with co-flowing and tee diffusers, the flow field along the diffuser will be fully mixed only if the local densimetric Froude number is larger than a critical value. By examining a range of experimental data, a critical value of about 2.5 is suggested [6] yielding a criterion for "shallow water" which is similar to Equation (7):

$$\frac{H}{B_o} \leq 2.5^{-2/3} \; \mathbb{F}_s^{4/3} \simeq 0.5 \, \mathbb{F}_s^{4/3} \tag{11}$$

A comparison of observed and predicted dilutions for situations involving shallow water and $L/H > 15$ is presented in Figure 5.

In a crossflow, dilution is observed to improve due to the partial separation of the individual plumes. For strong crossflows the dilution will approach the ratio of flows given by Equation (6) and hence will approach, but be somewhat less than, the dilution for a co-flowing diffuser. Of course the staged diffuser has the obvious advantage that its performance is independent of current direction!

Vertical Diffusers ($\alpha \sim 90^o$, $\beta \sim 0^o$)

Alternating Diffusers ($\beta \sim 0^o$, $\gamma \sim \pm 90^o$)

The three designs discussed previously have all involved the introduction by the diffuser of substantial horizontal momentum in order to induce entrainment flow. With the co-flowing and the tee designs, especially, the performance in an ambient current depends strongly on the orientation of the ambient flow with respect to the diffuser induced flow. A different strategy is to orient the nozzles vertically ($\alpha \sim 90^o$) thereby inducing no net horizontal momentum and thus reducing the directional preference. Similar overall performance, but without local hot spots immediately above the diffuser ports, may be obtained by alternating the diffuser ports ($\alpha \sim 0^o$, $\gamma = \pm 90^o$).

For large currents, the dilution downstream from the diffuser ports is given in either case by Equation (6) which follows from Equation (4) when $\cos \alpha = 0$. For smaller currents the diffuser performance (in shallow water) is governed by density-driven exchange flow [2]. The minimum dilution occurs when $V = 0$ and is given theoretically [2] by

$$S_a = \frac{(2 \; \mathbb{F}_H)^{2/3}}{\mathbb{F}_s^{2/3}} \; \frac{H}{B_o} \tag{12}$$

where $\mathbb{F}_H$ is a densimetric Froude number of the exchange flow system and is a function of interfacial friction. $\mathbb{F}_H$ ranges from .25 for no friction to less than .15 for large frictional effects. As with the momentum diffusers Equation (12) is derived for conditions of shallow water given [2] by

$$\frac{H}{B_o} < 1.84(1 + \cos^2 \alpha)^2 \mathbb{F}_s^{4/3} \tag{13}$$

Equation (12) was derived under the assumption of a uniform exchange flow in vertical planes perpendicular to the diffuser line, i.e., surface layer flow moving away from the diffuser, and an equal bottom layer flow moving toward the diffuser. Experiments conducted with nozzles oriented normal to the diffuser, $\gamma = \pm 90^o$, however, indicated that the entrainment flow entered predominantly from the ends of the diffuser while the mixed flow left along a path perpendicular to the diffuser as shown in Figure 2(e). This situation resulted in successive re-entrainment of the discharged water as flow migrated from the ends to the center of the diffuser and observed dilutions were considerably below those given by Equation (12). It was found that a uniform flow field could be obtained, however, and observation brought in line with Equation (12), if a non-uniform "nozzle control" was adopted as suggested in Figure 2(f). The nozzle distribution was shown theoretically to be

$$\gamma(y) = \pm \cot^{-1} \left[\frac{1}{\pi} \ell n \ \frac{1 + 2y/L}{1 - 2y/L} \right] \tag{14}$$

where the $\pm$ refers to the alternating nozzles [2]. A comparison between observed and predicted dilutions is indicated in Figure 6.

DESIGN COMPARISON

It is difficult to make a satisfactory comparison of the diffuser types because the performance measures discussed above are somewhat biased (eg., the maximum temperature predicted for a staged diffuser occurs in a narrow, relatively short region along the diffuser, while the temperature associated with the alternating diffuser is predicted for the whole near field) and, at best, address only one index of performance-- near field temperature. However, the exercise is useful in that it points out trends in the performance of the various diffuser types.

The design example considers a power plant situated near the coast. The receiving water is characterized by a straight coastline, a bottom with linear slope δ, and a range of alongshore current speeds $0 < V < V_{max}$. Situations with predominantly uni-directional currents as well as those with bi-directional currents are considered. The design objective is to build a diffuser with minimum length while meeting the following constraints:

1) The diffuser should be in water of depth H_o or greater, and
2) the maximum near field surface temperature rise should be less than ΔT_{max} under all conditions

Condition 2) suggests that for the alternating, staged and co-flowing diffuser the design velocity should be V = 0 while for the tee diffuser, the design condition should be $V = V_{max}$. The co-flowing diffuser is only considered for the case of uni-directional currents.

The required diffuser lengths for co-flowing, tee, staged and alternating diffusers under design conditions can be determined from Equations (5), (9), (10) and (12) respectively and are summarized below:

(Co-flowing)

$$L_c = \frac{2J_o\Delta T_o}{\rho c_\rho \Delta T_{max}^2 u_c (H_o + .5\delta L)} \tag{15}$$

(Tee)

$$L_t = \frac{2J_o\Delta T_o}{\rho c_\rho \Delta T_{max}^2 u_o H_o} \frac{1}{[(1 - \frac{10V^2\Delta T_o^2}{u_o^2 \Delta T_{max}^2})]} \tag{16}$$

(Staged)

$$L_s = \frac{6.9\ J_o\Delta T_o}{\rho c_\rho \Delta T_{max}^2 u_o (H_o + .5\delta L)} \tag{17}$$

(Alternating)

$$L_a = \frac{J_o}{\rho c_\rho (ag)^{1/2} 2\ \mathbb{F}_H \Delta T_{max}^{3/2} (H_o + .5\delta L)^{3/2}} \tag{18}$$

where J_o is the plant heat rejection rate, $J_o = \rho c_\rho Q_o \Delta T_o$, and ρ, c_ρ and a are the density, specific heat and coefficient of thermal expansion of water. Note that for the co-flowing, alternating and staged diffusers, where the diffuser extends offshore, the water depth is variable and an average value of $H = H_o + .5\delta L$ is used. For the tee diffuser the diffuser line is located in a depth of H_o. Also, in evaluating the alternating diffuser, $\mathbb{F}_H$ is strictly a function of water depth and diffuser length, but for this study, a constant value of .17 is used. This corresponds to a value of $\Phi = 1.0$ as defined in [2].

Equations (15), (16), (17) and (18) are presented in their particular form in order to isolate the effects of plant variables (J_o), condenser-cooling

system variables (ΔT_o and u_o) and environmental variables (V_{max}, H_o and ΔT_{max}). The sensitivity of the required pipe length to each of these variables is shown graphically in Figure 7 using as base case conditions $J_o = 7 \times 10^9$ BTU/hr (corresponding roughly to a 1000 MW_e nuclear unit), $\Delta T_o = 25^oF$, $U_o = 20$ fps, $H_o = 25$, $V_{max} = .5$ fps, and $\Delta T_{max} = 3^oF$. Values for ρc_p, a and δ were 62 BTU/ft^3- ^oF, .0001$^oF^{-1}$ and .02 respctively. Lengths for the co-flowing diffuser are indicated by a dashed line to stress the fact that they are only considered in a uni-directional current.

Several conclusions can be drawn from this comparative study. First the momentum diffusers show similar trends with performance improving with increasing H_o , u_o and ΔT_{max} and decreasing with increasing ΔT_o. In uni-directional currents where a co-flowing diffuser is appropriate, relatively short diffusers can be built to obtain any reasonable ΔT_{max}. Conversely, if there are moderate or strong currents then the tee design requires a relatively long diffuser and for design currents $\geq$ 0.7 fps this design seems impractical for the conditions tested and the stated objective. In these cases the staged diffuser appears to be a logical choice.

The alternating diffuser generally requires a longer length than the staged diffuser in order to meet a given ΔT_{max}. (And as discussed above, temperatures do not decrease below ΔT_{max} as rapidly.) However, as long as conditions of shallow water are met (Equation 13), the performance of the alternating diffuser is insensitive to either discharge velocity (u_o) or the combination of condenser flow rate-temperature rise ($Q_o - \Delta T_o$). This suggests that by using lower discharge velocities, the savings in pumping costs and the lower risk of mechanical damage incurred by organisms entrained in the discharge plume might outweigh the installation costs of a longer diffuser. Furthermore, the insensitivity of performance to ΔT_o suggests that the use of an alternating diffuser with a low condenser flow rate (low Q_o and high ΔT_o) may be desirable due to reduced entrainment and impingement losses at the cooling water intake, as well as lower pumping costs.

The plant load (J_o), temperature standard (ΔT_{max}) and water depth (H_o) have less influence on the design choice. Increases in H_o or decreases in ΔT_{max} favor slightly the alternating diffuser in comparison with the momentum diffusers, while an increase in J_o requires a somewhat less than proportionate increase in diffuser length due to the increase in effective water depth. This latter observation suggests possible economies of scale associated with combining discharges from several generating units.

SUMMARY

This paper has discussed the behavior of several basic types of submerged multi-port diffusers. The mechanics of each type are different. The co-flowing and tee diffusers use horizontal momentum to induce a flow behind the diffuser, while the staged diffuser relies on jet-like mixing along the sides of the diffuser; in each case dilution is controlled by the horizon-

zontal momentum of the discharge and buoyancy plays a secondary role. On the other hand, the dilution achieved by shallow water alternating diffusers is governed by buoyancy-driven exchange flow, and above a certain limit, the role of discharge momentum is insignificant.

The preceding example shows the sensitivity of each diffuser's performance to various plant, cooling system and environmental variables. Perhaps the most important conclusion to be drawn is that, depending on the combination of these variables and the design objectives, any of the four designs which were considered could be most appropriate in a given situation. It should be remembered, however, that this study considers primarily one performance standard-- near field temperature rise-- and that many other variables must enter into any actual design.

REFERENCES

1. Cederwall, K., "Buoyant Slot Jets Into Stagnant or Flowing Environments," California Institute of Technology, W.M. Kech Laboratory of Hydraulics and Water Resources, Report No. KH-R-25, April 1971.

2. Jirka, G., and D.R.F. Harleman, "The Mechanics of Submerged Multi-port Diffusers in Shallow Water," M.I.T., R.M. Parsons Laboratory for Water Resources and Hydrodynamics, Technical Report No. 169, 1973.

3. Harleman, D.R.F., G. Jirka, K.D. Stolzenbach, P.J. Ryan and E.E. Adams, Heat Disposal in the Water Environment M.I.T. Press, to be published Spring 1977.

4. Adams, E.E., "Submerged Multi-port Diffusers in Shallow Water with Current," S.M. Thesis, M.I.T., Department of Civil Engineering, June 1972.

5. Lee, J., "Modeling of Uni-directional Thermal Diffusers in Shallow Water," Ph.D. Thesis, M.I.T., Department of Civil Engineering, to be published June 1977.

6. Almquist, C.W., and K.D. Stolzenbach, "Staged Diffusers in Shallow Water," M.I.T., R.M. Parsons Laboratory for Water Resources and Hydrodynamics, Technical Report No. 213, 1976.

7. Anon, "Browns Ferry Nuclear Plant," Tennessee Valley Authority, Engineering Laboratory, Norris, Tennessee, Advanced Report No. 14, 1972.

8. Anon, "Perry Nuclear Power Plant, Thermal Hydraulic Model Study of Cooling Water Discharge," Acres American Inc., Buffalo, N.Y., 1974.

9. Anon, "Niagara Mohawk Power Corporation, Nine Mile Point Nuclear Power Station, Hydraulic Model Study of Thermal Discharge," Acres American Inc., Buffalo N.Y., 1974.

10. Anon, "Postoperational Hydrothermal Survey for James A. Fitzpatrick Nuclear Power Plant-Power Authority of the State of New York (June, August, and October Surveys)," Stone and Webster Engineering Corporation, Boston, MA, 1976.

Table 1

Advantages and Disadvantages of Diffuser Designs

Diffuser Types	Advantages	Disadvantages
Co-flowing	-- provides most efficient mixing under stagnant or co-flowing current conditions	-- poor performance in a counterflow -- provides no offshore momentum*
Tee	-- provides efficient mixing under stagnant or nearly stagnant current conditions -- provides offshore momentum*	-- poor performance in strong crossflow -- difficult to define worst case (maximum current speed) -- induces strong currents -- may require somewhat longer feeder line
Staged	-- may be designed to provide acceptable dilution in worst case (stagnant current) -- symmetrical performance with respect to current direction -- provides offshore momentum*	-- induces strong currents
Alternating or Vertical	-- symmetrical performance with respect to current direction -- induces lowest currents -- does not require high discharge velocities	-- requires large diffuser length to obtain high dilution -- provides no offshore momentum*

*in coastal areas

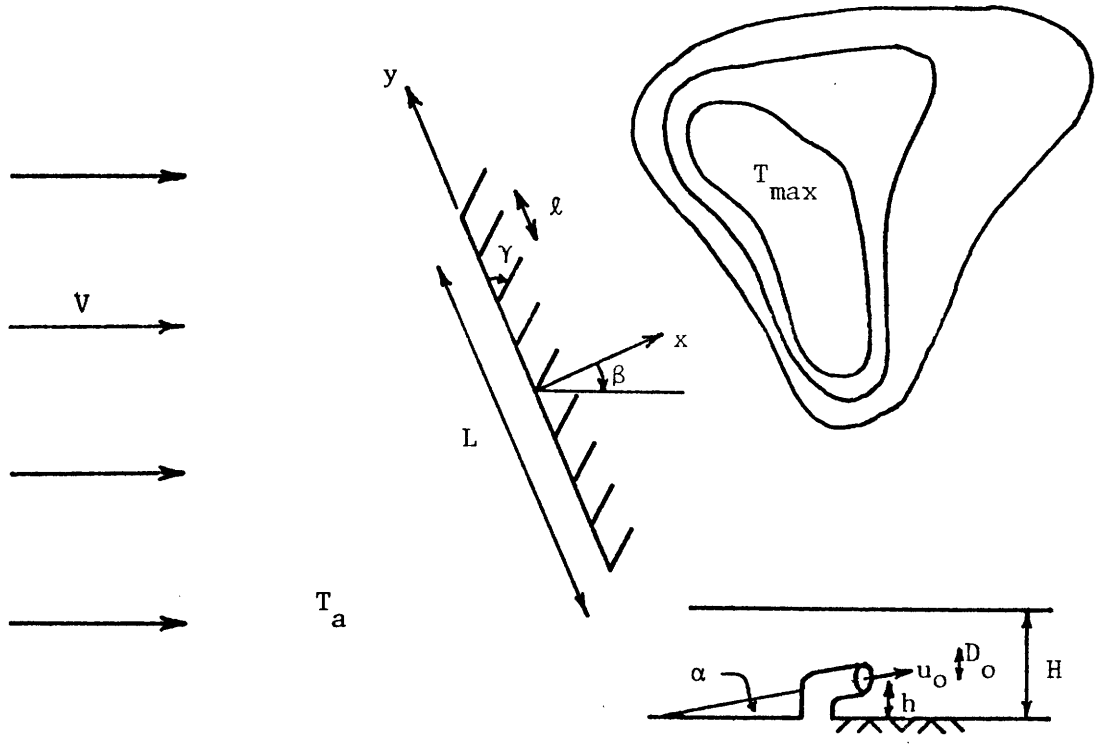

x,y = horizontal coordinates
V = ambient current velocity
L = diffuser length
ℓ = port spacing
N = number of ports L/ ℓ
α = angle between port and horizontal plane
β = angle between diffuser line and ambient current
γ = horizontal angle between port and diffuser line
H = water depth
h = elevation of port above the bottom
D_o = port diameter
u_o = discharge velocity
T_o = discharge temperature
T_a = ambient temperature

Figure 1. Definition Sketch

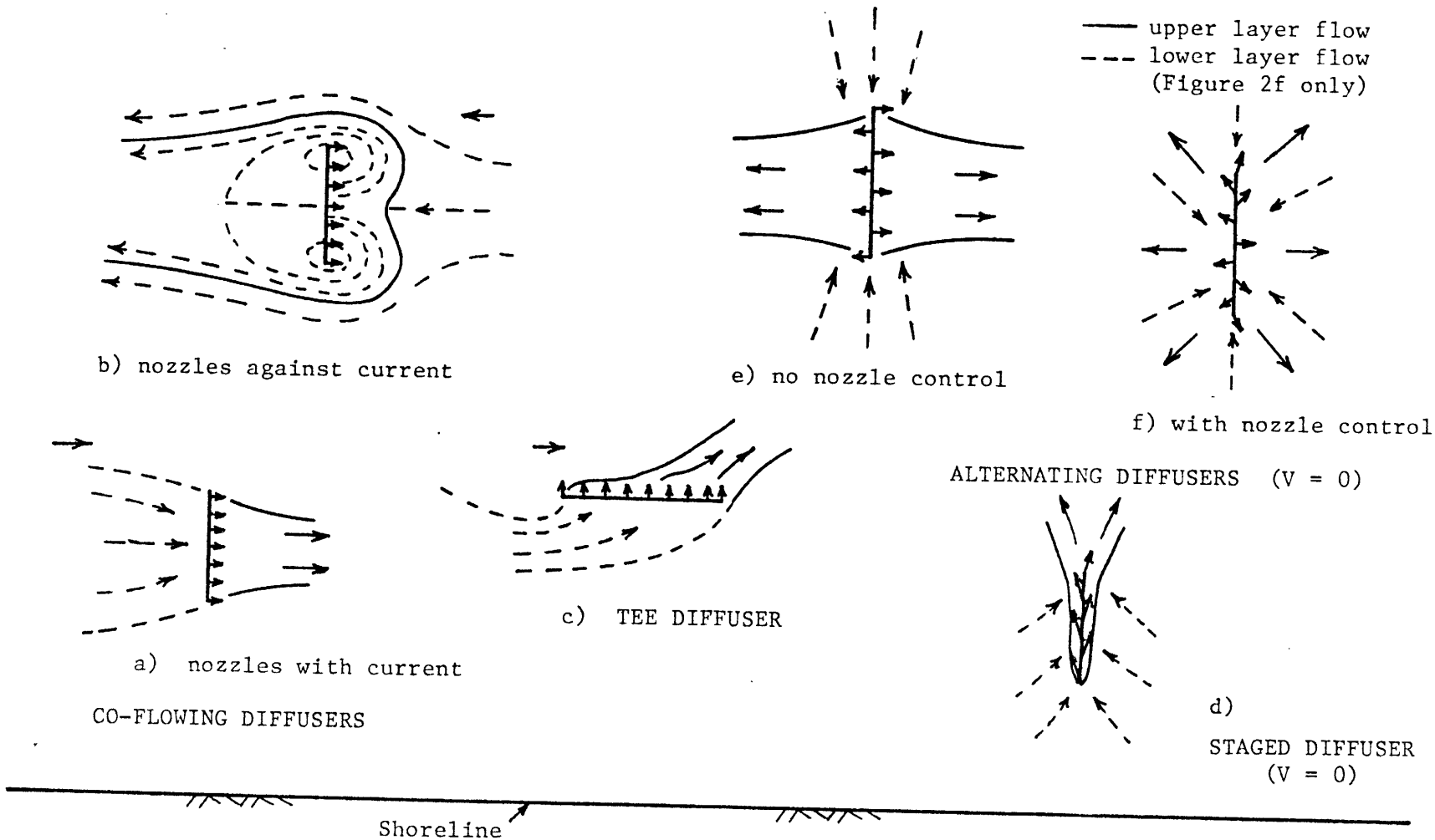

Figure 2. Geometry and Flow Fields Associated with Basic Diffuser Designs

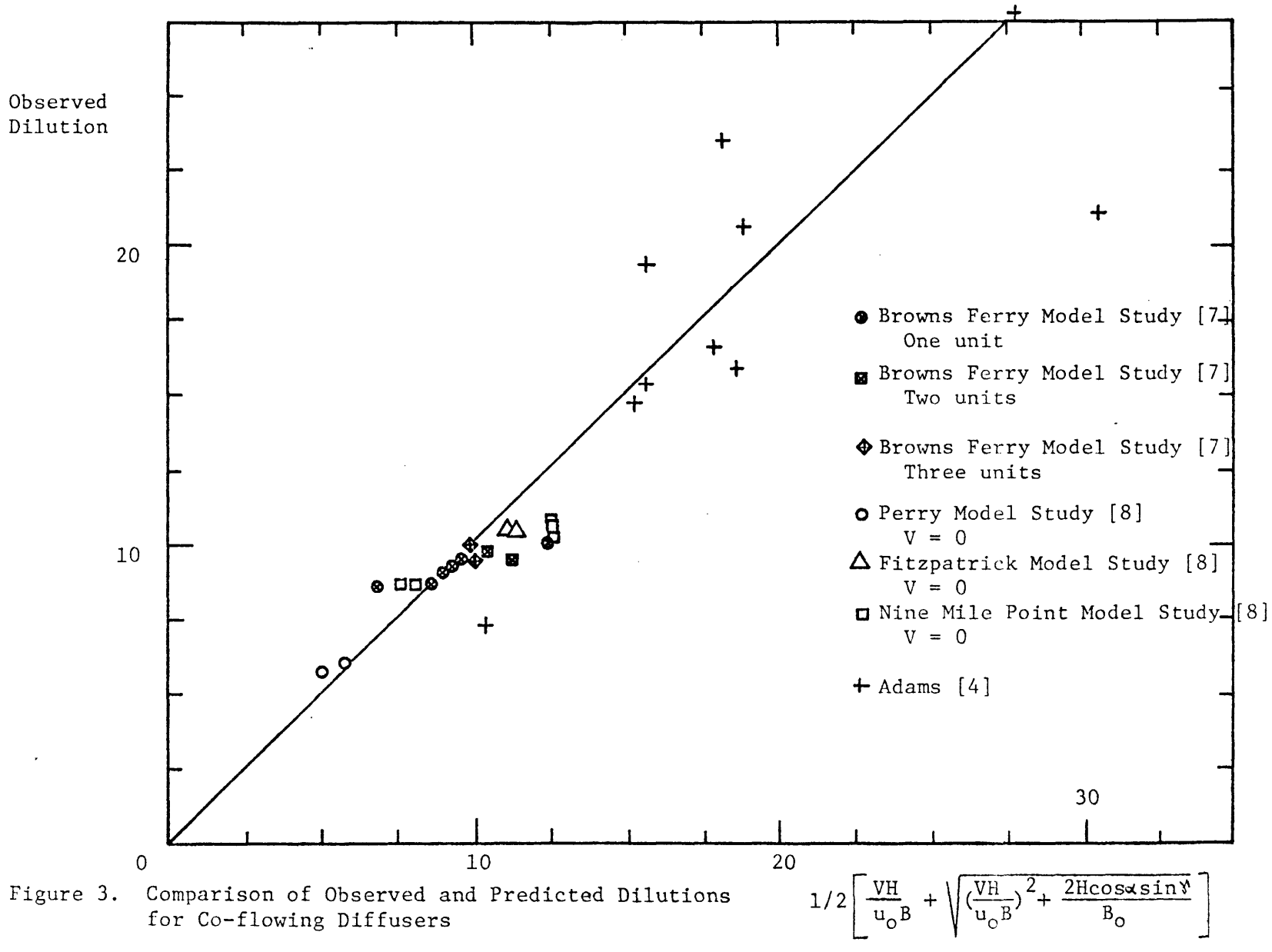

Figure 3. Comparison of Observed and Predicted Dilutions for Co-flowing Diffusers

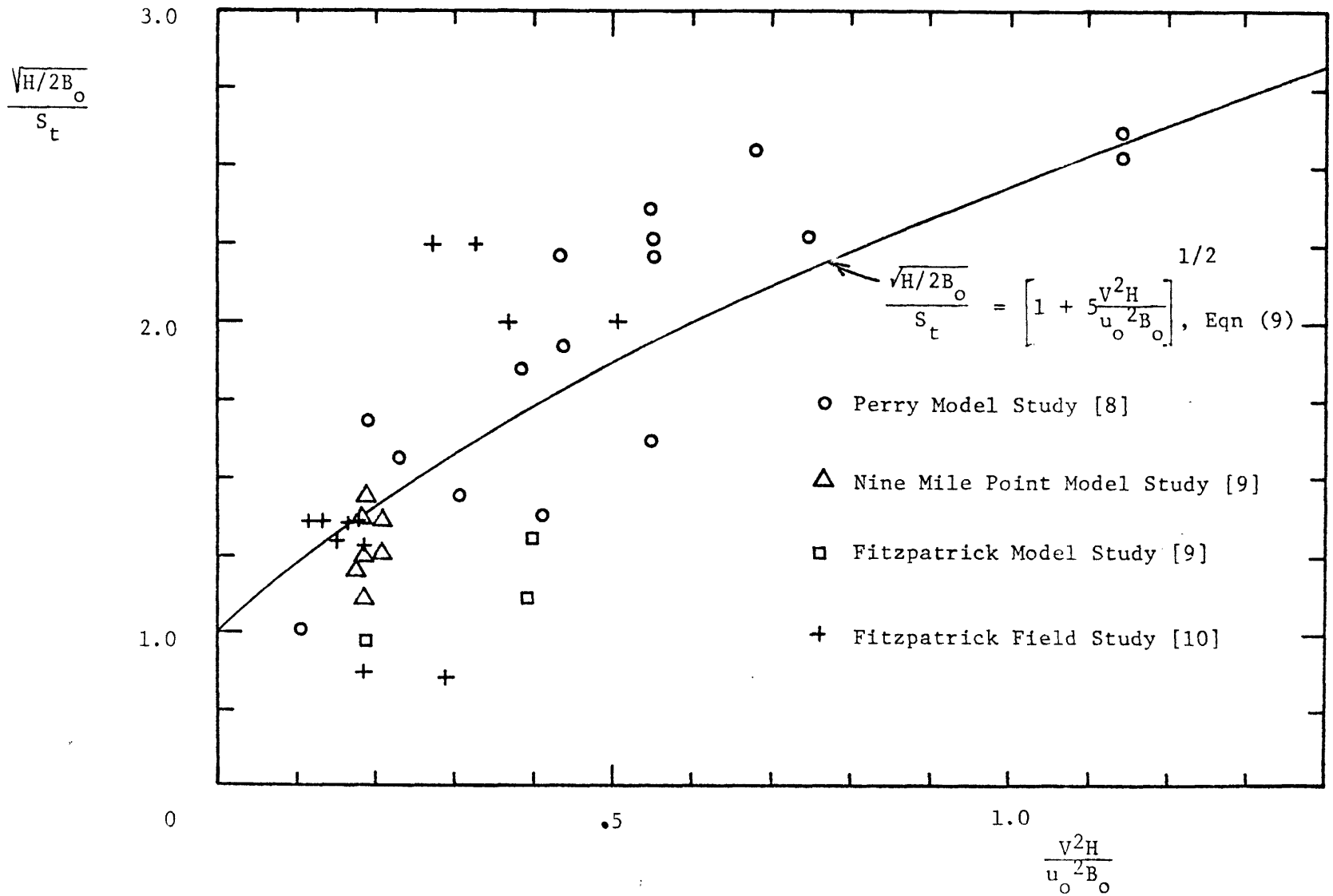

Figure 4. Observed Performance of a Tee Diffuser in a Current

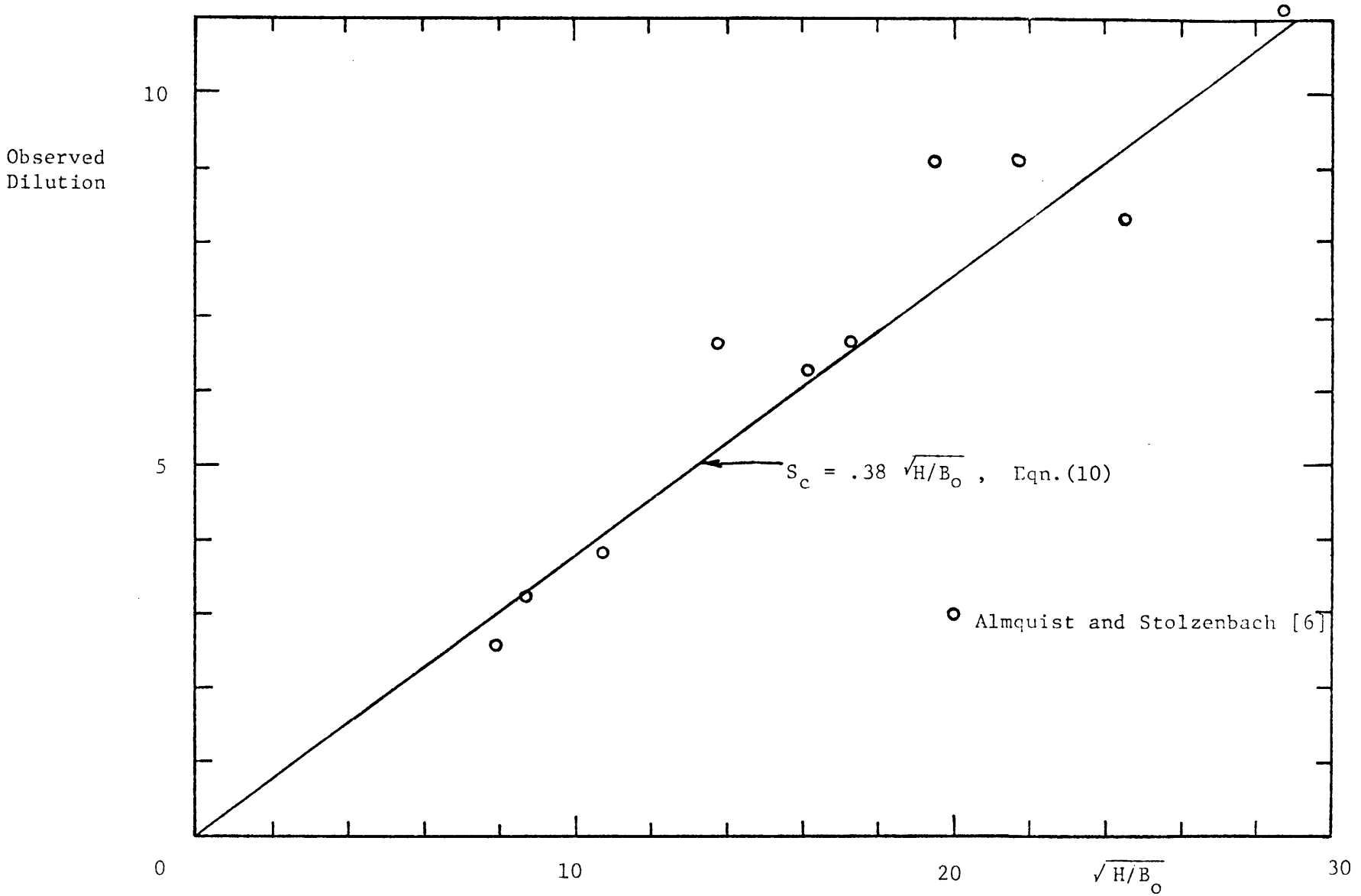

Figure 5. Comparison of Observed and Predicted Dilutions for Staged Diffusers, Adapted From [6].

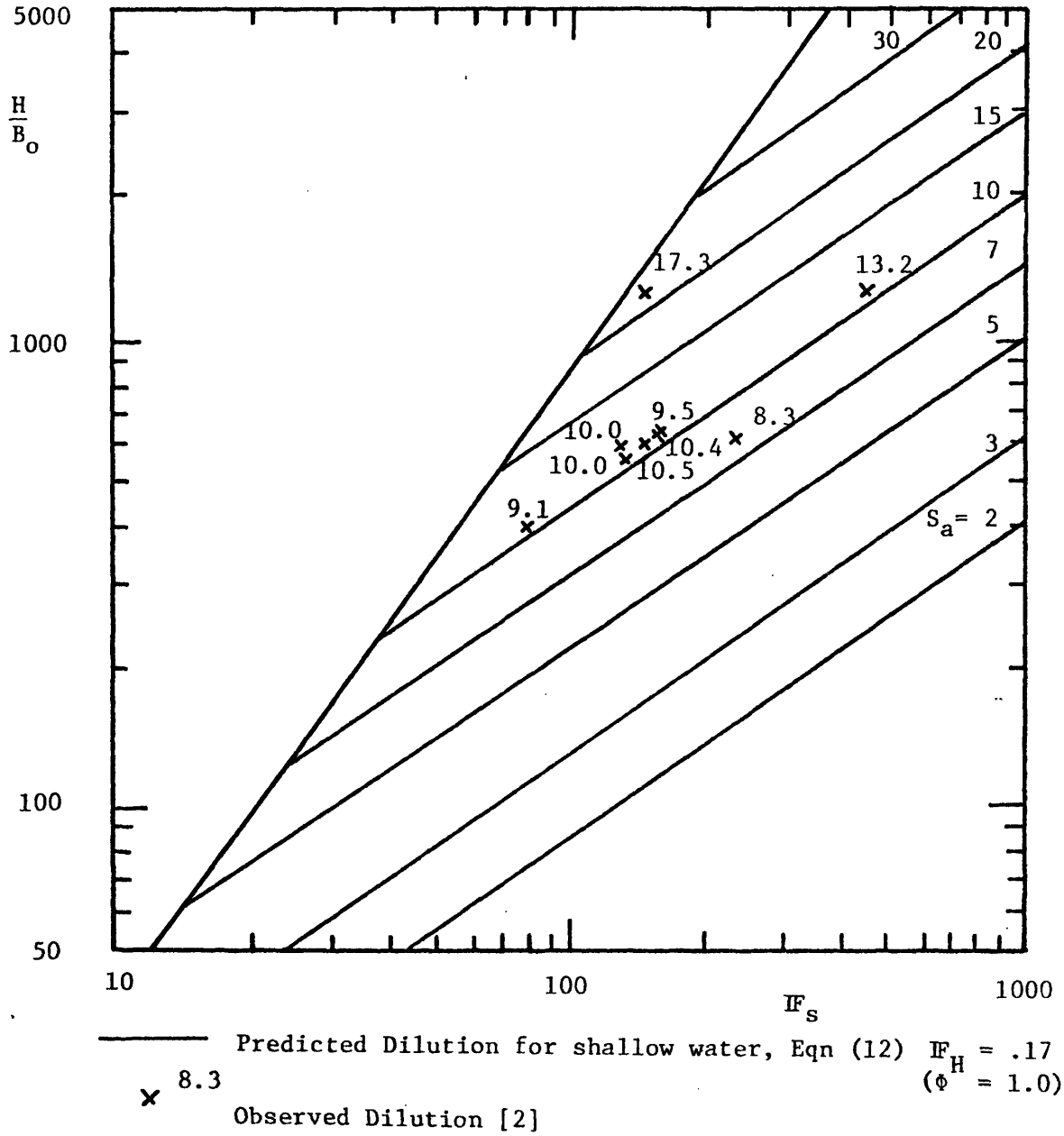

Figure 6. Comparison of Observed and Predicted Dilutions, for Alternating Diffusers

Adapted from [2]

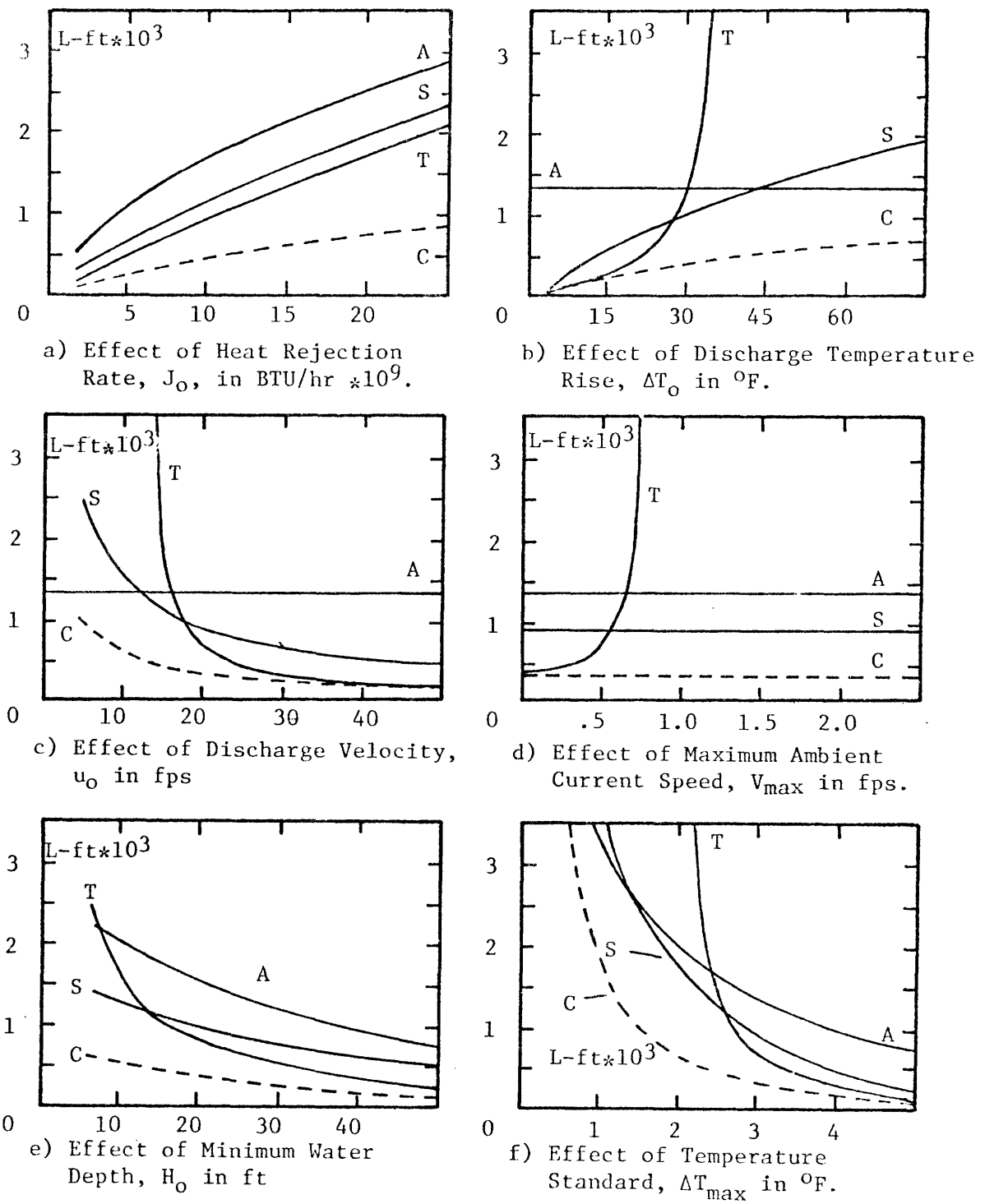

a) Effect of Heat Rejection Rate, J_o, in BTU/hr $*10^9$.

b) Effect of Discharge Temperature Rise, ΔT_o in ^oF.

c) Effect of Discharge Velocity, u_o in fps

d) Effect of Maximum Ambient Current Speed, V_{max} in fps.

e) Effect of Minimum Water Depth, H_o in ft

f) Effect of Temperature Standard, ΔT_{max} in ^oF.

Figure 7. Sensitivity of Diffuser Length to Plant, Diffuser, and Environmental Parameters for Co-flowing (C), Tee (T), Staged (S) and Alternating (A) Diffusers. Base Case: $J_o=7 \times 10^9$BTU/hr, $\Delta T_o=25^oF$, $u_o=20$fps, $V_{max}=.5$fps, $H_o=25$ ft, $\Delta T_{max}=3^oF$. ——— valid for uni- and bi-directional currents
------ valid for uni-directional currents only